ISTANBUL TECHNICAL UNIVERSITY ★ GRADUATE SCHOOL

FLYING AND HANDLING QUALITIES ORIENTED LONGITUDINAL ROBUST CONTROL OF A FIGHTER AIRCRAFT IN LARGE FLIGHT ENVELOPE

M.Sc. THESIS

Zafer KAÇAN

Department of Aeronautics and Astronautics Engineering

Aeronautics and Astronautics Engineering Programme

FEBRUARY 2022

ISTANBUL TECHNICAL UNIVERSITY ★ GRADUATE SCHOOL

FLYING AND HANDLING QUALITIES ORIENTED LONGITUDINAL ROBUST CONTROL OF A FIGHTER AIRCRAFT IN LARGE FLIGHT ENVELOPE

M.Sc. THESIS

Zafer KAÇAN
511181144

Department of Aeronautics and Astronautics Engineering

Aeronautics and Astronautics Engineering Programme

Thesis Advisor: Assoc. Prof. Emre KOYUNCU

FEBRUARY 2022

ISTANBUL TEKNİK ÜNİVERSİTESİ ★ LİSANSÜSTÜ EĞİTİM ENSTİTÜSÜ

UÇUŞ VE KULLANIM KALİTELERİNE DAYALI OLARAK BİR SAVAŞ UÇAĞI İÇİN GENİŞ BİR UÇUŞ ZARFI İÇERİSİNDE DAYANIKLI BOYLAMSAL KONTROLCÜ TASARIMI

YÜKSEK LİSANS TEZİ

Zafer KAÇAN
511181144

Uçak ve Uzay Mühendisliği Anabilim Dalı

Uçak ve Uzay Mühendisliği Programı

Tez Danışmanı: Doç. Dr. Emre KOYUNCU

ŞUBAT 2022

Zafer KAÇAN, a M.Sc. student of ITU Graduate School student ID 511181144 successfully defended the thesis entitled “FLYING AND HANDLING QUALITIES ORIENTED LONGITUDINAL ROBUST CONTROL OF A FIGHTER AIRCRAFT IN LARGE FLIGHT ENVELOPE”, which he prepared after fulfilling the requirements specified in the associated legislations, before the jury whose signatures are below.

Thesis Advisor :	**Assoc. Prof. Emre KOYUNCU** Istanbul Technical University	.....
Jury Members :	**Asst. Prof. İsmail BAYEZİT** Istanbul Technical University	.....
	Prof. Dr. Muammer KALYON Istanbul Commerce University	.....

Date of Submission : 12 January 2022
Date of Defense : 15 February 2022

To my family,

FOREWORD

Before anyting else, I want to express my gratitude to my family, my dad and my mom, who have been supporting me in every aspect of my life. Without them, none of my achievements have been accomplished and I would not be the person who I am now.

Then I want to thank my girlfriend Tuğçe Öcal, who is supporting me throughout my entire master degree. I want to thank her for supporting me, to soothe me every stressed moment I had, for sharing every cheerful memory we lived.

Then I want to thank my friends Bahadır Gökçeaslan, İrem Kırcı and Melis Özen, for keeping me alerted by making bets on my thesis study whether I succeed or fail. They sometimes got me going by applying reverse psychology but mostly supporting me and encouraging me to successfully finish my thesis study.

I want to thank Tolga Yiğit, my lead engineer in Turkish Aerospace, for feedbacks that he has given about my thesis study and also his contributions about control theory which has enlargen my knowledge during the time I find the chance to work with him.

Last, I want to thank my thesis advisor Assoc. Prof. Emre Koyuncu, for guiding me and widen my vision about aerospace applications throughout this thesis study.

February 2022

Zafer KAÇAN
Flight Control Law Design Engineer

TABLE OF CONTENTS

Page

ABBREVIATIONS

AGARD : Advisory Group for Aerospace Research and Development
AoA : Angle of Attack
AR : Aerial Recovery
CAP : Control Anticipation Power
CL : Climb
CO : Air to air Combat
CR : Cruise
D : Descend
DOF : Degree of Freedom
FBW : Fly by Wire
FHQ : Flying and Handling Qualities
FLCS : Flight Control System
GARTEUR : Group for Aeronautical Research and Technology in Europe
IBM : International Business Machines
L : Landing
LEF : Leading Edge Flap
LO : Loiter
LQR : Linear Quadratic Regulator
NASA : National Aeronautics and Space Administration
NDI : Nonlinear Dynamic Inversion
PA : Approach
PI : Proportional Integral
PID : Proportional Integral Derivative
RC : Reconnaissance
RMSE : Root Mean Square Error
RR : In Flight Refuelling
SVD : Singular Values Decomposition
TO : Take off
US : United States
WO : Wave-off / Go-around

SYMBOLS

$\boldsymbol{a}$	: Integrator coefficient of W_1 pre-compensator
$\boldsymbol{b_{ref}, b}$	: Wing span
$\boldsymbol{c_{ref}, \bar{c}}$	: Mean aerodynamic chord
$\boldsymbol{d}$	: Disturbance input
$\boldsymbol{g}$	: Gravitational acceleration
$\boldsymbol{h}$	: Altitude
$\boldsymbol{k}$	: Proportional coefficient of W_1 pre-compensator
$\boldsymbol{m}$	: Mass of the aircraft
$\boldsymbol{p_s}$	: Total pressure
$\boldsymbol{u}$	: Inputs
$\boldsymbol{x}$	: States
$\boldsymbol{x_{cg}}$	: Center of gravity position in x-axis
$\boldsymbol{x_{cg,ref}}$	: Reference center of gravity position in x-axis
$\boldsymbol{y}$	: Outputs
$\boldsymbol{u, v, w}$	: Body velocities
$\boldsymbol{p, q, r}$	: Body angular rates
$\boldsymbol{p_N, p_E}$	: Position in NED frame, north and east
$\boldsymbol{q_{ss}}$	: Steady-state pitch rate
$\boldsymbol{A, B, C, D}$	: Linear system matrices
$\boldsymbol{C_{x,t}, C_{y,t}, C_{z,t}}$	: Total force coefficients around body axis
$\boldsymbol{C_{l,t}, C_{m,t}, C_{n,t}}$	: Total moment coefficients around body axis
$\boldsymbol{C_x, C_y, C_z}$	: Clean body force coefficients around bodu axis
$\boldsymbol{C_l, C_m, C_n}$	: Clean body moment coefficients around body axis
$\boldsymbol{F_{x,A}, F_{y,A}, F_{z,A}}$	: Total aerodynamic forces in body axis
$\boldsymbol{L_A, M_A, N_A}$	: Total aerodynamic moments in body axis
$\boldsymbol{I_x, I_y, I_z, I_{xz}}$	: Moment of inertias

C_{x_q} : Force coefficient in x-axis due to pitch rate

C_{y_r} : Force coefficient in y-axis due to roll rate

C_{z_q} : Force coefficient in z-axis due to pitch rate

C_{l_p} : Moment coefficient in x-axis due to roll rate

C_{l_r} : Moment coefficient in x-axis due to yaw rate

C_{m_q} : Moment coefficient in y-axis due to pitch rate

C_{n_r} : Moment coefficient in z-axis due to yaw rate

C_{n_p} : Moment coefficient in z-axis due to roll rate

DB : Dropback

K : Controller

K_1 : Feedforward controller

K_2 : Feedback controller

L : Loop transfer function

G : Plant

G_s : Shaped plant

G_d : Disturbance plant

G_p : Uncertain plant

G_m : Gain margin

P_s : Phase margin

G_s : Sensitivity function

G_s : Complementary sensitivity function

M^{-1}, N : Left coprime factorization of plant G

Q_c : Dynamic pressure

S_{ref} : Wing aera

Th : Thrust

T : Temperature

V_t : Velocity

W : Weight

W_1 : Pre-compensator

W_2 : Post-compensator

W_i : Steady-state gain

X, Z : Solutions of ricatti equations

α : Angle of attack

$\boldsymbol{\beta}$: Angle of sideslip

$\boldsymbol{\delta_a}$: Aileron deflection

$\boldsymbol{\delta_e}$: Elevator deflection

$\boldsymbol{\delta_h}$: Horizontal tail deflection

$\boldsymbol{\delta_{lef}}$: Leading edge flap deflection

$\boldsymbol{\delta_r}$: Rudder deflection

$\boldsymbol{\delta_{sb}}$: Speedbrake deflection

$\boldsymbol{\delta_{th}}$: Thrust level percentage

$\boldsymbol{\epsilon}$: Robust stability margin

$\boldsymbol{\rho}$: Air density

$\boldsymbol{\overline{\sigma}, \underline{\sigma}}$: Maximum and minimum singular values

$\boldsymbol{\phi, \theta, \psi}$: Euler angles

$\boldsymbol{\Delta C_{x,lef}}$: Change in force in x-axis due to lef deflection

$\boldsymbol{\Delta C_{x,sb}}$: Change in force in x-axis due to speedbrake deflection

$\boldsymbol{\Delta C_{x,lef}}$: Change in force in x-axis due to lef deflection

$\boldsymbol{\Delta C_{x_{q,lef}}}$: Change in force in x-axis due to pitch rate due to lef deflection

$\boldsymbol{\Delta C_{y,lef}}$: Change in force in y-axis due to lef deflection

$\boldsymbol{\Delta C_{y,\delta_a=20°}}$: Change in force in y-axis when aileron deflection is 20 degrees

$\boldsymbol{\Delta C_{y,\delta_a=20°,lef}}$: Change in force in y-axis when aileron deflection is 20 degrees due to lef deflection

$\boldsymbol{\Delta C_{y,\delta_r=30°}}$: Change in force in y-axis when rudder deflection is 30 degrees

$\boldsymbol{\Delta C_{y_r,lef}}$: Change in force in y-axis due to yaw rate due to lef deflection

$\boldsymbol{\Delta C_{z,lef}}$: Change in force in z-axis due to lef deflection

$\boldsymbol{\Delta C_{z,sb}}$: Change in force in z-axis due to speedbrake deflection

$\boldsymbol{\Delta C_{z_q,lef}}$: Change in force in z-axis due to pitch rate due to lef deflection

$\boldsymbol{\Delta C_{l,lef}}$: Change in moment in x-axis due to lef deflection

$\boldsymbol{\Delta C_{l,\delta_a=20°}}$: Change in moment in x-axis when aileron deflection is 20 degrees

$\boldsymbol{\Delta C_{l,\delta_a=20°,lef}}$: Change in moment in x-axis when aileron deflection is 20 degrees due to lef

$\boldsymbol{\Delta C_{l,\delta_r=30°}}$: Change in moment in x-axis when rudder deflection is 30 degrees

$\boldsymbol{\Delta C_{l_r,lef}}$: Change in moment in x-axis due to yaw rate due to lef deflection

$\boldsymbol{\Delta C_{l_p,lef}}$: Change in moment in x-axis due to roll rate due to lef deflection

$\Delta C_{m,lef}$: Change in moment in y-axis due to lef deflection

$\Delta C_{m,sb}$: Change in moment in y-axis due to speedbrake deflection

$\Delta C_{m_{q,lef}}$: Change in moment in y-axis due to pitch rate du to lef deflection

ΔC_{m} : Change in moment in y-axis

$\Delta C_{m,ds}$: Change in moment in y-axis due to deep stall

$\Delta C_{n,lef}$: Change in moment in z-axis due to lef deflection

$\Delta C_{n,\delta_a=20^\circ}$: Change in moment in z-axis when aileron deflection is 20 degrees

$\Delta C_{n,\delta_a=20^\circ,lef}$: Change in moment in z-axis when aileron deflection is 20 degrees due to lef

$\Delta C_{n,\delta_r=30^\circ}$: Change in moment in z-axis when rudder deflection is 30 degrees

$\Delta C_{n_{r,lef}}$: Change in moment in z-axis due to yaw rate due to lef deflection

$\Delta C_{n_{p,lef}}$: Change in moment in z-axis due to roll rate due to lef deflection

ΔC_{n_β} : Change in moment in z-axis due to sideslip angle

$\|.\|_1$: 1 norm

$\|.\|_2$: 2 norm

$\|.\|_\infty$: Infinity norm

$\|.\|_H$: Hankel norm

$[.]^T$: Transpose

LIST OF TABLES

Page

LIST OF FIGURES

Page

FLYING AND HANDLING QUALITIES ORIENTED LONGITUDINAL ROBUST CONTROL OF A FIGHTER AIRCRAFT IN LARGE FLIGHT ENVELOPE

SUMMARY

In the scope of this thesis study, robust control design apprach has been applied to F-16 aircraft which is aimed to satisfy Level 1 FHQ within the specified flight envelope.

First, a brief information about the histoy of flight mentioned in the introduction chapter. This historical storyline starts from the early sketches of Leonardo da Vinci and extends along to Wright Brothers who had achieved the first sustainable, controlled heavier than air flight. Then the innovations in aerospace industry is mentioned along with the advances in technology at the same time. The milestone successes are explained which has brought us to realize the design of fly-by-wire flight control algoritms. Then a literature review of the documents about the F-16 aircraft, FHQ criteria, multivariable robust control applications and mathematical backgroud of this approach. The structure of the thesis has outlined.

Then, F-16 aircraft has been presented along with the aerodynamic data and how the force and moment of the aircraft is related with the aerodynamic and thrust data. The presented data of the F-16 aircraft was obtained from the researches of NASA Langley Research Center which is based on wind tunnel test results of the F-16 aircraft. The mathematical model of the F-16 aircraft is introduced. This mathematical model includes the airframe spacifications, the mass data, the systems that represent actuator and sensor and the environmental data which gives the atmospheric properties with respect to the flight condition of the aircraft. Then, the trim and linearization algorithms are introduced for the steady-state wings level flight condition. The inputs, states and outputs related to the longitudinal motion of the aircraft has been identified and the resultant state space linear system which represents the characteristics of the aircraft is obtained. The longitudinal modes which are phugoid and the short-period mode are mentioned.

Next, the flying and handling qualities to evaluate the performance of the aircraft are emphasized. The reason for the use of flying and handling qualities are determined and related with the pilot evaluations Cooper-Harper ratings. The suggested flying and handling qualities are explained for the use of both design guidance and evaluation criteria. It is mentioned that the CAP criterion is used as design guideline whereas the Bandwidth and Dropback criteria are used as evaluation criteria for the aircraft in the both frequency and time domain. The corresponding flying and handling qualitieslevels are detailed for the criteria and related intervals for the properties are supported with the graphical representations.

The robust control approach is introduced while mentioning the background of the method. The norm definitions are done and the feedback properties are given in the related chapter of this thesis in order to associating the design purposes with the feedback properties. The relationships between the open-loop characteristics and

closed loop results are identified and the loop-shaping aproach is emphasized. Yhen the uncertainty definitions are identified. The classes of uncertainty and where they are reasoned for is explained. An uncertainty definition which is suitable for the use in this thesis is mentioned. Then the H_∞ Loop Shaping approach is expressed. The normalized coprime factorization method is explained and the design of both one degree of freedom and two degrees of freedom H_∞ Loop Shaping approaches are detailed with the design steps.

Then, the control structure used in this thesis is explained. It is aimed to design a pitch rate controller which will results in Level 1 flying and handling qualities within a specified flight envelope. The design has been made for one design point and then the resulted parameters are used for the whole flight envelope. This enables to overcome the complexity of gain scheduling manner and provides robustness against any probable loss of air data such as angle of attack. The controller architecture of NASA research was presented for the longitudinal axis. Then the optimization structure to find the design parameters which ensures that the pitch rate demand flight control law results in Level 1 flying and handling qualities within a specified flight envelope. The root mean square approach has been applied in optimization phase. It is purposed that the time responses of 5 different design points after step input should follow a desired transfer function response specified during the design of the two degrees of freedom H_∞ Loop Shaping algorithm as close as possible. Moreover, in order to satisfy the specified flying and handling qualities, time delay parameter is included in the optimization cost which makes the optimization multiobjective optimization with a weigthed sum cost function.

The resultant optimized parameters for the design of two degrees of freedom H_∞ Loop Shaping architecture is given. The results of both nominal design point and the responses of 5 different design points along the flight envelope are presented. The flying and handling qualities evaluations are shown. Then the performance and stability robustness results are associated with the results. The comparison study between the two degrees of freedom H_∞ Loop Shaping algorithm and the NASA control structure which emphasizes a classical PI controller has been presented.

The results are satisfactory as all the design points resulted in Level 1 flying and handling qualities responses in both frequency and time domain. It is seen that the control architecture is successful for performance and stability robustness as all uncertain plants are following the nominal response and no frequency response has crossed a nichols exclusion zone defined. The two degrees of freedom H_∞ Loop Shaping algorithm outperformed the NASA PI controller as Level 2 results are seen for NASA PI controller responses. The use of two degrees of freedom H_∞ Loop Shaping structure lowered the time delays as it was purposed in the optimization goals as the effective time delay results are less than the NASA PI controller.

UÇUŞ VE KULLANIM KALİTELERİNE DYALI OLARAK BİR SAVAŞ UÇAĞI İÇİN GENİŞ BİR UÇUŞ ZARFI İÇERİSİNDE DAYANIKLI BOYLAMSAL KONTROLCÜ TASARIMI

ÖZET

Bu tez çalışması kapsamında, F-16 uçağı için belirlenen uçuş zarfı boyunca seviye 1 uçuş ve kullanım kalitesi sonucu veren bir dayanıklı kontrol sistemi tasarımı yapılması amaçlanmıştır.

Öncelikle, uçuşun tarihi hakkında genel bir bilgi başlangıç bölümünde bulunabilir. Bu tarihi bilgi bütünü rönesans döneminde Leonardo da Vinci'nin eskizlerinden Wright kardeşlerin ilk sürdürülebilir ve kontrol edilebilir uçuşuna kadar olan zaman dilimi içerisindeki bilimadamlarının havacılık bilimine katkılarından bahsedilir. Daha sonra havacılığın gelişimi o dönemdeki sanayi atılımları ile beraber ilişkilendirilir. Bizi şu anda "fly-by-wire" terimi ile uçuş kontrol yasalarını tasarlamamıza yol açan her bir kilometre taşı bu bölüm kapsamında değinilen noktalar arasındadır. F-16 uçağı, uçuş ve kullanım kaliteleri, çok değişkenli dayanıklı kontrol uygulamaları ve bunların matematiksel arkaplanları hakkında bir literatür taraması sunulmuştur ve tez boyunca değinilecek bölümlerdeki konular özetlenmiştir.

Sonrasında, F-16 uçağının aerodinamik ve motor verilerinin nasıl kuvvet ve moment denklemleri ile ilişkili olduğu anlatılmıştır. Bu bölümde sunulan aerodinamik ve motor verileri 1970'lerde NASA Langley Araştırma Merkezi'nde yapılan rüzgar tüneli sonuçlarını kapsar. F-16 uçağının matematiksel modeli tanıtılır. Bu matematiksel model hareket denklemlerini, hava aracı modelini, ağırlık ve kütle verilerini, eyleyici ve sensör modellerinin matematiksel yaklaşımlarını ve uçağın uçuş koşuluna bağlı olarak değişen atmosferik özellikleri yansıtan modelleri içermektedir. Trim ve doğrusallaştırma algoritmalarını sabit durumda, kanat seviyeleri eşit bir uçuş durumu için aktarılmıştır. Hava aracı modelinin boylamsal eksendeki değişkenleri ile ilgili olan giriş, durum ve çıkışları lineerleştime sonucunda oluşan durum uzayı denklemleri ile ilişkilendirimiştir. Uçağın boylamsal modları olan phugoid ve short-period modları ve bu modları nelerin etkilediği aktarılmıştır.

Daha sonra, uöağın performans kriterlerini ölçecek olan uçuş ve kullanım kalitesi kriterleri aktarılmıştır. Uçuş ve kullanım kalitesi kriterlerinin kullanım nedenleri belirtilmiş ve bu kriterler pilot değerlendirmeleri olan Cooper-Harper değerlendirme ölçütleri ile ilişkilendirilmiştir. Önerilen uçuş ve kullanım kriterleri hem tasarım kılavuzu hem de değerlendirme ölçütleri için kullanılmak üzere detaylandırılmıştır. CAP kriterinin tasarım kılavuzu olarak kullanılması, Bandwidth ve Dropback kriterlerinin de değerlendirme ölçütleri olarak kullanıldığı aktarılmıştır. Sonuçlara karşılık gelen uçuş ve kullanım kalitesi kriterlerinin hem sayısal aralıkları hem de grafiksel gösterimleri seviye sonuçları ile ilişkilendirilmiştir.

Sonrasında dayanıklı uçuş kontrol yaklaşımı, bu yaklaşımın arkaplanıyla beraber yansıtılmıştır. Norm tanımları yapılmış, geri besleme özelliklerinin açık çevrim

sonuçları ile nasıl ilişkilendirilebileceği aktarılmıştır. Açık çevrim sonuçları ve bu sonuçları kapalı çevrim geri besleme sonuçlarıyla ilişkileri detaylandırılmıştır. Loopshaping yaklaşımı bu ilişkiler üzerinden anlatılmıştır. Uçuş kontrol yasaları tasarımı ve değerlendirilmesi kapsamında kullanılacak olan belirsizlik tanımları verilmiştir. Sonrasında ise H_∞ Loop Shaping yaklaşımı anlatılmıştır. Normalize edilmiş asal faktorizasyon yöntemi açıklanmış ve hem bir serbestlik dereceli hem de iki serbestlik dereceli H_∞ Loop Shaping yaklaşımı tasarım aşamaları ile beraber detaylandırılmıştır.

Daha sonra bu tez kapsamında kullanılacak olan kontrol mimarisi açıklanmıştır. Belirlenen bir uçuş zarfı içerisinde seviye 1 uçuş ve kullanım kalitesi sonuçlarını veren bir yunuslama hızı kontrol sistemi tasarlamak bu tezin asıl amacıdır. Böylece uçuş zarfında yer alan tek bir noktada yapılan tasarım ile beraber kazanç düzenlemeye ait bütün kompleks yapı ortadan kaldırılmış olur. Dahası, uçuş süresince oluşabilecek olan hücum açısı gibi hava verisi kaybı risklerine karşı da dayanıklı bir uçuş kontrol sistemi elde edilmiş olunur. Sonrasında, NASA araştırmasında yer alan PI kontrolcü yapısı ile bir karşılaştırma yapılmıştır. Bahsedilen uçuş kontrol algoritması amaçlarına ulaşmak için bir optimizasyon çalışması yapma ihtiyacı doğmuştur. Bu kapsamda belirlenen uçuş zarfı boyunca seviye 1 uçuş ve kullanım kalitesi sonuçlarını verecek olan bir yunuslama hızı talep uçuş kontrol sistemi parametreleri optimizasyon yardımı ile bulunmuştur. Optimizasyon sırasında "root mean square" yaklaşımı kullanılmıştır. Buradaki amaç, uçuş zarfı içerisindeki tek bir noktada tasarlanan uçuş kontrol sistemi kazançlarının kullanıldığı 5 farklı tasarım noktasındaki cevapların, iki serbestlik dereceli H_∞ Loop Shaping algoritması için belirlenen ideal bir sistem cevabını olabildiğince yakından takip edebilmesidir. Root mean square yaklaşımı da bu aradaki farkların azaltılması için kullanılmıştır. Hatta, gerekli uçuş ve kullanım kalitesi kriterlerini karşılayabilmek için zaman gecikmesi parametresi de optimizasyon amaç fonksiyonuna eklenmiş ve optimizasyon çok amaçlı bir optimizasyon problemine dönüşmüştür. Burasa zaman gecikmesinde kullanılan kısıtlama, bu parametrenin izin verilen bir değeri geçmemesidir. Optimizasyon amaç fonksiyonu ağırlıklı değerlendirme yöntemi haline getirilmiş ve optimizasyon problemi çözülmüştür.

Bu optimizasyon probleminin çözümü sonucunda istenen uçuş ve kullanım kalitesi değerlerini veren bir kazanç değerleri grubu elde edilmiştir. Bu değerlerin kullanıldığı bir tasarım noktasında tasarlanan iki serbestlik dereceli H_∞ Loop Shaping uçuş kontrol algoritması, bu noktada belirlenen uçuş ve kullanım kalitesi kriterlerini seviye 1 olarak karşılayabilmektedir. Daha sonra uçuş zarfı boyunca gereken analizleri yapmak için belirlenen 5 noktada bu uçuş kontrol algoritmasının hem frekans uzayındaki hem zaman uzayındaki cevapları alınmıştır. Bu alınan cevapları uçuş ve kullanım kalitesi kriterlerine yansıtılmıştır. Bir karşılaştırma çalışması yapmak üzere, iki serbestlik dereceli H_∞ Loop Shaping uçuş kontrol algoritması ile NASA araştırmasında yer alan klasik kontrol metodlarının uygulandığı boylamsal eksendeki PI kontrolcüsü ile elde edilen cevaplar kıyaslanmıştır.

Yapılan tasarım sonucunda elde edilen sonuçlar tasarım amaçlarının başarıyla gerçekleştirildiğini göstermektedir. Uçuş zarfının orta bölgesinde belirlenen bir nokta için yapılan iki serbestlik dereceli H_∞ Loop Shaping uçuş kontrol algoritması elde edilen aynı kazançlar ile, uçuş zarfının 4 köşesinde yer alan diğer tasarım noktalarında uygulanmıştır. Elde edilen sonuçlara göre, hem uçuş zarfının orta bölgesindeki tasarım noktasında, hem de uçuş zarfının köşelerine denk gelen diğer tasarım noktalarında istenen uçuş ve kullanım kalitesi kriterlerine ulaşılmıştır. Hem zaman uzayında hem de frekans uzayında daha önceki bölümlerde belirlenen "Bandwidth" ve "Dropback"

uçuş ve kullanım kalitesi sonuçları seviye 1 sınırları içerisinde yer almaktadır. Bu sonuçlar ayrıca performans ve stabilite açısından da dayanıklıdır. Sonuçlar incelendiğinde, zarfın her noktasındaki tasarım noktalarının belirsizlikler içeren cevapları, belirsizlik içermeyen "nominal" durumdaki cevapları hem zaman hem de frekans uzayında takip etmektedir. Uçuş zarfındaki belirsizlikler içeren frekans cevapları nichols grafiği üzerindeki nichols kısıtlama bölgesinden geçmemektedir. Bu da uçuş zarfı boyunca ele alınan tasarım noktalarında, uçuş kontrol algoritmasının dayanıklı bir stabiliteye sahip olduğunu göstermektedir. Ayrıca performans kıyaslaması amacı ile NASA araştırmasında yer alan PI kontrolcüsü ile beraber bir karşılaştırma çalışması yürütülmüştür. Bı kıyaslamada, iki serbestlik dereceli H_∞ Loop Shaping uçuş kontrol algoritmasının NASA dökümanındaki PI kontrolcüsünden daha iyi performans gösterdiği görülmüştür. NASA PI kontrolcüsü ile yürütülen uçuş ve kullanım kalitesi kriterleri sonuçlarında bazı bölgelerde seviye 2 sonuçlar görülürken, iki serbestlik dereceli H_∞ Loop Shaping uçuş kontrol algoritmasında bu noktalardaki bütün sonuçlar seviye 1 ile sonuçlanmaktadır. Dahası, optimizasyon amacı olarak ele alınana zaman gecikmesi sonuçlarının da iki serbestlik dereceli H_∞ Loop Shaping uçuş kontrol algoritması için NASA PI kontrolcüsünden daha iyi sonuçlar verdiği gözlemlenmiştir.

1. INTRODUCTION

The idea of flight has always been one of the most challenging quest throughout the history of mankind. The aspiration to fly is as old as the human imagination. Human examined the birds for ages to understand the physics behind the flight. Even the word “aviation” is said to be used first by Frech writer and former naval officer Gabriel La Landelle as “avier” which is derived from the Latin word “avis” that means bird in English.[1] Unfortunately, man had unsucceed flying like a bird since the human anatomy differs from birds by means of the mass and muscle build.

Early flying machine studies were conducted by Leonardo da Vinci during Rennesaince era. He had drawed hundreds of sketches of his design “ornithopter”. This concept differs from the predecessors as it does not rely only on a pair of mechanical wings but it features a set of foot pedals and lever to get the machine into the air.[2] Later studies based on lighter than air concepts such as hot air baloons. In 1783, Montgolfier had succeeded the first-ever manned balloon flight. On 21 November 1783, Montgolfier hot air balloon made its maiden flight at Paris by completing 25 minutes of flight[3].

The major leap had been achieved in 19th century with the studies of Sir George Cayley who is known as the father of aeronautics lived between 1773 and 1854. He defined four main forces acting on the aircraft during flight which are lift, drag, weight and thrust on his article “On Aerial Navigation”[4] at 1810. He suggested the idea that the air vehicle should have a velocity enough to support the weight in order to retain its relative position in the air. His studies on wings are leaded the design of the the heavier than air concepts such as gliders.

Otto Lilienthal followed the ideas of Sir George Cayley and designs 18 different glider models and succeeded over 2000 flights until his tragic death in 1896 after stall of a glider in flight. The control of the glider was enabled by the body movements of the pilot by changing the centre of gravity.

During the industrial revolution, many technological advancements were achieved especially on the design of internal combustion engines. During this era, the internal combustion engines are designed in a way that they generate more power while losing weight so they became applicable to mount on gliders. This advancement enabled the gliders to maintain their air speed during the flight. The Wright brothers, Orville and Wilbur Wright had understood the concept and built one of the first wind tunnels of the world in order to study on physics of flight. Over the years, they tested hundreds of airfoils and established a database for lift and drag characteristics. Finally, wright brothers had invented the airplane and achieved the first-ever sustained and controlled heavier than air flight on 17 December 1903. The aircraft Wright Flyer can be seen in the Figure 1.1 below.

Figure 1.1 : The Wright Flyer.

Orville Wright shared his enthusiasm with a quote below[3].

"The exhilaration of flying is too keen, the pleasure too great, for it to be neglected as a sport."

After this great achievement, the aircraft industry gained immense acceleration all over the world. Robert Esnault-Pelterie patented the "joystick" for flight control and in 1908, the aircraft Bleriot VIII became the first-ever aircraft that uses joystick to monitor flight control surfaces. The aerospace industry continued to grow during the World War I and World War II. During this time zone, the aircrafts were used for various purposes such as reconnasaince, bomber, fighter and delivery missions. Many

well known aircraft companies were established in these years such as Boeing, de Havilland, Lockheed, Northrop, Fokker, Piper, and Douglas. The early aircrafts used mechanical linkage between the pilot inputs to joystick and rudder pedals to primary control surfaces such as pulleys and push rods. As the industry for many areas growed during the World War I and World War II, the capabilities of the aircrafts were enhanced too. They began to fly faster, higher and further. In the period from 1910's to 1930's researches of scientists are focused on stability derivatives, the response of disturbances and calculated the response to applications of control[5]. In 1924, Gates asssumed that the flight controls were shaped according to the certain laws[6]. The early flight control applications were focused on navigational control as well as angle of attack and attitude control which enables the aircraft fly transatlantic routes. Thanks to the developments on the automatic control, in 1947 a Douglas C-54 aircraft becomes the first-ever fully automatic controlled aircraft from the take-off to landing with no human hand touched the controls. A special IBM equipment controlled the aircraft by selecting radio stations, course, speed, flap settings and landing gear position with a program stored on punched cards[5].

As the aircrafts get bigger and heavier, the loads which pilot have to command were increased so the control schemes redevised to reduce the pilot workload to maintain the control. Hydro-mechanical systems entered service during this era to use hydrolic power to assist the pilot during flight to decrease pilot load in the cockpit. This systems enabled the development of larger aircrafts such as Boeing 707[6].Taking account of the world wars era with the technological advancements, especially introduction of the jet engine to the aircraft industry and the aerodynamic benefits of the elements which have deficiencies in stability, required a new research area which is flight control design. During this era, very familiar contributions to control theory had been accomplished by Nyquist, Bode, Nichols, Philips and Evan's root locus developed in this period[5]. The term "stability augmentation" introduced in the late 1940's. With the help of feedback control, the application of stability augmentor actuators enabled aircrafts to have desired stability characteristics. The yaw damper, short-period damper, roll damper, sideslip augmentor and longitudinal augmentor as well as other inventions were invented during this era combined the feedback theories and understanding of stability leads to the control law development in the following decades.

As the capabilites of the aircrafts enlarged, the mission of the stability augmentation has changed from simple damping to cover much broather scope[5]. Besides ensuring the stability, a flight control system should prevent any deficiencies during the flight. This leads to control augmentation systems.

The advancements on the feedback control and electrical technology had leaded a new era in the flight control area. A Fly-by-Wire(FBW) system uses electrical wires and computers rather than pulleys and push rods in order to manipulate the primary control surfaces of the aircraft. This enables more reliable operation of the aircraft as manual controls suffer from the mechanical deficiencies[6]. The pilot commands is translated into analogue signals which are reaches the flight computer via wires. The signal then operatess the actuation systems that deflects the control surfaces. After deflection of the control surfaces, a feedback signal detected from sensors are feeded to the flight computer to detect an error between commanded signal and the measured signal. A FBW system and its components can be seen from the Figure 1.2 below.

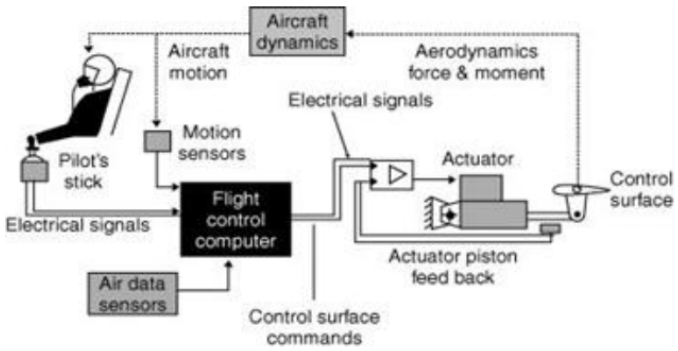

Figure 1.2 : A FBW system and its components.

The lightweight and more reliable FBW stability and command augmentation sytems provide other functions to be applied to the control law of the aircraft. General Dynamics F-16 is the first example that used fully FBW system in modern fighters in 1970's. The flight control laws of F-16 also includes envelope limiting functions that limits the pilot inputs at certain fligth conditions.

The success of FBW systems is a big achievement such that applications expands another areas of aerospace such as civil transportation. Airbus introduced A320 aircraft with fully equipped FBW system while Boeing produced 777 as a first full-time FBW application of its brand however 757 and 767 includes partial FBW control systems[5].

A sample block diagram of the FBW flight control system law can be seen in the Figure 1.3 below.

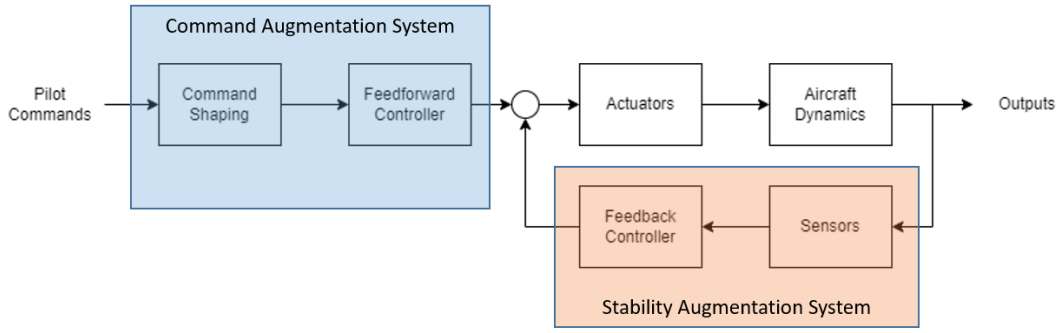

Figure 1.3 : Block diagram of the FBW control law.

As the appliacation of the FBW control laws spreads quickly to the design of various air vehicles, a set of evaluation criteria and standards which defines the performance of the closed loop system emerges as requirements. Studies of AGARD[7], Department of Defence Interface Standard[8][9][10] and NASA[11] proposes a set of flying and handling qualites for the design and evaluation of the aircrafts in military perspective.

Numerous techniques are existant to design a flight control law algorithm in the literature. There are proposed modern techniques such as linear quadratic regulator (LQR), eigenstructure assignment, nonlinear dynamic inversion(NDI), pole-placement[12] and H_∞ techniques[13] as well as the classical PID control methods.

1.1 Purpose of Thesis

The purpose of this thesis to design a robust flight control algorithm using H_∞ Loop Shaping technique which ensures Level 1 FHQ within a specified flight envelope defined. Then the performance of this designed control law is evaluated with respect to the selected criteria and then a comparison study is conducted with the existant control architecture studied before by NASA. It is aimed that to result better FHQ evaluation than the pre-existant NASA controller.

1.2 Literature Review

A literature survey has been completed for the purprose of better understanding of previous studies and gain insight about the current status of the metodologies applied in the aircraft flight control subject. The topics can be groupped as the aircraft research, flight handling and qualities and applications to the flight control algorithms design process, studies on robust and multivariable control.

In 1979, NASA published a technical paper TP1538 which covers the aerodynamic properties of General Dynamics YF-16 aircraft[14]. Besides the broad information of aerodynamic properties, this paper includes control system schemes in roll, pitch and yaw axis. The envelope protection algorithms such as AoA limiting and spin prevention functions are detailed. Post–stall characteristics of YF-16 are demonstrated. A later study has detailed the structure of the FLCS of F-16 aircraft[15] and the fuctions of flight control law design.

In 1969, Cooper and Harper proposed a pilot rating scale in order to evaluate the handling qualities of the aircraft[11]. In 1980, Air Force Wright Aeronautical Labs prepared a set of flying qualities of piloted aircrafts for military purposes to define desired flying and handling qualities[8]. This document aimed to assure flying qualities that ensures certain mission performance levels and presents as design guideline for the flight control law engineers. The research on the criteria for desired handling qualities proceeds and in 1982, AGARD published a document[7] which gathers the studies on flying and handling qualities of the military aircrafts of numereous researchers. In 1994, Mitchell, Hoh, Aponso and Klyde developed proposed revisions to the flying qualities military standard MIL-STD-1797A[10]. Gibson presented his master thesis study focused on design methodologies for handling qualities in fly by wire aircrafts[16] after working in the industry many years. Then in 2004, a more broadscale document of MIL-STD-1797A has been published by Department of Defense[9].

In 1998, Gautrey studied set of flying qualities design requirements for transport aircraft using Gibson's criterions in both time and frequency domain and military specifications[17]. In 2001, Tichler, Lee and Colburne evaluated various flight control system design methods such as PID, LQR, dynamic inverse and H_∞ using a set of handling qualities criteria[18]. Tichler also continued to study on control law design

and handling qualities optimization for longitudinal[19] and lateral-directional[20] axes.

In 1988, Glover and Doyle proposed a solution method to obtain all stabilizing controllers to achieve a certain H_∞ bounds[21].

In 1989, Glover and McFarlane handled the robust stabilization problem based on normalized coprime factorization method[22] and extends this idea on H_∞ loop shaping in 1990 and details the procedure of H_∞ Loop Shaping method[23].

In 1993, Limbeer studies further about the H_∞ Loop Shaping method and proposed an architecture of H_∞ Loop Shaping with 2 degrees-of –freedom controller approach[24].

In 1991, Hyde demonstrated multivariable control laws with H_∞ approach on a VSTOL aircraft[25].

In 1996, Wright Laboratory published a document which subjects the multivariable control design guidelines[26] with the contributions of Lockheed Martin and Honeywell.

In 1997, GARTEUR published a research report on robust control with the contributions of different institutes and companies[27]. This report includes numerous methods for robust control vatying from the nonlinear dynamic inversion to H_∞ synthesis.

In 2001, Bates, Kureemun and Postletwaite introduced an uncertainty definition to be applied on nominal plant in order to represent the input multiplicative uncertainty[28]. ADMIRE presented a report which presents the aerodynamic data model also includes the uncertainty modelling and data for the aerodynamic derivatives in 2005[29].

In 1999, Zhou and Doyle published a book based on robust control and its essentials which includes the definitions of H_∞ norms, uncertainty types and solution methods for robust controllers[30].

In 2001, Sidi published a book on the design of robust systems along with the experiences he had from the industrial applications[31].

In 2001, Skogestad and Postletwaite published a book which covers the subjects from the classical feedback control to multivariable control and robust stability and performance analyses[32]. This book also introduces the applications of robust control algorithms into MATLAB software.

1.3 Hypothesis

The 2 degree of freefom H_∞ Loop Shaping technique enables the determination of a ideal transfer function to be followed by the system. The characteristics of this ideal transfer function can be defined in time domain by taking account of the FHQ requirements. The pre-determined ideal transfer function which satisfies the FHQ requirements results in that the system response is coherant with the specified requirements so the system is expected to give similar FHQ evaluations with the ideal transfer function. By generalizing this idea to a specified flight envelope and determining the controller parameters as well as the ideal transfer function should result in a flight control law algorithm which gives Level 1 FHQ criteria evaluations within the flight envelope specified earlier. This feature enables the aircraft result in good flying and handling qualities within the flight envelope without the gain scheduling so the system is said to be robust against any loss of flight instrument data such as angle of attack. A pitch rate controller ensures the desired FHQ critera since the evaluations of FHQ responses are mainly focuses on the pitch rate and relatively pitch attitude responses.

1.4 Thesis Outline

In the scope of this thesis longitudinal control with of the F-16 aircraft H_∞ Loop Shaping method is presented with the evaluation of FHQ analysis. Then a comparison study completed with two controllers which are designated H_∞ Loop Shaping controller and the PI controller presented in the technical report of the NASA[14].

Chapter 2 details the specifications of the F-16 aircraft. The aerodynamic calculations are given as well as the propulsion modelling. Equations of motion are presented. The actuator and sensor models are given with the athmosphere model used in the mathematical model of the aircraft. The inputs, states and outputs of the aircraft model are determined and then the algorithms for trim and linearization are presented. The longitudinal aircraft modes, phugoid and short-period mode are defined as well as the linear approximated state-space models are given finally.

Chapter 3 presents the Flying and Handling Qualities. First, classification of different aircrafts are defined since the related FHQ criteria differs each other with respect to different aircraft classes and flight regimes. Then, the reason for determining the FHQ

levels are detailed by relating the Cooper-Harper ratings of the pilot to the relevant FHQ Levels. Suggested FHQ criteria for the evaluation of longitudinal axis are defined and detailed with mathematical and graphical representations.

Chapter 4 defines the mathematical background of the control method of H_∞ Loop Shaping first and then gives brief information about the feedback structures and related transfer functions. It is demonstrated that how this transfer functions affects the closed loop behaviour. The loop shaping approach is detailed by determining how the frequency response should be shaped in order to get good closed loop results in both frequency and time domain. The uncertainty concept is introduced and types of uncertainties are detailed. The demonstration of the uncertainty which will be used for both in the design and analysis sections is made. Finally, the method H_∞ Loop Shaping is presented with 1 degree of freedom and 2 degree of freedom approximations.

Chapter 5 presents the control problem. The choice of controlled parameter of the aircraft is selected and related control architecture is demonstrated. The flight envelope which the aircraft is aimed to have Level 1 FHQ is defined. Open loop responses corresponding to this flight envelope are examined. The PI controller in the NASA technical paper is given for the purpose of comparison study. Last, the optimization problem is defined which purposes to find optimization variables to keep the aircraft in Level 1 FHQ within the selected flight envelope.

Chapter 6 presents the results of this thesis study. First, the results of the optimization is given with the comparison of how optimization changed the primitive results. Then the results of optimized nominal design point is presented as well as the results of the different design points within the flight envelope defined in previous chapter. The performance and stability robustness of the flight control algorithm is examined. Then, finally the results of the comparison study with the longitudinal PI controller is demonstrated.

Chapter 7 interprets the results of this thesis study and details possible further studies based on the subjects adressed in the scope of this thesis study.

2. AIRCRAFT

The mathematical model of the F-16 aircraft which will be used as a plant model for longitudinal flight control law design is modelled in Simulink environment. The model is composed of a couple of submodels as follows:

- Airframe
- Propulsion
- Weight&Balance
- Actuator
- Sensor
- Environment
- Controller

2.1. Airframe

Airframe model involves the calculations of the aerodynamic coefficients, total force and moments as a result of aerodynamic coefficients and contributions from propulsion model and 6 DOF equations of motion model. Also, the mass and dimensional information about the plant model is given in the Table 2.1 below.

Table 2.1 : Mass and dimensional data of the plant model.

Mass Characteristics		Dimensional Information		Surface Deflections	
Weight $[N]$	91188	Wing Span $[m]$	9,144	Horizontal Tail [°]	$\pm$ 25
I_x $[kgm^2]$	12875	Wing Area $[m^2]$	27,87	Ailerons [°]	$\pm$ 21,5
I_y $[kgm^2]$	75674	MAC, $\bar{c}$ $[m]$	3,45	Rudder [°]	$\pm$ 30
I_z $[kgm^2]$	85552	$x_{cg,ref}$	0,35 $\bar{c}$	LEF [°]	25
I_{xz} $[kgm^2]$	1331			Speed Brake [°]	60

2.2.1 Aerodynamic Model

The aerodynamic model of the plant model consists of the wind tunnel test results of the YF-16 [14]. Aerodynamic forces and moments are calculated in the body axis of

the airframe as seen in the equations from 1.2 to 1.7. The aerodynamic data presented here is valid for AoA values from -20° to +90°, AoS values between ±30° and mach numbers from 0.2 to 0.6. The plant model YF-16 also includes a LEF that schedules according to the values of AoA, dynamic pressure and static pressure. The formula for the calculation of deflection of the LEF can be seen in the equation 2.1.

$$\delta_{lef} = 1.38\frac{2s + 7.25}{s + 7.25}\,\alpha - 9.05\,\frac{\bar{q}}{p_s} + 1.45 \tag{2.1}$$

$$\begin{aligned} C_{x,t} = {} & C_x(\alpha, \beta, \delta_h) + \Delta C_{x,\text{lef}}\left(1 - \frac{\delta_{lef}}{25}\right) + \Delta C_{x,sb}(\alpha)\left(\frac{\delta_{sb}}{60}\right) \\ & + \frac{\bar{c}q}{2V_t}\left[C_{x_q}(\alpha) + \Delta C_{x_{q,lef}}(\alpha)\left(1 - \frac{\delta_{sb}}{25}\right)\right] \end{aligned} \tag{2.2}$$

$$\begin{aligned} C_{y,t} = {} & C_y(\alpha, \beta) + \Delta C_{y,\text{lef}}\left(1 - \frac{\delta_{lef}}{25}\right) \\ & + \left[\Delta C_{y,\delta_{a=20^\circ}} + \Delta C_{y,\delta_{a=20^\circ,lef}}\left(1 - \frac{\delta_{lef}}{25}\right)\right]\left(\frac{\delta_a}{20}\right) \\ & + \Delta C_{y,\delta_{r=30^\circ}}\left(\frac{\delta_r}{30}\right) \\ & + \frac{b}{2V_t}\left\{\left[C_{y_r}(\alpha) + \Delta C_{y_{r,lef}}(\alpha)\left(1 - \frac{\delta_{lef}}{25}\right)\right]r\right. \\ & \left. + \left[C_{y_p}(\alpha) + \Delta C_{y_{p,lef}}(\alpha)\left(1 - \frac{\delta_{lef}}{25}\right)\right]p\right\} \end{aligned} \tag{2.3}$$

$$\begin{aligned} C_{z,t} = {} & C_z(\alpha, \beta, \delta_h) + \Delta C_{z,\text{lef}}\left(1 - \frac{\delta_{lef}}{25}\right) + \Delta C_{z,sb}(\alpha)\left(\frac{\delta_{sb}}{60}\right) \\ & + \frac{\bar{c}q}{2V_t}\left[C_{z_q}(\alpha) + \Delta C_{z_{q,lef}}(\alpha)\left(1 - \frac{\delta_{lef}}{25}\right)\right] \end{aligned} \tag{2.4}$$

$$\begin{aligned} C_{l,t} = {} & C_l(\alpha, \beta, \delta_h) + \Delta C_{l,lef}\left(1 - \frac{\delta_{lef}}{25}\right) \\ & + \left[\Delta C_{l,\delta_{a=20^\circ}} + \Delta C_{l,\delta_{a=20^\circ,lef}}\left(1 - \frac{\delta_{lef}}{25}\right)\right]\left(\frac{\delta_a}{20}\right) \\ & + \Delta C_{l,\delta_{r=30^\circ}}\left(\frac{\delta_r}{30}\right) \\ & + \frac{b}{2V_t}\left\{\left[C_{l_r}(\alpha) + \Delta C_{l_{r,lef}}(\alpha)\left(1 - \frac{\delta_{lef}}{25}\right)\right]r\right. \\ & \left. + \left[C_{l_p}(\alpha) + \Delta C_{l_{p,lef}}(\alpha)\left(1 - \frac{\delta_{lef}}{25}\right)\right]p\right\} + \Delta C_{l_\beta}(\alpha)\beta \end{aligned} \tag{2.5}$$

$$
\begin{aligned}
C_{m,t} = {} & C_m(\alpha,\beta,\delta_h)\eta_{\delta_h}(\delta_h) + \mathrm{C_{z,t}}\left(x_{cg,ref} - x_{cg}\right) \\
& + \Delta C_{m,lef}\left(1 - \frac{\delta_{lef}}{25}\right) + \Delta C_{m,sb}(\alpha)\left(\frac{\delta_{sb}}{60}\right) \\
& + \frac{\bar{c}q}{2V_t}\left[C_{m_q}(\alpha) + \Delta C_{m_{q,lef}}(\alpha)\left(1 - \frac{\delta_{lef}}{25}\right)\right] + \Delta C_m(\alpha) \\
& + \Delta C_{m,ds}(\alpha,\delta_h)
\end{aligned} \tag{2.6}
$$

$$
\begin{aligned}
C_{n,t} = {} & C_n(\alpha,\beta,\delta_h) + \Delta\mathrm{C_{n,lef}}\left(1 - \frac{\delta_{lef}}{25}\right) - C_{y,t}\left(x_{cg,ref} - x_{cg}\right)\frac{\bar{c}}{b} \\
& + \left[\Delta C_{n,\delta_{a=20^\circ}} + \Delta C_{n,\delta_{a=20^\circ},lef}\left(1 - \frac{\delta_{lef}}{25}\right)\right]\left(\frac{\delta_a}{20}\right) \\
& + \Delta C_{n,\delta_{r=30^\circ}}\left(\frac{\delta_r}{30}\right) \\
& + \frac{b}{2V_t}\left\{\left[C_{n_r}(\alpha) + \Delta C_{n_{r,lef}}(\alpha)\left(1 - \frac{\delta_{lef}}{25}\right)\right]r\right. \\
& \left. + \left[C_{n_p}(\alpha) + \Delta C_{n_{p,lef}}(\alpha)\left(1 - \frac{\delta_{lef}}{25}\right)\right]p\right\} + \Delta C_{n_\beta}(\alpha)\beta
\end{aligned} \tag{2.7}
$$

where,

$$\Delta C_{x,lef} = C_{x,lef}(\alpha,\beta) - C_x(\alpha,\beta,\delta_h = 0^\circ)$$

$$\Delta C_{y,lef} = C_{y,lef}(\alpha,\beta) - C_y(\alpha,\beta)$$

$$\Delta C_{y,\delta_{a=20^\circ}} = C_{y,\delta_{a=20^\circ}}(\alpha,\beta) - C_y(\alpha,\beta)$$

$$\Delta C_{y,\delta_{a=20^\circ},lef} = C_{y,\delta_{a=20^\circ},lef}(\alpha,\beta) - C_{y,lef}(\alpha,\beta) - \left[C_{y,\delta_{a=20^\circ}}(\alpha,\beta) - C_y(\alpha,\beta)\right]$$

$$\Delta C_{y,\delta_{r=30^\circ}} = C_{y,\delta_{r=30^\circ}}(\alpha,\beta) - C_y(\alpha,\beta)$$

$$\Delta C_{z,lef} = C_{z,lef}(\alpha,\beta) - C_z(\alpha,\beta,\delta_h = 0^\circ)$$

$$\Delta C_{l,lef} = C_{l,lef}(\alpha,\beta) - C_l(\alpha,\beta,\delta_h = 0^\circ)$$

$$\Delta C_{l,\delta_{a=20^\circ}} = C_{l,\delta_{a=20^\circ}}(\alpha,\beta) - C_l(\alpha,\beta,\delta_h = 0^\circ)$$

$$\Delta C_{l,\delta_{a=20^\circ},lef} = C_{l,\delta_{a=20^\circ},lef}(\alpha,\beta) - C_{l,lef}(\alpha,\beta) - \left[C_{l,\delta_{a=20^\circ}}(\alpha,\beta) - C_l(\alpha,\beta,\delta_h = 0^\circ)\right]$$

$$\Delta C_{l,\delta_{r=30^\circ}} = C_{l,\delta_{r=30^\circ}}(\alpha,\beta) - C_y(\alpha,\beta,\delta_h = 0^\circ)$$

$$\Delta C_{m,lef} = C_{m,lef}(\alpha,\beta) - C_m(\alpha,\beta,\delta_h = 0^\circ)$$

$$\Delta C_{n,lef} = C_{n,lef}(\alpha,\beta) - C_n(\alpha,\beta,\delta_h = 0^\circ)$$

$$\Delta C_{n,\delta_{a=20^\circ}} = C_{n,\delta_{a=20^\circ}}(\alpha,\beta) - C_n(\alpha,\beta,\delta_h = 0^\circ)$$

$$\Delta C_{n,\delta_{a=20°,lef}} = C_{n,\delta_{a=20°,lef}}(\alpha,\beta) - C_{n,lef}(\alpha,\beta) - \left[C_{n,\delta_{a=20°}}(\alpha,\beta) - C_n(\alpha,\beta,\delta_h = 0°)\right]$$

$$\Delta C_{n,\delta_{r=30°}} = C_{n,\delta_{r=30°}}(\alpha,\beta) - C_n(\alpha,\beta,\delta_h = 0°)$$

Total aerodynamic forces and moments resulting from the coefficients mentioned above are expressed in the equations from 2.8 to 2.13. The subscript "A" specifies that these forces and moments are resulting from the aerodynamic coefficients.

$$F_{x_A} = Q_c\, S_{ref}\, C_{x,t} \tag{2.8}$$

$$F_{y_A} = Q_c\, S_{ref}\, C_{y,t} \tag{2.9}$$

$$F_{z_A} = Q_c\, S_{ref}\, C_{z,t} \tag{2.10}$$

$$L_A = Q_c\, S_{ref}\, b_{ref}\, C_{l,t} \tag{2.11}$$

$$M_A = Q_c\, S_{ref}\, c_{ref}\, C_{m,t} \tag{2.12}$$

$$N_A = Q_c\, S_{ref}\, b_{ref}\, C_{n,t} \tag{2.13}$$

2.2.2 Equations of Motion

The equations of motion of the aircraft are defined in the body axes as all forces and moments are given in body axes too. Later, velocities defined in three body axes are transformed to wind axes by transfomations[33] in equations 2.14 and 2.15 in order to use wind axes to have information about velocity, and aerodynamic angles AoA and AoS terms in the state vector of the plant. The definitions of axes and aerodynamic angles can be seen in the Figure 2.1 below.

$$C_{s/bf} = \begin{bmatrix} \cos\alpha & 0 & \sin\alpha \\ 0 & 1 & 0 \\ -\sin\alpha & 0 & \cos\alpha \end{bmatrix} \tag{2.14}$$

$$C_{w/s} = \begin{bmatrix} \cos\beta & \sin\beta & 0 \\ -\sin\beta & \cos\beta & 0 \\ 0 & 0 & 1 \end{bmatrix} \tag{2.15}$$

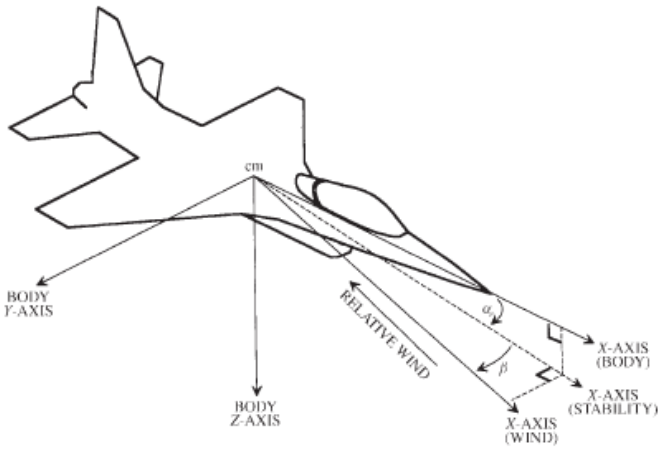

Figure 2.1 : Definitions of axes and aerodynamic angles. [33]

The force equations are defined as in the equations 2.16 to 2.18. Subscripts "A" and "T" determines whether the force in relative axes resulting from aerodynamic or thrust subsystems.

$$\dot{u} = rv + qw - g\sin\theta + (F_{x_A} + F_{x_T})/m \tag{2.16}$$

$$\dot{v} = -ru + pw + g\sin\phi\cos\theta + (F_{y_A} + F_{y_T})/m \tag{2.17}$$

$$\dot{w} = qu - pv + g\cos\phi\cos\theta + (F_{z_A} + F_{z_T})/m \tag{2.18}$$

The angular rates of the aircraft are computed from the equations 2.19 to 2.21.

$$\Gamma\dot{p} = I_{xz}(I_x - I_y + I_z)pq - [I_z(I_z - I_y) + I_{xz}^2]qr + I_z L_A + I_{xz} N_A \tag{2.19}$$

$$I_y\dot{q} = (I_z - I_x)pr - I_{xz}(p^2 - r^2) + M_A \tag{2.20}$$

$$\Gamma\dot{r} = [(I_x - I_y)I_x + I_{xz}^2]pq - I_{xz}(I_x - I_y + I_z)qr + I_{xz} L_A + I_x N_A \tag{2.21}$$

where

$\Gamma = I_x I_z - I_{xz}^2$

The euler angles which are computed from the angular rates using the kinematic equations are denoted in equations 2.22 to 2.24.

$$\dot{\phi} = p + \tan\theta\,(q\sin\phi + r\cos\phi) \tag{2.22}$$

$$\dot{\theta} = q\cos\phi - r\sin\phi \tag{2.23}$$

$$\dot{\psi} = (q\sin\phi + r\cos\phi)/\cos\theta \tag{2.24}$$

Finally navigation equations are calculated as seen as equation 2.25.

$$\begin{bmatrix} \dot{p_N} \\ \dot{p_E} \\ \dot{h} \end{bmatrix} = \begin{bmatrix} c_\theta c_\psi & -c_\phi s_\psi + s_\phi s_\theta c_\psi & s_\phi s_\psi + c_\phi s_\theta c_\psi \\ c_\theta s_\psi & c_\phi c_\psi + s_\phi s_\theta s_\psi & -s_\phi c_\psi + c_\phi s_\theta s_\psi \\ s_\theta & -s_\phi c_\theta & c_\phi c_\theta \end{bmatrix} \begin{bmatrix} u \\ v \\ w \end{bmatrix} \tag{2.25}$$

Then, body axes force equations are transformed into the wind components using equations 2.26 to 2.27 below

$$\dot{V_t} = \frac{u\dot{u} + v\dot{v} + w\dot{w}}{V_t} \tag{2.26}$$

$$\dot{\alpha} = \frac{u\dot{w} - w\dot{u}}{u^2 + w^2} \tag{2.27}$$

$$\dot{\beta} = \frac{V_t\dot{v} - v\dot{V_t}}{V_t\sqrt{u^2 + w^2}} \tag{2.28}$$

Finally, the state vector to be used in the scope of this thesis is obtained as below.

$$x = [V_t\ \alpha\ \beta\ p\ q\ r\ \phi\ \theta\ \psi\ p_N\ p_E\ h]^T$$

2.2 Propulsion

The engine is modelled according to the Technical Paper 1538 published by NASA[14]. Flowcharts based on the value of P_1 and P_3 determines the thrust value generated by the engine. Actual power P_3, is calculated according to the equation 2.29 below.

$$P_3 = \int \frac{1}{\tau_T}(P_2 - P_3)dt \tag{2.29}$$

The engine time constant τ_T and P_2 are calculated depending on the values of $P_1$and P_3 as seen in the equations 2.30 and 2.31.

$$P_2 = \begin{cases} P1 & if\ P_1 < 50\ and\ P_3 < 50 \\ 40 & if\ P_1 < 50\ and\ P_3 \geq 50 \\ 60 & if\ P_1 \geq 50\ and\ P_3 < 50 \\ P1 & if\ P_1 \geq 50\ and\ P_3 \geq 50 \end{cases} \tag{2.30}$$

$$1/\tau_T = \begin{cases} f(P_2 - P_3) & if\ P_1 < 50\ and\ P_3 < 50 \\ 5.0 & if\ P_1 < 50\ and\ P_3 \geq 50 \\ f(P_2 - P_3) & if\ P_1 \geq 50\ and\ P_3 < 50 \\ 5.0 & if\ P_1 \geq 50\ and\ P_3 \geq 50 \end{cases} \tag{2.31}$$

The engine time constant is a function of P_2 and P_3 in some cases as equation 2.31 describes. Following Figure 2.2 shows the relasionship between engine time constant and P_2 and P_3. Finally, engine thrust in x-axis is calculated by using equation 2.32.

$$Th = \begin{cases} Th_{idle} + (Th_{mil} - Th_{idle})\left(\frac{P_3}{50}\right) & if\ P_3 < 50 \\ \frac{Th_{mil}(Th_{max} - Th_{mil})\left(\frac{P_3}{50}\right)}{50} & if\ P_3 \geq 50 \end{cases} \tag{2.32}$$

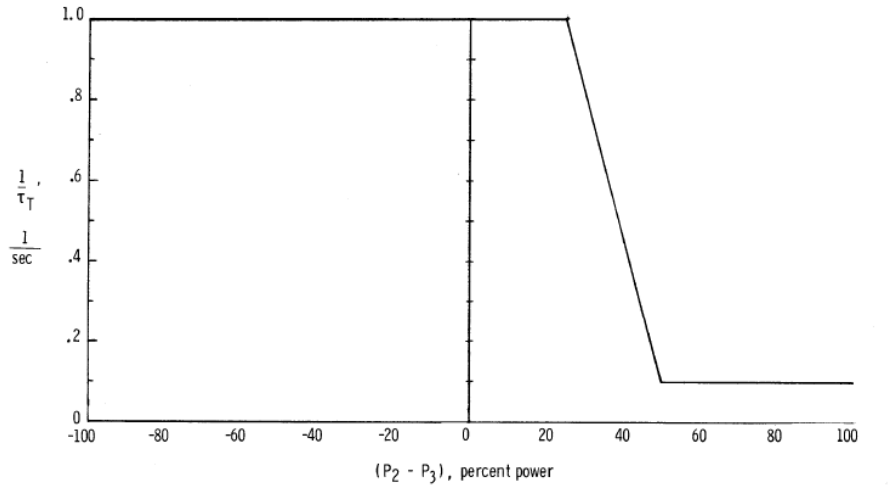

Figure 2.2 : Variation of inverse of thrust time constant with incremental power command. [14]

Also, Figure 2.3 shows the relationship between the reference percent power P_1 and percent throttle travel.

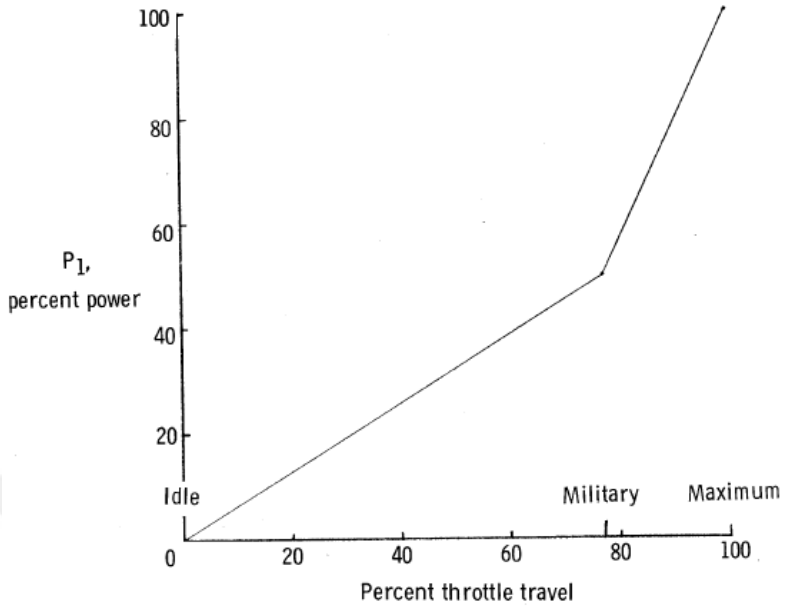

Figure 2.3 : Power variation with throttle position. [14]

2.3 Actuator and Sensors

The mathematical model of the sensors and actuators are modelled as a first order transfer function as follows[14].

$$G_{actuator} = G_{sensor} = \frac{20.2}{s + 20.2}$$

2.4 Environment

Atmosphere model calculates the pressure, temperature, air density, gravity and mach number informations by taking altitude and true air speed as inputs. Equation sets are taken from the US Standard Atmosphere specifications[34]. Different equations are valid for different atmosphere layers. In the scope of this thesis, only equations for troposphere and stratosphere equations are in interest. The temperature value is calculated as in equation 2.33.

$$T(°K) = \begin{cases} T_0 - hL & if\ h < 11000\ m. \\ T_0 - 11000L & if\ h \geq 11000\ m. \end{cases} \quad (2.33)$$

where, L denotes the lapse rate assuming that $0.0065\,°K/m$, T_0 describes the temperature at sea level which is taken as $288.15\,°K$ and h is the altitude in meters. Pressure is calculated as in equation 2.34 below.

$$P(Pa) = \begin{cases} P_0\left(\frac{T}{T_0}\right)^{\frac{g}{LR}} & if\ h < 11000\,m. \\ P_0\left(\frac{T}{T_0}\right)^{\frac{g}{LR}} e^{\frac{g(11000-h)T_0}{RT}} & if\ h \geq 11000\,m. \end{cases} \quad (2.34)$$

where, R denotes the gas constant taken as $287{,}0531\frac{J}{kg}/°K$ for air, P_0 is the sea level air pressure which is $101325\ Pa$ and g is the gravitational acceleration assumed as constant at a value of $9{,}8066\ m/s^2$. Air density is calculated as in the equation 2.35.

$$\rho = \begin{cases} \rho_0\left(\frac{T}{T_0}\right)^{\frac{g}{LR}-1} & if\ h < 11000\,m. \\ \rho_0\left(\frac{T}{T_0}\right)^{\frac{g}{LR}-1} e^{\frac{g(11000-h)T_0}{RT}} & if\ h \geq 11000\,m. \end{cases} \quad (2.35)$$

where, ρ_0 is the sea level air density assumed as $1.225\ kg/m^3$. Then the mach number is obtained by using the equation 2.36.

$$Mach = V/\sqrt{\gamma RT} \quad (2.36)$$

where, γ is the ratio of specific heats assumed as 1.4 and V_t is true air speed. Dynamic pressure is calculated as in equation 2.37.

$$\bar{q} = \frac{1}{2}\rho V_t^2 \quad (2.37)$$

2.5 Trim

Trim can be defined as an equilibrium point of the aircraft model. In order to simulate an aircraft, initial conditions for equations of motion and inputs are needed. Initial conditions resulted from trim condition which can not be defined randomly. Trim defines a static balance which means that if the aircraft remains steady in velocity, altitude and attitude would not change with time so moments and forces are constant

for specified condition. In order to obtain linear matrices for the design of the controller, a trim condition must be found. Then linearization around this trim point will give the linear system matrices. Trim problem is a root finding problem with certain constraints. As mentioned before, trim condition is a steady state condition which involves the derivatives of moment and force terms which are velocity, angle of attack, angle of sideslip, roll rate, pitch rate and yaw rates are equal to zero[33] as in equation 2.38.

$$\dot{V}_t = \dot{\alpha} = \dot{\beta} = \dot{p} = \dot{q} = \dot{r} = 0 \tag{2.38}$$

In addition, steady-state wings level trim condition which is the condition to obtain linear matrices in the scope of this thesis involves the following terms in equation 2.39 to be equal to zero.

$$\phi = \dot{\phi} = \dot{\theta} = \dot{\psi} = p = q = r = 0 \tag{2.39}$$

The trim problem is solved by using Newton Raphson method which is a root-locating problem [35]. The method is an iterative process which terminates when error is lower than the specified criteria. The equation 2.40 is used to guess the next point for the solution of the problem.

$$x_{i+1} = x_i - \frac{f(x_i)}{f'(x_i)} \tag{2.40}$$

Termination criteria can be seen in the equation 2.41.

$$\epsilon = \frac{x_i - x_{i-1}}{x_i} \tag{2.41}$$

For the scope of this trim problem, iterative root-locating problem is terminated successfully when the termination criteria is lower than 10^{-8}. Otherwise, a new guess for the solution of the problem is made by using equation 1.39. The flowchart of the trim algorithm can be seen in the Figure 2.4.

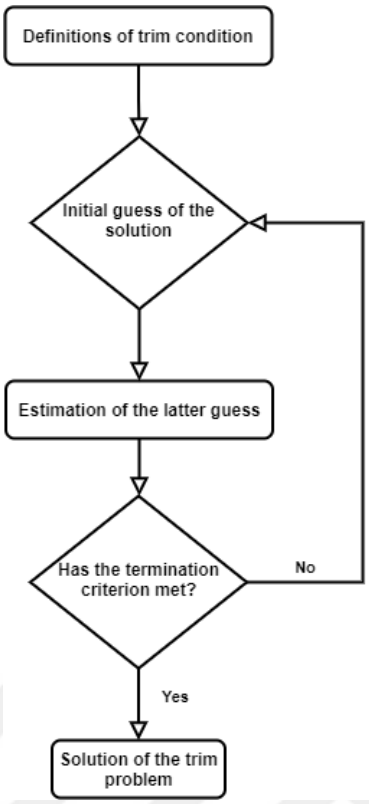

Figure 2.4 : Algorithm for the solution of the trim problem.

In order to determine the trim conditions, altitude and mach values should be defined and then the trim algorithm finds the control surface deflections, throttle level and euler angles of the aircraft which maintains the equlibrium point for the simulation.

2.6 Linearization

The linearization of the nonlinear aircraft model is done by using central difference theorem[36]. It is assumed that the linearized system represents the characteristics of the nonlinear plant near the trim point to be linearized for the small perturbations. In order to apply central difference theorem, one term among states and inputs perturbed small in amplitude positively and negatively then the effect of this perturbation represented by the equation 2.42 below.

$$F_{ij} = \frac{f_i(x_0 + \Delta x_j, u_0) - f_i(x_0 - \Delta x_j, u_0)}{2\Delta \mathrm{x_j}} \tag{2.42}$$

Subscript i describes i^{th}equation is in interest while subscript j interpretes that the j^{th} term of input or state is perturbed at one time only. Only the values of couple equations are calculated in linearization which are $V_t, \alpha, \beta, p, q, r, \phi$ and θ equations represents

the nonlinear behaviour of the aircraft. The resultant linear matrices as a result of linearization is as in equation 2.43.

$$\begin{aligned} \dot{x} &= Ax + Bu \\ y &= Cx + Du \end{aligned} \tag{2.43}$$

while,

$$\begin{aligned} x &= [V_t \quad \alpha \quad \beta \quad p \quad q \quad r \quad \phi \quad \theta]^T \\ u &= [\delta_{th} \quad \delta_e \quad \delta_a \quad \delta_r]^T \\ y &= [V_t \quad \alpha \quad \beta \quad p \quad q \quad r \quad \phi \quad \theta]^T \end{aligned}$$

The equation 1.41 is valid for the motion of the aircraft in all axes. The longitudinal and lateral-directional axes may be decoupled since the effect of perturbations in different axis are negligible. State and input vectors are decoupled as follows in the equation 2.44.

$$\begin{aligned} x_{long} = [V_t \quad \alpha \quad q \quad \theta]^T, \quad x_{lat-dir} = [\beta \quad p \quad r \quad \phi]^T \\ u_{long} = [\delta_{th} \quad \delta_e]^T, \quad u_{lat-dir} = [\delta_a \quad \delta_r]^T \end{aligned} \tag{2.44}$$

The state and control matrices of longitudinal motion can be expressed as follows[2] in equation 2.45.

$$\begin{bmatrix} \dot{V}_t \\ \dot{\alpha} \\ \dot{q} \\ \dot{\theta} \end{bmatrix} = \begin{bmatrix} X_V + X_{T_V}\cos\alpha & X_\alpha & 0 & -g\cos\gamma \\ Z_V - X_{T_V}\sin\alpha & Z_\alpha & V_{T_e} + Z_q & -g\sin\gamma \\ M_V + M_{T_V} & M_\alpha + M_{T_\alpha} & M_q & 0 \\ 0 & 0 & 1 & 0 \end{bmatrix} x + \begin{bmatrix} X_{\delta_{th}}\cos\alpha & X_{\delta_e} \\ -X_{\delta_{th}}\sin\alpha & Z_{\delta_e} \\ M_{\delta_{th}} & M_{\delta_e} \\ 0 & 0 \end{bmatrix} u \tag{2.45}$$

Longitudinal behaviour of the aircraft can be interpreted in to two approaches such as long period(phugoid) and short-period.

2.6.1 Phugoid mode

Long period or the phugoid model is an interchange of the potential and kinetic energies about the equilibrium point.[37] It is assumed that the angle of attack and pitch rate differences are negligible.

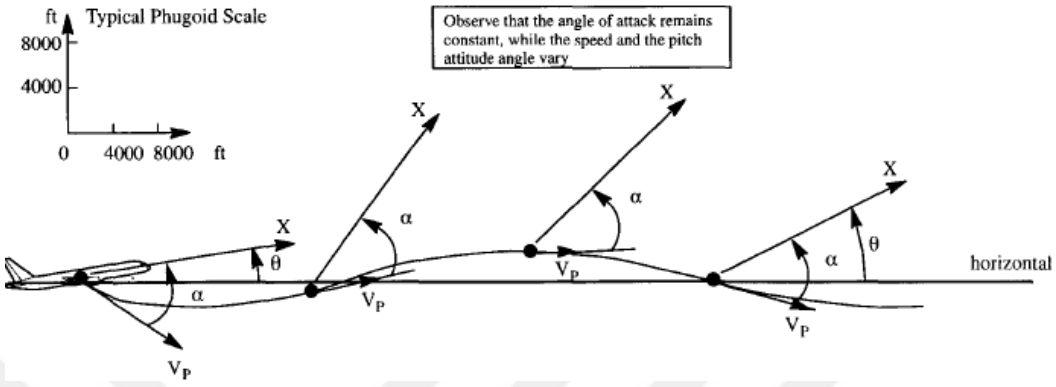

Figure 2.5 : The phugoid mode. [38]

As the pitch attitude angle of the aircraft increases, the aricraft loses speed while gaining altitude, in reverse, as the aircraft loses altitude and thus, increases speed, the pitch attitude angle is decreases as seen as Figure 2.5 above.

Since the angle of attack and pitch rate terms are negligible, the state space matrices for phugoid approximation can be degraded as in equation 2.46.

$$\dot{x}_{ph} = A_{ph}x_{ph} + B_{ph}u_{ph} \tag{2.46}$$

where,

$$x_{ph} = [V_t \quad \theta], u_{ph} = [\delta_{th}], A_{ph} = \begin{bmatrix} D_V & -g \\ -\frac{L_v}{V_0} & 0 \end{bmatrix}, B_{ph} = \begin{bmatrix} D_{\delta_{th}} \\ 0 \end{bmatrix}$$

2.6.2 Short period mode

The speed and attitude change is negligible for short-period approximation. There is an interchange between the angle of attack and pitch rate as seen in the Figure 2.6.

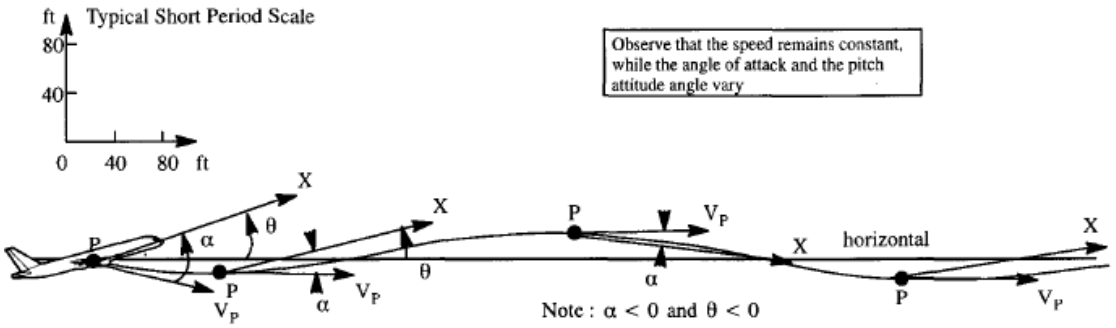

Figure 2.6 : The short period mode. [38]

The angle of attack and pitch rate differences are significant in short-period mode so, the pitch attitude and speed related terms are discarded from the longitudinal state-space eqation to form the short-period sytem as seen in equation 2.47.

$$\dot{x}_{sp} = A_{sp}x_{sp} + B_{sp}u_{sp} \tag{2.47}$$

where,

$$x_{sp} = [\alpha \quad q], u_{sp} = [\delta_e], A_{sp} = \begin{bmatrix} -\frac{L_\alpha}{V_0} & 1 - \frac{L_q}{V_0} \\ M_\alpha & M_q \end{bmatrix}, B_{sp} = \begin{bmatrix} -L_{\delta_e} \\ M_{\delta_e} \end{bmatrix}$$

3. FLYING AND HANDLING QUALITIES

As aircrafts are equipped by Fly-by-Wire flight control systems, a search for the flying qualities of the aircraft has risen up. These flying qualities determines whether the aircraft is capable of performing defined mission tasks succesfully. There are couple of classifications in order to clarify the needs for the aircraft control law design standards. Following subsections defines the needs and divisions of the aircraft and standards for the design.

3.1 Aircraft Classification

In order to evaluate the performance of the aircraft, the mission tasks which the aircraft will perform during its flights needs to be determined. There are couple aircraft classes each focuses a specific purpose. While some aircrafts are aimed to be designed to carry payloads, some aircrafts are designed to perform combat, carry bombs or support the other aircrafts as a fuel tank. These purposes defines the needs for flight control algorithm purposes. For this reason each aircraft for different purposes have its own evaluation criteria to be satisfied. There are four different aircraft classes that comes forward which have common purposes with respect to their mission tasks during their flights as seen as the Table 3.1.

Table 3.1: Airplane classes. [33]

Airplane Classes	
Class I:	Small, light airplanes.
Class II:	Medium weight, low-to-medium-maneuverability airplanes.
Class III:	Large, heavy, low-to-medium-maneuverability airplanes.
Class IV:	High-maneuverability airplanes.

Class I aircrafts defined as the small light airplanes such as light utility, primary trainer and light observation. Class II aircraft are known as medium weight, low-to-medium-maneouverability airplanes such as antisubmarine, reconnaissance, tactical bomber and heavy attack. Class III airplanes which are large heavy, low-to-medium maneouverability aircrafts can be sampled as heavy bomber, heavy transport/cargo/tanker and trainer for Class III and last high maneouverability aircrafts

such as fighter-inceptor, attack and observation aircrafts are groupped as Class IV aircraft [9]. The purpose of this thesis is to design a control algorithm law for F-16 aircraft, thus the Class IV aircraft standards will be followed throughout in this thesis.

3.2 Flight Phase Categories

The term “flight phase” is a significant feature for the definition of the flight handling quality level description. The aircraft performs different tasks during its mission from take-off to landing. Every different task needs different desired characteristics and relatively different definiton of satisfactory response. In order to evaluate the performance of the aircraft during different mission tasks, numerous flight phases are degraded to three flight phase categories based on their similar flight characteristics. The nonterminal flight phases such as air-to-air combat(CO), aerial recovery(AR), reconnaissence(RC) and In-flight refuelling(reciever)(RR) which have common characteristics of requirement of maneouvering, precision tracking or precise path-control are groupped as Category A. Other nonterminal flight phases such as cruise(CR), loiter(LO), descend(D) and climb(CL) which do not require precision tracking however they require accurate flight-path control which uses gradual maneouvers are groupped as Category B. Last, terminal flight phases such as take-off(TO), approach(PA), landing(L) and waveoff/go-around(WO) which require accurate flight-path control using gradual maneouvers are groupped as Category C flight phase category.

3.3 Levels and Qualitive Suitability of Flying Qualities

In order to clarify flying qualities, a well accepted scale in flight and simulation tests which named Cooper-Harper Handling Qualities Ratings are taken into the consideration as a guideline for definitions of desired and adequate performance of the aircraft[10]. The term “Handling Qualities” are defined as the qualities or characteristics of an aircraft which affects the ease and precision of which the pilot to perform the tasks required in support of an aircraft role[11]. According to the Cooper-Harper Ratings, the quality of the flight during the mission scenerio is rated ona a scale from 1-10 as seen as the Table 3.2.

Table 3.2: Examples of pilot rating scales. [10]

Cooper Rating	Cooper Descriptor	ψ Value	ψ Descriptor
1	Excellent, Includes Optimum	1.00	Excellent Handling Qualities
2	Good, Pleasant to Fly	3.70 3.71	Good Handling Qualities Pleasant Handling Qualities
3	Satisfactory, but with some Mildly Unpleasant Characteristics	5.66	Some Mildly Unpleasant Characteristics
4	Acceptable, but with Unpleasant Characteristics	6.04	Improvement is Requested
5	Unacceptable for Normal Operation [Primary Mission Accomplished? "Doubtful"]	7.08	Pilot Compensation Required for Acceptable Performance in Mission is too High
6	Acceptable for Emergency Conditions Only [Primary Mission Accomplished? "Doubtful"]	7.48	Requires Sunstantial Pilot Skill and Attention to Retain Control and Continue Mission
7	UnacceptableEven for Emergency Condition [Can be Landed? "Doubtful"]	8.00	Mandatory Improvement Required
8	Unacceptable - Dangerous [Can be Landed? "No"]	9.00	Nearly Uncontrollable
9	Unacceptable - Uncontrollable [Can be Landed? "No"]	10.00	Uncontrollable
10	Motions Possibly Violent Enough to Prevent Pilot Escape	-	(No ψ Equivalent)

These 10 rating is associated with 3 qualitive degrees of flight handling. First three cooper levels describes “Satisfactory” level while the next three levels which are the cooper ratings 4, 5 and 6 means the handlig quality of the aircraft is “Acceptable”. Finally the cooper ratings 7, 8 and 9 describes the “Controllable” aircraft response while cooper rating 10 means the control will be lost during some portion of required operation as seen as the Table 3.3 below.

Also these three proficiency levels of the flight handling qualities can be related with the levels of handling qualities as Level 1 means “Satisfactory”, Level 2 describes “Acceptable” and last, Level 3 indicates “Controllable” aircraft responses. However, it should be noted that Level 3 may not be identified as safe. The controllability is questionable for the cooper harper ratings of 8 and 9 [9]. Satisfactory aircraft response defines the good enough respsonse without improvement which is best category [11]. The situation which requires some increased pilot workload despite the flying qualities are adequate to complete the mission is called “Acceptable”. Last, “Controllable” flying qualities defined as there is a need for excessive pilot workload or the mission effectivenes is inadequate however the aircraft is controllable during the mission flight

phase [9]. These three handling quality levels will be used as a criteria for the control law algorithm design performance.

Table 3.3: Relationships between pilot ratings and flying qualities levels. [33]

Aircraft Characteristics	Demands on Pilot in Selected Task or Required Operation	Pilot Rating	Flying Qualities Level
Excellent; highly desirable	Pilot compensation not a factor for desired performance	1	1
Good; negligible deficiencies	as above	2	
Fair; some mildly unpleasant deficiencies	Minimal pilot compensation required for desired performance	3	
Minor but annoying deficiencies	Desired performance requires moderate pilot compensation	4	2
Moderately objectionable deficiencies	Adequate performance requires considerable pilot compensation	5	
Very objectionable but tolerable deficiencies	Adequate performance requires extensive pilot compensation	6	
Major deficiencies	Adequate performance not attainable with maximum tolerable pilot compensation controllability not in question	7	3
Major deficiencies	Considerable pilot compensation required for control	8	
Major deficiencies	Intense pilot compensation required to retain control	9	
Major deficiencies	Control will be lost during some portion of requested operation	10	

3.4 Selected Flight Handling Qualities Criteria

The sections above describes the class of the aircraft, flight phases and flight handling quality for which the aircraft will be evaluated in compliance with. There are also certain criteria which needs to be clarified depending on the response type of the to be designed flight control law. In the scope of this thesis, rate response of the aircraft will be controlled so consistent flight handling qualities need to be selected in order to evaluate the performance of the aircraft. The Table 3.4 below, sets a group of criteria to be clarified with respect to response type of the aircraft.

Since the short-period behaviour of the aircraft to be controlled in the scope of this thesis by controlling the pitch rate of the aircraft, it is best to choose bandwidth and dropback criteria as design criteria for the flight control law algorithm. These criteria will be detailed more in the following sections.

Table 3.4: Roadmap for short-term pitch response criteria. [10]

RESPONSE-TYPE	SPECIFICATION AND DESIGN CRITERIA	CRITERIA FOR DESIGN GUIDANCE ONLY	CRITERIA NOT ACCEPTABLE
Conventional	Bandwidth (or CAP) Plus Dropback	ω_{sp} T_{θ_2}, Neal Smith Gibson Nichols-Chart Boundaries	TPR
Rate or RCAH	Bandwidth Plus Dropback	CAP ω_{sp} T_{θ_2}, Neal Smith Gibson Nichols-Chart Boundaries TPR	None
Attitude-Augmented (including ACAH and GCGH)	Bandwidth	None	Dropback CAP ω_{sp} T_{θ_2}, Neal Smith Gibson Nichols-Chart Boundaries

3.4.1 Bandwidth criteria

The pitch attitude response for the longitudinal channel of the aircraft shall satisfy the limits seen in the Figure 3.1 below.

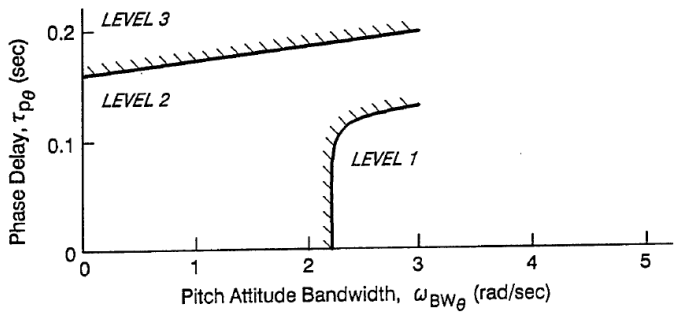

Figure 3.1 : Pitch attitude bandwidth criteria evaluation template. [10]

The bandwidth ω_{BW_θ} and phase delay τ_{p_θ} are calculated from the frequency response of the pitch attitude bandwidth response of the aircraft. A sample frequency response can be seen in the Figure 3.2 along with the bandwidth definitions of phase and gain.

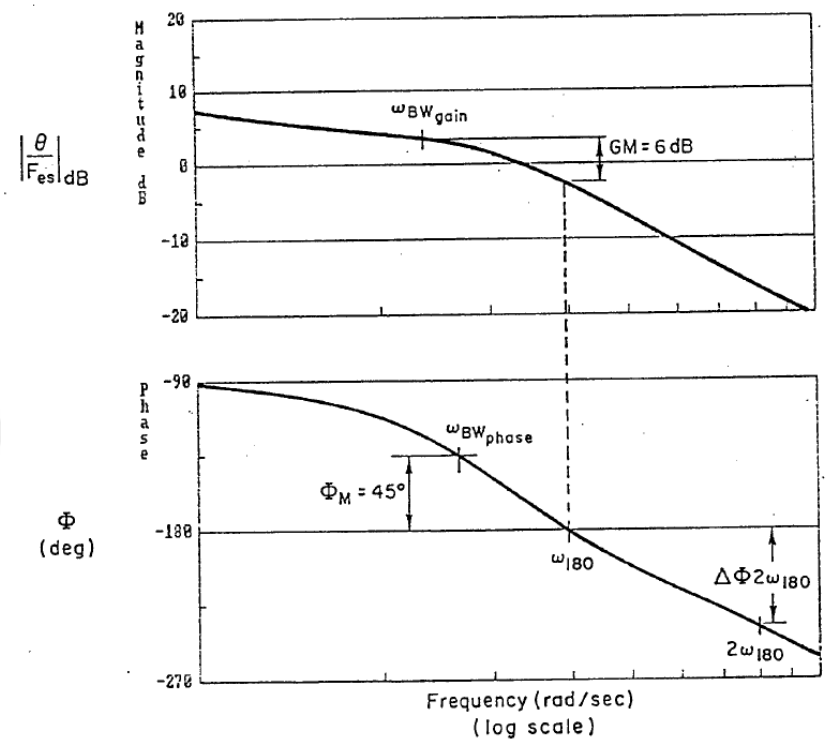

Figure 3.2 : Definitions of bandwidth and phase delay terms. [10]

According to the bandwidth criteria, for rate response type of aircraft, accepted bandwidth is the lesser of $\omega_{BW_{gain}}$ or $\omega_{BW_{phase}}$. Formula of the phase delay is given in Equation 3.1 below.

$$\tau_p = \frac{\Delta\phi_{2_{w_{180}}}}{57.3\omega_{180}} \tag{3.1}$$

In order to satisfy Level 1 flying handling quality, the pitch attitude response of the aircraft should satisfy at least 2.2 rad/sec of bandwidth and maximum of 0.12 sec phase delay. The respective plot for which the response of the aircraft will be evaluated is given in the Figure 3.3 below.

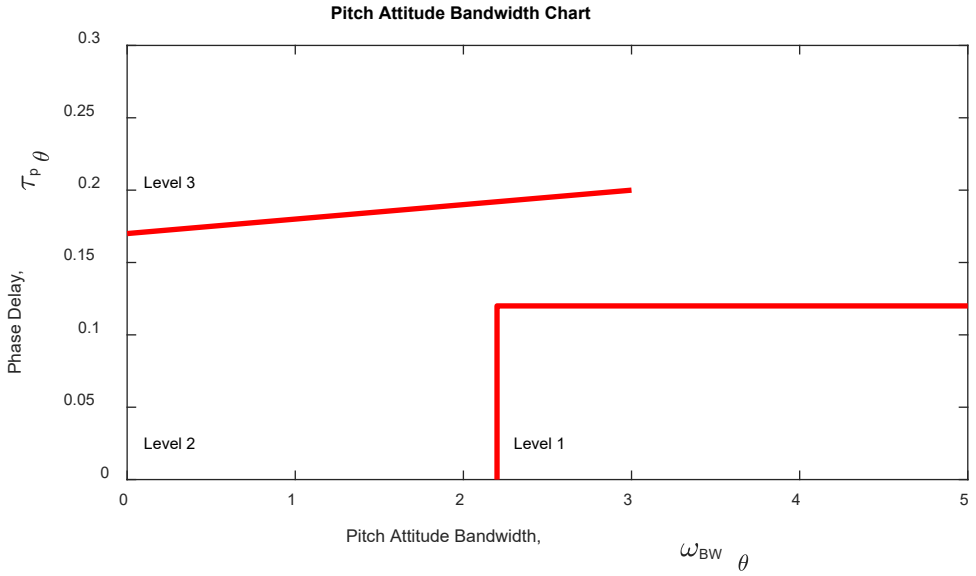

Figure 3.3 : Pitch attitude bandwidth criteria FHQ level limits.

3.4.2 Control anticipation power (CAP)

Control Anticipation Power is defined as the ratio of initial pitching acceleration to steady state normal acceleration as seen in the equation 3.2 where the last expression is an approximation for aircraft with negligible control system dynamics and tail effect for which the term $\frac{V}{g}\frac{1}{T_{\theta_2}}$ can be approximated to n/α [9].

$$CAP = \frac{\ddot{\theta}}{\Delta n_{z_{ss}}} = \frac{\omega_{sp}^2}{\frac{V}{g}\frac{1}{T_{\theta_2}}} g^{-1} sec^{-2} \tag{3.2}$$

Also the equation 3.3 below gives the relationship between the parameter n/α and C_{L_α} [9].

$$\frac{n}{\alpha} = \frac{C_{L_\alpha}\bar{q}S}{W} \tag{3.3}$$

Appereantly, CAP parameter specifies the characteristics of the short period dynamics as it sets limits for short period natural frequency and paramater n/α respectively. This limits can be seen in the Figure 3.4 below.

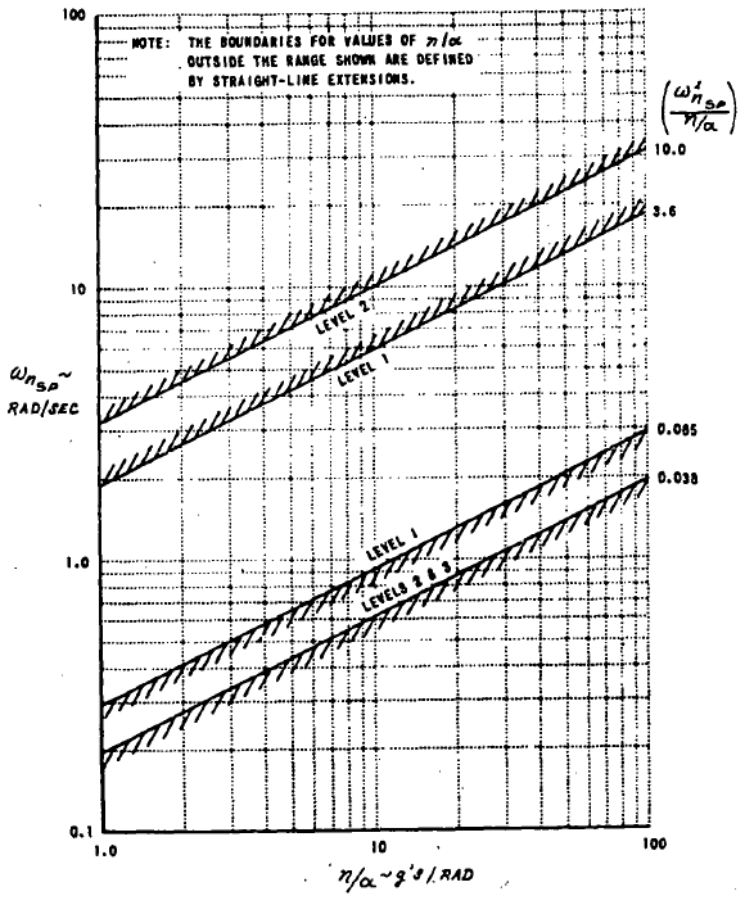

Figure 3.4 : Short-period frequency requirements – Category B flight phases. [8]

3.4.3 Dropback criteria

Dropback criteria evaluates the aircraft response in time domain. A simple step input is the best way to present and study handling information which gives a time response history with an excellent graphical form. Although the pure step input is not applicable in practice, it gives great insight for aircraft characteristics [16].

A couple of relationships between pitch attitude, flight path angle, flight path angle rate, velocity, g and pitch rate can be seen from the Figure 3.5. From this figure it can be easily understood that the angle of attack is the difference between the pitch attitude and flight path angle, there is a delay in both pitch attitude and flight path angle responses. The delay difference between these two metrics is an important parameter for longitudinal flight characteristics which can be shown as in equation 3.4 and equation 3.5

$$T_{\theta 2} = \frac{DB}{q_{ss}} + 2\zeta_{sp}\omega_{sp} \tag{3.4}$$

where,

$$t_\gamma = 2\zeta_{sp}\omega_{sp} \tag{3.5}$$

By rearranging the formula for time lag constant between attitude Θ and flight path γ the parameter in equation 3.6 "the attitude dropback ratio" which is significant for dropback criteria obtained.

$$\frac{DB}{q_{ss}} = T_{\theta 2} - 2\zeta_{sp}\omega_{sp} \tag{3.6}$$

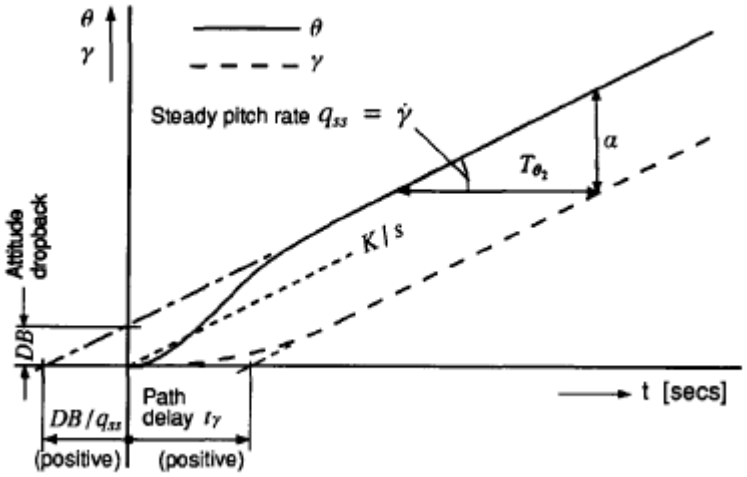

Figure 3.5 : Detailed atittude and flight path relationships. [16]

Different responses related to the longitudinal characteristics of the aircraft can be seen in the Figure 3.6 below.

There is a couple observations for this criteria known as Gibson Criteria as follows [16]

- Negative and unpredictable reponse for both tracking and flight path related with the negative dropback
- Fine tracking is associated with the attitude dropback ratio between 0 to 0.25 commented as "The nose follows the stick".
- "Bobbling", "continuous oscillations" are related with the increasing attitude dropback.

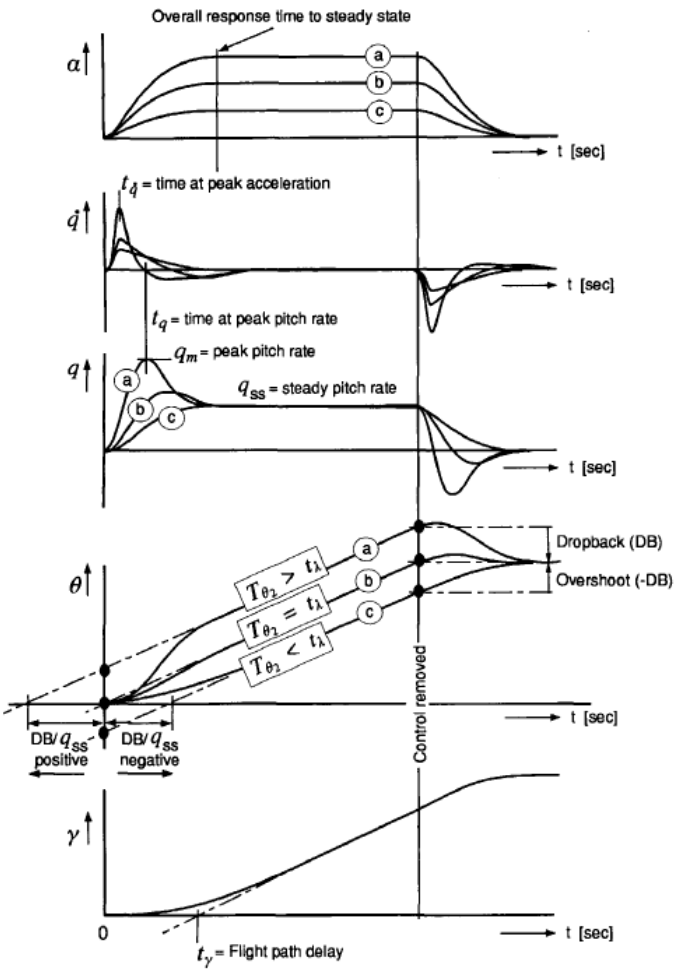

Figure 3.6 : Generic short period pitch time responses. [16]

There is different approaches for dropback criteria which offered by Gibson[16], a MIL-STD-1797A mentions a modified version of this criteria. It is ideal to use the dropback criteria without affection of time delay as it is a measure of mid frequency abrubtness[9]. The only way to get negative attitude dropback ratio is to have large flight path delay as it can be seen in the Eq above. The definition of the standard refuses to use the flight path delay as it reduces the attitude dropback ratio without affecting the pitch rate overshoot[9]. The definition in MIL-STD-1797A will be used as a design guide and evaluation criteria for the longitudinal control law algorithm to be designed throughout this thesis.

The purpose is to keep the attitude dropback ratio and pitch rate overshoot values within the area specified as “satisfactory” in the Figure 3.7 below.

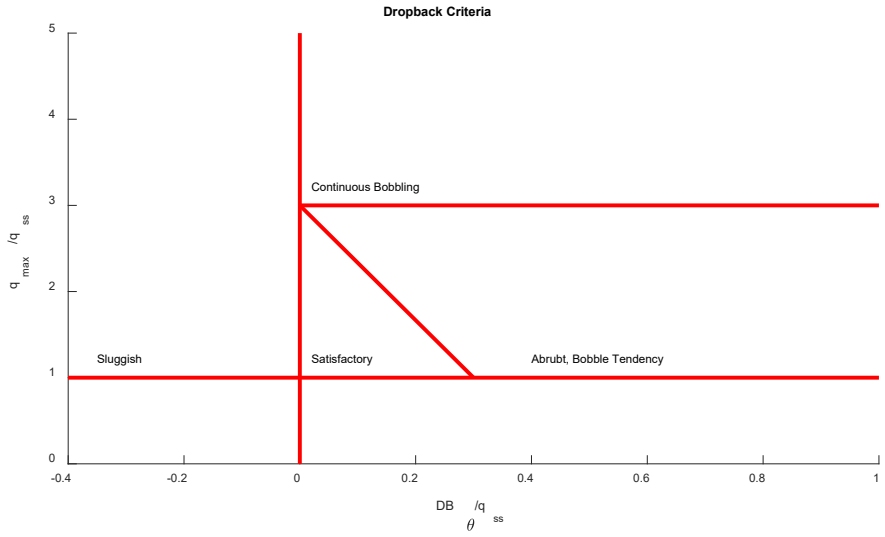

Figure 3.7 : Dropback criteria FHQ level limits.

Also military standards[8] sets limits of the effective time delay in pitch response. Effective time delay determined by a point where a tangent line to the maximum slope of pitch rate response crosses the time axis as seen as in the Figure 3.8 below.

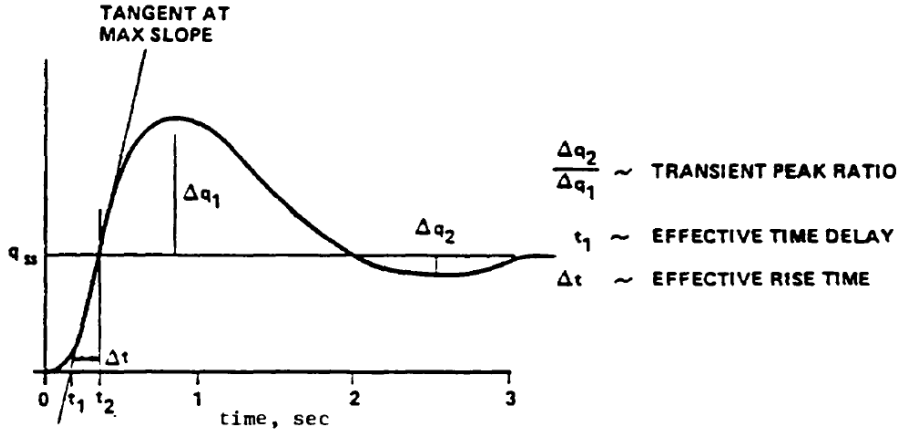

Figure 3.8 : The definition of effective time delay criteria. [9]

The values which defines the bounds of effective time delay criteria is given in the Table 3.5 below.

Table 3.5: Effective time delay FHQ level limits.

Level	Effective Time Delay
1	$t_1 \leq 0.12\ sec$
2	$0.12\ \text{sec} < t_1 \leq 0.17\ sec$
3	$0.17\ sec < t_1$

4. H INFINITY LOOP SHAPING

In this chapter, linear algebra basics with H norms are explained. Then, the feedback control and its properties are mentioned along with the open-loop response and how to shape the open loop frequency response. Definition and classifications of different type of uncertainties are defined. Last, design procedures of H_∞ Loop Shaping controller with different approaches are mentioned with their advantages.

4.1 H_2 and H_∞ Norms

In order to determine the size of any variable x which may be scalar signal, a vector, a matrix or a system transfer function, different types of norms can be defined[31]. A norm of the variable $\boldsymbol{x}$ is any real number which satisfies the following criteria.

i) $\|x\| \geq 0$

ii) $\|x\| = 0 \Leftrightarrow x = 0$

iii) $\|ax\| = |a|\|x\|, \quad \forall a \epsilon R$

iv) $\|x + y\| \leq \|x\| + \|y\|,$

Achieving the certain performance criteria besides providing the internal stability is the most important purpose of the design of a control system[32]. The size of the related signals are a way to show the performance of the control system. Norm of a signal is used to determine the size of the related signal. A simple 1-norm of a time domain scalar function can be seen in the equation 4.1 below.

$$\|x(t)\|_1 = \int_{-\infty}^{\infty} |x(t)| dt \tag{4.1}$$

The 2-norm of a time-domain scalar function which is related to the energy[25] can be seen in the equation 4.2.

$$\|x(t)\|_2 = \left[\int_{-\infty}^{\infty} |x(t)|^2 dt\right]^{\frac{1}{2}} \tag{4.2}$$

According to the definition in the equation 5.2, a p-norm can be defined as in the equation 4.3.

$$\|x(t)\|_p = \left[\int_{-\infty}^{\infty} |x(t)|^p dt\right]^{\frac{1}{p}} \tag{4.3}$$

So, an ∞-norm can be defined as in the equation 4.4.

$$\|x(t)\|_\infty = \sup_t |x(t)| = \lim_{t\to\infty} [|x(t)|^p]^{\frac{1}{p}} \tag{4.4}$$

The definitions of the norms on the time-domain scalar functions can be extended to definitions of norms of the scalar sytem functions as in the equation 4.5 and 4.6 which may be named as H_2 and H_∞ norms .

$$\|G\|_2 = \sqrt{\frac{1}{2\pi}\int_{-\infty}^{\infty} |G(j\omega)|^2 d\omega} \tag{4.5}$$

$$\|G\|_\infty = \sup_\omega |G(j\omega)| \tag{4.6}$$

The H_∞ norm defines the distance from the origin to the farthest point of the transfer function G in the nyquist plane as well as it means the maximum value on the Bode magnitude plot of G[32].

The term "Singular Value Decomposition" (SVD) is a beneficial tool in matrix analysis[30]. The corresponding singular values is a good measures of the size of the matrix. Assuming , $A \in \mathbb{R}^{\boldsymbol{mxn}}$, there exists unitary matrices in equation 4.7 and 4.8 below.

$$U = [u_1, u_2, \dots, u_m] \in \mathbb{R}^{mxm} \tag{4.7}$$

$$V = [v_1, v_2, \dots, v_n] \in \mathbb{R}^{nxn} \tag{4.8}$$

where $u_1, u_2, \dots, u_m$ are vectors in $\mathbb{R}^{mx1}$ and $v_1, v_2, \dots, v_n$ are vectors in $\mathbb{R}^{nx1}$. These U and V matrices satisfiy the equation 4.9.

$$A = U\Sigma V^*, \Sigma = \begin{bmatrix} \Sigma_1 & 0 \\ 0 & 0 \end{bmatrix} \tag{4.9}$$

where,

$$\Sigma_1 = \begin{bmatrix} \sigma_1 & 0 & \dots & 0 \\ 0 & \sigma_2 & \dots & 0 \\ \vdots & \vdots & \ddots & \vdots \\ 0 & 0 & \dots & \sigma_p \end{bmatrix}$$

and,

$\sigma_1 > \sigma_2 > \cdots > \sigma_p \geq 0, p = \min\{m, n\}$

Here, σ values are called singular values of the matrix A. Maximum and minimum values of the singular values are defined in equation 4.10 and 4.11 respectively.

$$\overline{\sigma}(A) = \sigma_{max}(A) = \sigma_1 \tag{4.10}$$

$$\underline{\sigma}(A) = \sigma_{min}(A) = \sigma_p \tag{4.11}$$

4.2 Feedback Control and Loop Shaping

A basic feedback control system architecture is seen in the Figure 4.1 below. Here, r defines reference input signal, d is the disturbance input, y is the output, n is noise input, y_m is the measured output while K represents controller, G is plant and last, G_d defines the disturbance system. The input to the controller K is $r - y_m$ where $y_m = y + n$, so the input to the plant is given in the equation 4.12.

$$u = K(s)(r - y - n) \tag{4.12}$$

The purpose of control is the generate u signal which will minimize the control error e in equation 4.13 while noise signal is not taken into account.

$$e = r - y \tag{4.13}$$

The output of the system can be written as in equation 4.14.

$$y = G(s)u + G_d(s)d \tag{4.14}$$

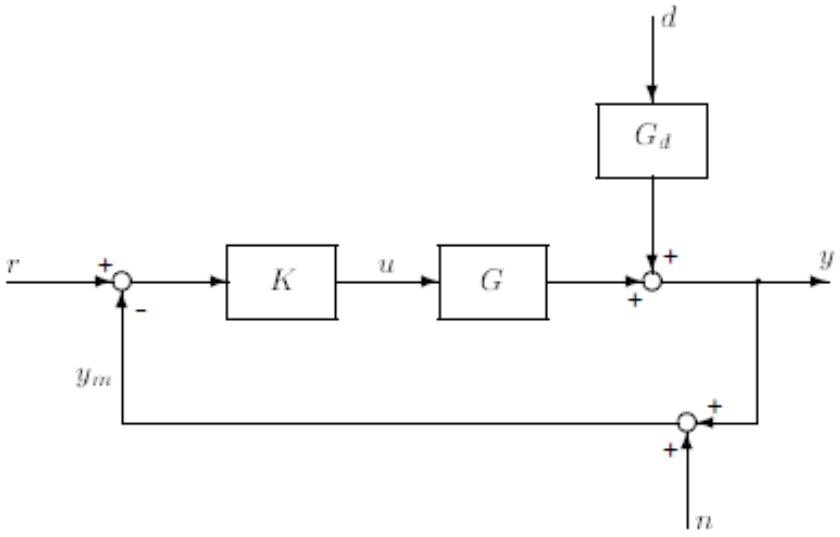

Figure 4.1 : Block diagram of one-degree-of freedom feedback control system. [32]

Reshaping the equation above gives more detailed equation 4.15.

$$\begin{aligned} y &= GK(r - y - n) + G_d d \\ (I + GK)y &= GKr + G_d d - GKn \end{aligned} \tag{4.15}$$

And the closed loop response of the sytem seen in the equation 4.16.

$$y = GK(I + GK)^{-1}r + (I + GK)^{-1}G_d d - GK(I + GK)^{-1}n \tag{4.16}$$

Here, $L = GK$ denotes the "loop transfer function". A couple of definitions can be made according to the loop transfer function. First, sensitivity function defined as in equation 4.17.

$$S = \frac{I}{I + GK} = \frac{I}{I + L} \tag{4.17}$$

Sensitivity function is a measure of disturbance rejection as it is related to the disturbance input in equation 4.16 above. In order to have a good disturbance rejection characteristics, sensitivity function should have low gain values at lower frequencies. In other words, largest singular value of the sensitivity function $\bar{\sigma}(S) < 1$ over a frequency range where disturbance effects are meaningful[3]. Second, complementary sensitivity function is defined as in equation 4.18.

$$T = \frac{GK}{I + GK} = \frac{L}{I + L} \tag{4.18}$$

The complementary sensitivity function relates the closed loop system output to the reference input thus it is related with the tracking of the reference signal. In order to have a good reference tracking performance, complementary sensitivity function should have a value of 1 at lower frequencies. Moreover, the complementary sensitivity function is a measure of how noise affects the closed loop output so at higher frequencies, complementary sensitivity function should have low gain values in frequency response.

When the equations 4.17 and 4.18 are combined together, it can be seen that the sensitivity function and complementary sensitivity function are inversely proportional to each other at the specified frequency. The relationship can be seen in the equation 4.19.

$$S + T = I \tag{4.19}$$

So, there are typical design specifications based od sensitivity and complementary sensitivity functions such $|S(jw)| \ll 1$ at low frequencies and $|T(jw)| \ll 1$ at high frequencies[39].

To sum up the discussion above, in order to have a good disturbance rejection characteristics, sensitivity function should have lower gain values at lower frequencies. The only way to accomplish this is the having loop gain transfer function higher gains at low-frequency range such as $(-\infty, \omega_l)$ in equation 4.20.

$$\underline{\sigma}(L) = \underline{\sigma}(GK) \gg 1 \tag{4.20}$$

In the other hand, complementary sensitivity function should have low magnitudes in order to satisfy noise reduction. If the singular values of loopgain transfer function goes to zero, the magnitude of complementary sensitivity function gets smaller too. Thus, for a high-frequency range (ω_h, ∞), loop transfer fuction should have low gains as in equation 4.21.

$$\overline{\sigma}(L) = \overline{\sigma}(GK) \ll 1 \tag{4.21}$$

The relations in equation 4.20 and 4.21 can be related to the desired loop shape in the Figure 4.2 below. The procedure of loopshaping design is to add dynamic control networks in front of the known plant in order to satisfy the properties such as gain margin, phase margin, bandwidth and steady state error by analysing the loop shape $L(j\omega)$ [31] .

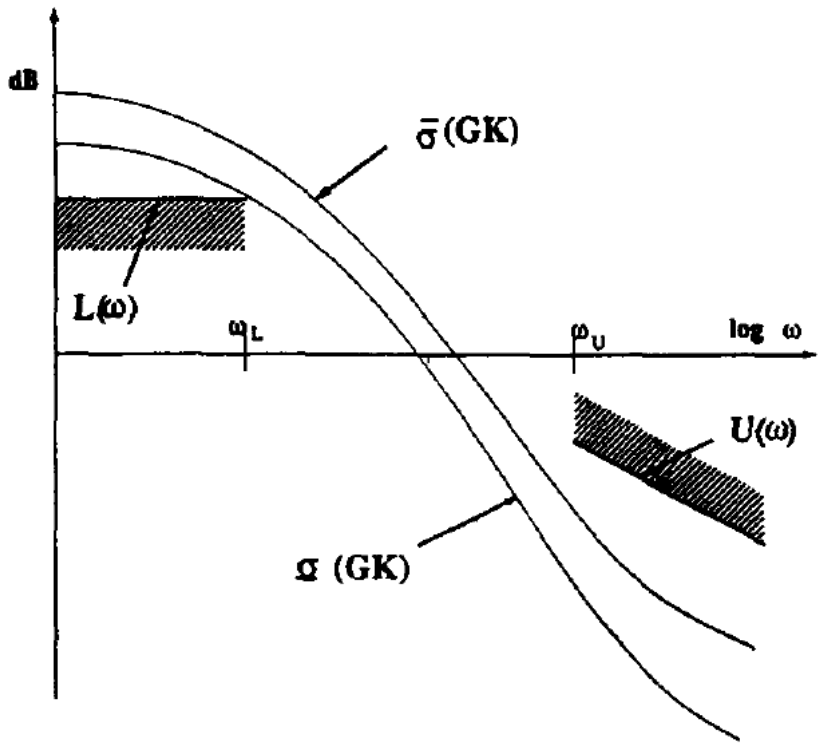

Figure 4.2 : Singular values of the open loop-transfer function. [23]

The loop shaping approach aims to shape the frequency response of the open loop transfer function with the controller K to reach the closed loop system design requirements.

4.3 Uncertainties

A control system is said to be robust if it is insensitive to differences between the model of the system used for designing the controller and the actual system[32]. The differences between the model and the actual system are named as model/plant mismatch or model uncertainty. An uncertainty set is the mathematical representation of model uncertainty. A system is said to be robustly stable if the system maintains its stability under all uncertainty set that defined. A system is said to have robust performance if the performance criteria is met for all the plants in uncertainty set.

Uncertainy of the plant model can have a variety of origins such as[32];

- The parameters in the linear model that are only known approximately
- The parameters in the linear model that changes because of nonlinearity or due to operating conditions.
- Measurement errors
- Eventhough the model is so detailed, it is preferred to work with a simpler model that has low order. Then the neglected dynamics are represented as uncertainty.
- The controller is implemented in a different form that the one has obtained.

A variety of the uncertainty sources may be groupped into three categories as below.

- **Parametric Uncertainty:** The structure of the model is known however some parameters remain uncertain. In order to model this type of uncertainty, parameters are bounded between their maximum and minimum values which is valid for most pyhsical systems[31].
- **Neglected and Unmodelled Dynamics Uncertainty:** The model is uncertain because of the missing dynamics, the lack of the knowledge of the physical process. Any kind of system will likely to have this kind of uncertainty. Structural modes with unpredictible dynamics which appear in high frequencies may be given as an example for airframe systems[31].
- **Lumped Uncertainty:** A couple of uncertainty sources of parametric/unmodelled dynamics combined into a lumped uncertainty of a chosen structure. The lumped uncertainty which is easy to be modelled in

frequency domain[32] is described as a multiplicative uncertainty form as seen as Figure 4.3 and the formula is in equation 4.22.

$$G_p(s) = G(s)\big(1 + \omega_I(s)\Delta_I(s)\big); \qquad |\Delta_I(j\omega)| \leq 1 \ \forall\omega \tag{4.22}$$

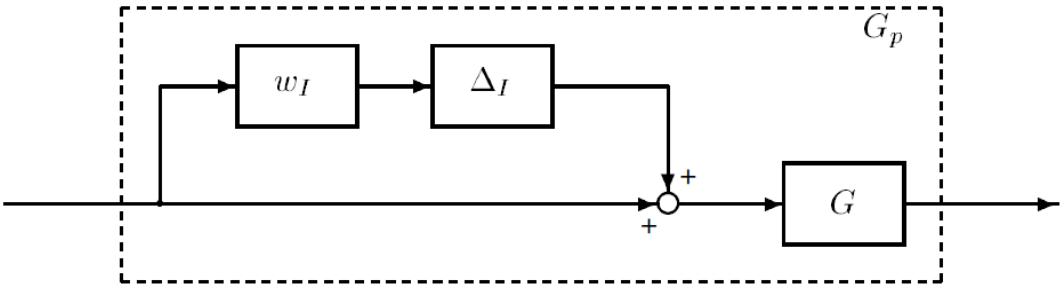

Figure 4.3 : Plant with multiplicative uncertainty. [32]

Gain and phase margins are poor measures of stability robustness for single-loop systems and multivariable systems[28]. A novel approach tests the robustness based on the "worst case" scenario for uncertain plants.

Nichols plot can be very useful when analysing the stability of the system. The open-loop response between the actuator and the error signal of the system formed by breaking the loop at the specified point in the Figure 4.4 should avoid a specific region in the Nichols plot.

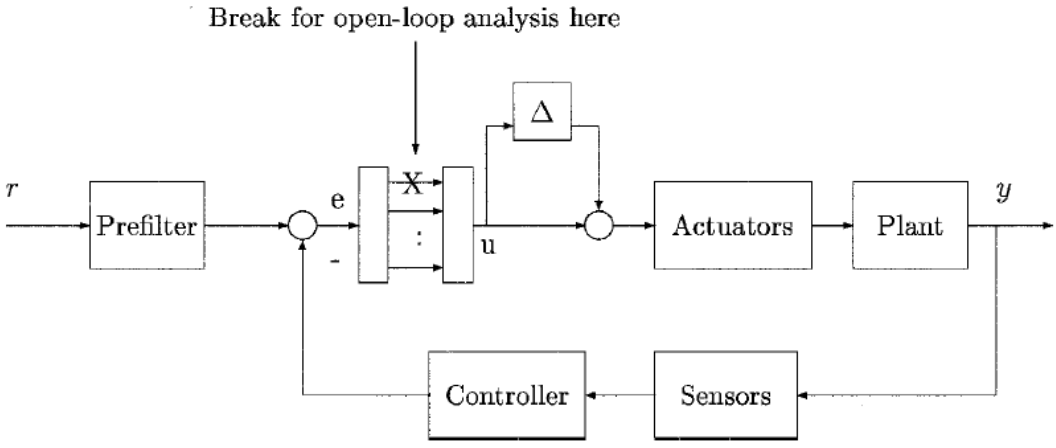

Figure 4.4 : Breaking the loop for open loop analysis. [28]

The exculison regions are seen in the Figure 4.5 below.

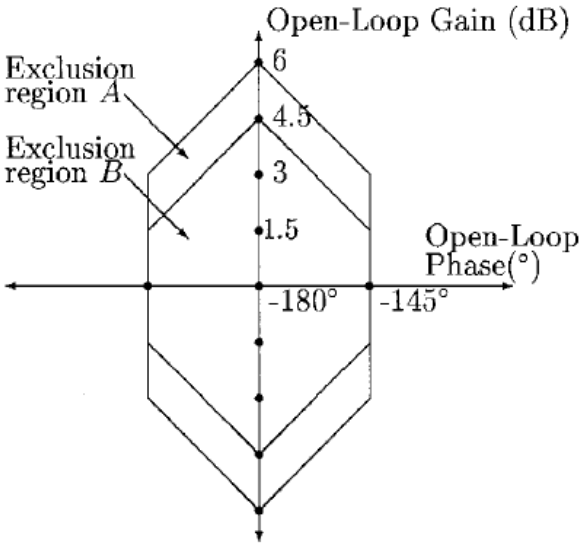

Figure 4.5 : Nichols plane exclision regions. [28]

When dealing with multivariable plants and large number of uncertainties, analysing every combination of uncertainty for each loop requires a vast amount of computational time. The stability robustness is guaranteed with the identification of the worst-case sceneario. The elliptical region in the Figure 4.6 can be represented as in equation 4.23 below.

$$\frac{|L(j\omega)|_{dB}^2}{G_m^2} + \frac{(\angle L(j\omega) + 180)^2}{P_m^2} = 1 \tag{4.23}$$

where,

$G_m = 20\ log_{10}(a + r)$, and $P_m = \cos^{-1}(\frac{a^2 - r^2 + 1}{2a})$

$L(j\omega)$ defines the open loop transfer function while G_m and P_m determines gain and phase margins respectively. The term a and r represents the centre and radius of a circle respectively in Nyquist plane which the exculusion zone in Nichols plane was mapped. Exclusion region A provides gain and phase margins of $\pm 6dB / \pm 36.87°$ while exclusion region B provides $\pm 4.5dB / \pm 28.44°$.

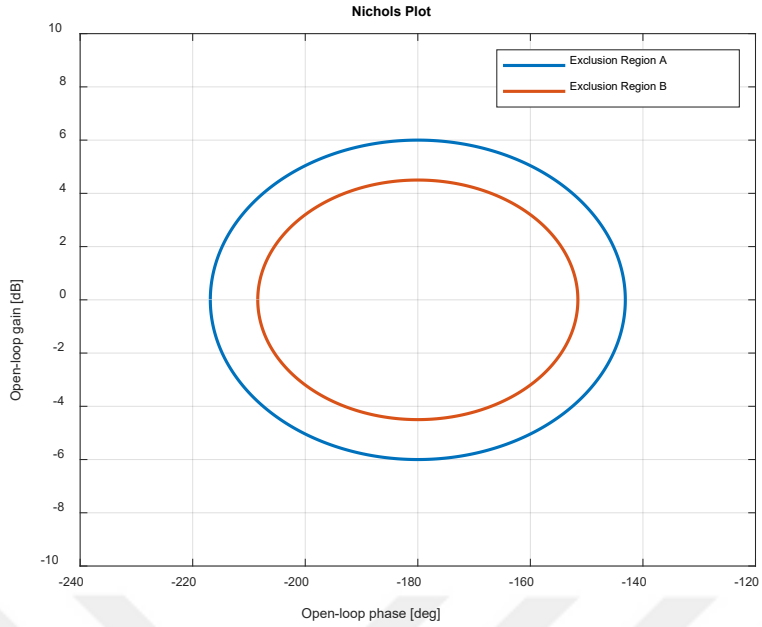

Figure 4.6 : Elliptical nichols plane exclusion regions.

The equivalent exclusion regions on Nyquist plane can be seen in the Figure 4.7.

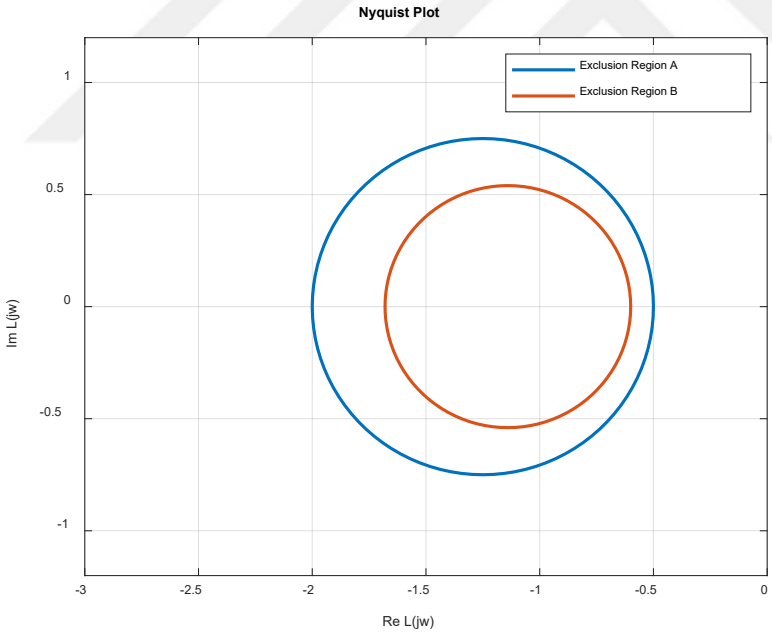

Figure 4.7 : Circular nyquist plane exclusion regions.

The exclusion region A represents a circle in Nyquist plane with a center at -1.25 and a radius of 0.75 while exclusion region B represents a circle with a center at -1.14 and a radius of 0.54.

An uncertain plant with the multiplicative input uncertainty which represents exclusion region A is given in equation 4.24 and will be used as a uncertainty metric throughout in this thesis hereafter.

$$P_{unc}(s) = 1.25P(s)(1 + 0.6\Delta_{\mathrm{M}}) \tag{4.24}$$

while, $P(s)$ is the nominal plant, $P_{unc}(s)$ is the plant with uncertainties and Δ_M is the uncertainty magnitude.

4.4 H_∞ Loop Shaping

The H_∞ loop shaping procedure which will be described below is a combination of H_∞ robust stabilization and loop shaping procedures as proposed by McFarlane and Glover[22]. The theory based on two steps which are the augmentation of the open-loop plant with pre and post compensators to have an ideal loop shape mentioned earlier. Next, the shaped plant is robustly stabilized with respect to coprime factor uncertainty using H_∞ optimization. In the following chapters, H_∞ robust stabilization problem will be examined first and then a methodology for designing H_∞ loop shaping controller will be presented.

4.4.1 Normalized coprime factorization

Modelling the uncertainty by stable norm bounded dynamic matrix perturbations is a common practice however the use of single stable perturbation restricts the plant and perturbed plant models have either the same number of unstable poles or the same number of unstable zeros[39]. In order to prevent this phenemenon, two stable perturbations can be used for each one of the factors in a coprime factorization of the plant. A stabilization of the plant G is done with a left coprime factorization as seen in the equation 4.25.

$$G = M^{-1}N \tag{4.25}$$

where both M and N are stable. Then a perturbed plant model G_p can be seen in the equation 4.26.

$$G_p = (M + \Delta_M)^{-1}(N + \Delta_N) \tag{4.26}$$

where, Δ_M and Δ_N are stable unknown transfer functions which represent the uncertainty in the nominal plant model G. The purpose of the robust stabilization is not only to stabilize the plant G but to stabilize all the perturbed plant family G_p defined as in equation 4.27.

$$G_p = \{(M + \Delta_M)^{-1}(N + \Delta_N) : \|\Delta_N \, \Delta_M\|_\infty < \epsilon\} \tag{4.27}$$

where $\epsilon > 0$ is the stability margin which is the maximum value that maintains stability[40]. The problem of the robust stabilization of normalized coprime factor plant desriptions is to maximize this stability margin value[39]. The H_∞ robust stabilization problem can be schemetized as in the Figure 4.8 below.

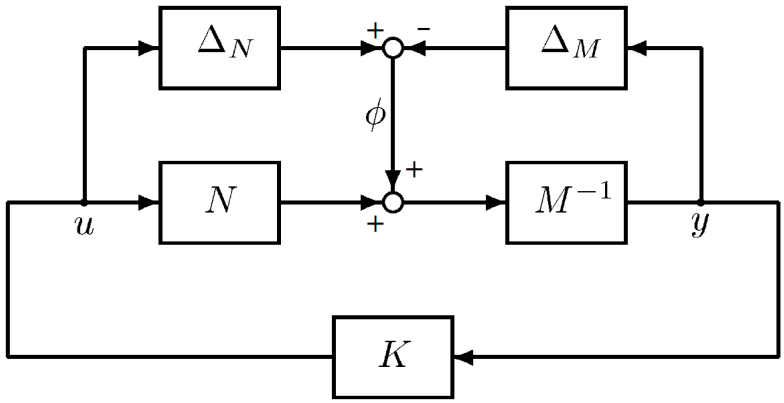

Figure 4.8 : H_∞ robust stabilization problem. [32]

The system is said to be robustly stable if and only if the nominal feedback system is stable and the equation 4.28 is valid. The maximum stability margin is given in the equation 4.29.

$$\gamma \triangleq \left\| \begin{bmatrix} K \\ I \end{bmatrix} (I - GK)^{-1} M^{-1} \right\|_\infty \leq \frac{1}{\epsilon} \tag{4.28}$$

$$\gamma_{min} = \epsilon_{max}^{-1} = \{1 - \|N \, M\|_H^2\}^{-\left(\frac{1}{2}\right)} = \left(1 + \rho(XZ)\right)^{\frac{1}{2}} \tag{4.29}$$

where, $\|.\|_H$ denotes the Hankel norm, ρ means spectral radius X and Z are the unique positive solutions of the riccati equations for a state-space realization (A, B, C, D) of the plant, respectively given in the equations 4.30 and 4.31.

$$(A - BS^{-1}D^TC)^TX + X(A - BS^{-1}D^TC) - XBS^{-1}B^TX + C^TR^{-1}C = 0 \quad (4.30)$$

$$(A - BS^{-1}D^TC)Z + Z(A - BS^{-1}D^TC)^T - ZC^TR^{-1}CZ + BS^{-1}B^T = 0 \quad (4.31)$$

where,

$R = I + DD^T$ and $S = I + D^TD$

And all stabilizing controller which guarantees equation 4.28 is given by in equation 4.32 for a specified $\gamma > \gamma_{min}$.

$$K = \begin{bmatrix} A + BF + \gamma^2(L^T)^{-1}ZC^T(C + DF) & \gamma^2(L^T)^{-1}ZC^T \\ B^TX & -D^T \end{bmatrix} \quad (4.32)$$

where,

$F = -S^{-1}(D^TC + B^TX)$ and $L = (1 - \gamma^2)I + XZ$

4.4.2 H_∞ one degree of freedom loop shaping design

Use of robust stabilization only does not able to present the insight to any performance requirements aimed by the designer. Thus, it is not very much in use in practice[32]. Shaping the singular values of the open-loop plant with the use of pre and post compensators presents flexibility to work with the "shaped plant"[22]. The shaped plant is given in equation 4.33 assuming W_1 is pre-compensator and the W_2 is the post compensator.

$$G_s = W_2GW_1 \quad (4.33)$$

The shaped plant and the controller can be seen in the Figure 4.9 below.

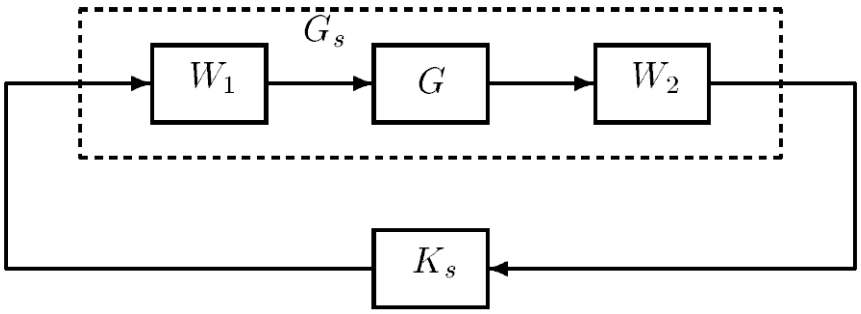

Figure 4.9 : The shaped plant and controller. [32]

The feedback controller for the plant G is given in the equation 4.34 below.

$$K = W_1 K_s W_2 \tag{4.34}$$

A procedure for designing the H_∞ one degree of freedom loop shaping controller is presented below[25].

- Scale the outputs such that one unit of cross-coupling into each of the outputs is equally undesirable.
- Scale all inputs to reflect the relative actuator bandwidth capabilities.
- Re-order the inputs such as the plant is as diagonal as possible.
- Choose pre and post compensator such that the singular values of the shaped plant is desirable. High gains of loopshape transfer function in the low frequency region is prefferable[32]. Also, roll-off rates of approximately $20\ dB/decade$ at the desired bandwidths and more in the high frequency regions are desired.
- Robustly stabilize the shaped plant G_s. Comment on the maximum stability margin ϵ. The values $\epsilon > 0.25$ and relatively $\gamma < 4$ is accepted as an indicator of successful design[32]. If desired criteria are not met, return to the selection of the weights and make a new selection.
- Implement the controller. A implementation seen in the Figure 4.10 is useful.

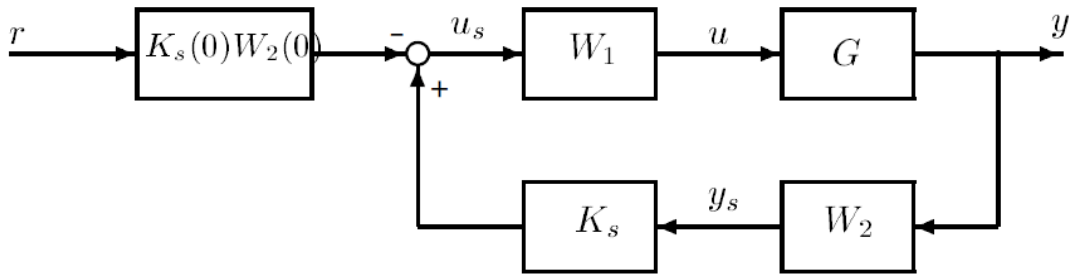

Figure 4.10 : A pratical implementation of the loop-shaping controller. [32]

4.4.3 H_∞ two degrees of freedom loop shaping design

Many practical real world control problems contains two degrees of freedom control architecture[32]. These two degrees represents the measurement or feedback signals and commands or reference signals. Two degrees of freedom controllers outperforms one degree of freedom ones in the case of the stringent time domain specifications. The general two degrees of freedom control structure can be seen in the Figure 4.11 below.

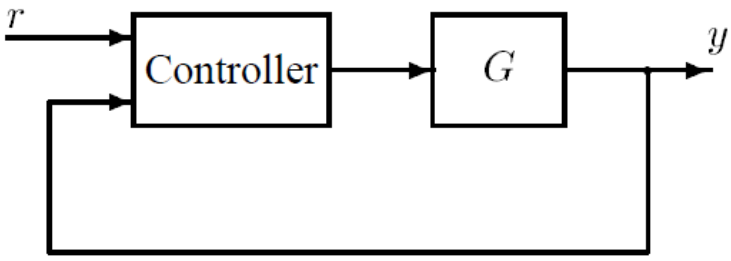

Figure 4.11 : General two degrees-of-freedom feedback controller scheme. [32]

A feedback controller purposes to meet the robust stability and disturbance rejection in the same manner as in the one degree of freedom controller case. An additional prefilter is added to the controller structure in order to force the closed loop system to follow the specified model T_{ref}, reference model. The two degrees of freedom control structure with the normalized coprime factorization scheme can be seen in the Figure 4.12 below.

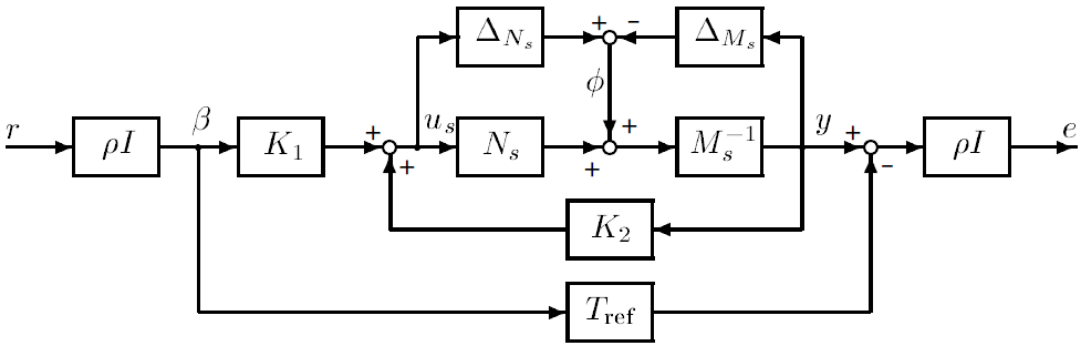

Figure 4.12 : Two degrees-of-freedom H_∞ loop-shaping design problem. [32]

In two degrees of freedom controller design process, the purpose is to find a controller $K = [K_1 \quad K_2]$ such that the H_∞ norm of the transfer function between $[r^T \ \phi^T]^T$ and

$[u_s^T\ y^T\ e^T]$ is minimized for the shaped plant $G_s = GW_1$. The control signal u_s can be seen in the equation 4.28 below.

$$u_s = [K_1 \quad K_2]\begin{bmatrix}\beta \\ y\end{bmatrix} \tag{4.35}$$

where K_1 is the prefilter and the K_2 is the feedback controller. β denotes the scaled reference signal while y represents the output. The prefilter ensures the closed loop transfer function follows the reference model T_{ref} by satisfying the equation 4.36.

$$\left\|(I - G_sK_2)^{-1}G_sK_1 - T_{ref}\right\|_\infty \leq \gamma\rho^{-2} \tag{4.36}$$

T_{ref} is the ideal model which represents the time domain specifications that the designer desires. ρ is the model matching parameter selected by designer is directly proportional to the performance at the expense of robustness. The problem is noe becomes to minimize the H_∞ norm of the 3x2 matrix in equation 4.37.

$$\begin{bmatrix}u_s \\ y \\ e\end{bmatrix} = \begin{bmatrix}\rho(I - K_2G_s)^{-1}K_1 & K_2(I - G_sK_2)^{-1}M_s^{-1} \\ \rho(I - G_sK_2)^{-1}G_sK_1 & (I - G_sK_2)^{-1}M_s^{-1} \\ \rho^2[(I - G_sK_2)^{-1}G_sK_1 - T_{ref}] & \rho(I - G_sK_2)^{-1}M_s^{-1}\end{bmatrix}\begin{bmatrix}r \\ \phi\end{bmatrix} \tag{4.37}$$

The problem in equation 4.30 turns into a H_∞ norm minimization problem between ϕ and $[u_s^T \quad y^T]^T$ and the two degrees of freedom problem reverts into an ordinary H_∞ loop shaping controller. In order to place the two degrees of freedom problem into the standard control configuration, generalized plant is defined as in equation 4.38.

$$\begin{bmatrix}u_s \\ y \\ e \\ \beta \\ y\end{bmatrix} = \begin{bmatrix}P_{11} & P_{12} \\ P_{21} & P_{22}\end{bmatrix}\begin{bmatrix}r \\ \phi \\ u_s\end{bmatrix} \tag{4.38}$$

while,

$$P_{11} = \begin{bmatrix}0 & 0 \\ 0 & M_s^{-1} \\ -\rho^2T_{ref} & \rho M_s^{-1}\end{bmatrix}, P_{12} = \begin{bmatrix}I \\ G_s \\ \rho G_s\end{bmatrix}, P_{21} = \begin{bmatrix}\rho I & 0 \\ 0 & M_s^{-1}\end{bmatrix} \text{ and } P_{22} = \begin{bmatrix}0 \\ G_s\end{bmatrix}$$

Moreover, if the desired closed-loop transfer function and shaped plant have the state-space realizations in equation 4.39 and 4.40, the generalized plant is given in the equation 4.41 [24].

$$G_s = \begin{bmatrix} A_s & B_s \\ C_s & D_s \end{bmatrix} \tag{4.39}$$

$$T_{ref} = \begin{bmatrix} A_r & B_r \\ C_r & D_r \end{bmatrix} \tag{4.40}$$

$$P = \begin{bmatrix} A_p & B_p \\ C_p & D_p \end{bmatrix} \tag{4.41}$$

while,

$$A_p = \begin{bmatrix} A_s & 0 \\ 0 & A_r \end{bmatrix}, B_p = \begin{bmatrix} 0 & (B_s D_s^T + Z_s C_s^T) R_s^{-\frac{1}{2}} \\ B_r & 0 \end{bmatrix} B_s, C_p = \begin{bmatrix} 0 & 0 \\ C_s & 0 \\ \rho C_s & -\rho^2 C_r \\ 0 & 0 \\ C_s & 0 \end{bmatrix}$$

and $D_p = \begin{bmatrix} 0 & 0 & I \\ 0 & R_s^{\frac{1}{2}} & D_s \\ -\rho^2 D_r & \rho R_s^{\frac{1}{2}} & \rho D_s \\ \rho I & 0 & 0 \\ 0 & R_s^{\frac{1}{2}} & D_s \end{bmatrix}$

Here, $R_s = I + D_s D_s^T$ and Z_s is the unique positive solution of the equation 4.31. The problem is solved as discussed in the section 4.4.1 and then the final two degrees of freedom H_∞ loop shaping controller is implemented as in the Figure 4.13 below.

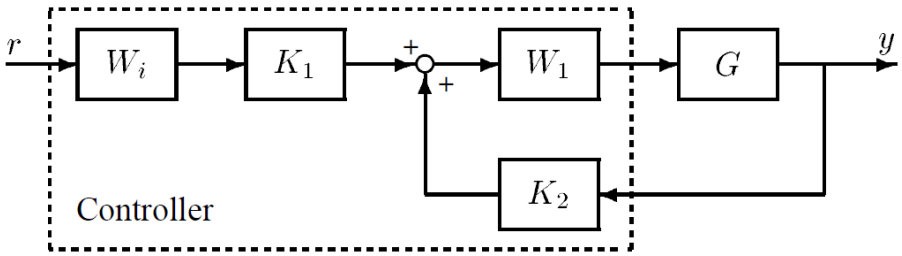

Figure 4.13 : Two degrees-of-freedom H_∞ loop-shaping controller implementation. [32]

Here, W_i is the steady state gain matching parameter which can be calculated by using the formula in equation 4.42.

$$W_i = \left[W_o \left(I - G_s(0) K_2(0) \right)^{-1} G_s(0) K_1(0) \right]^{-1} T_{ref}(0) \tag{4.42}$$

5. CONTROLLER ARCHITECTURE

The controller methodology presented in the previous chapter was introduced in the longitudinal axis of the aircraft in order to satisfy stability, tracking performance and disturbance rejection. The dynamics of the aircraft chages dramatically within the different areas of the flight envelope. The purpose of the controller designer is to keep the aircraft inside the Level 1 Flying and Handling Qualities along the flight envelope. Thus, various gain selections may be applied for different points of the flight envelope due to changing dynamics of the aircraft. Then, the controller is formed by interpolating these gains which are adjusted according to the a scheduling parameter between the selected operating points[41]. This scheduling parameter may be altitude, mach or the dynamic pressure which is a mathematical expression of altitude and mach. This design method is called “gain scheduling”. Although gain scheduling controllers are practical and powerful method for the control of nonlinear systems[41], they increase system complexity due to the requirement for design for various points. Robust controllers can solve this complexity by ensuring satisfactory performance throughout a design envelope with the design of one point[42].

In the scope of this thesis study, a 2 degree-of-freedom H_∞ Loop Shaping controller is designed in order to satisfy longitudinal FHQ requirements throughout the flight envelope with one design point. An optimization process has been carried out to satisfy “Level 1 FHQ” criteria for all the points inside the flight envelope. A nominal controller had been designed first and then resulting responses at the corners of the flight envelope were examined with respected to the ideal response. Minimization of the differences from ideal response in the time domain satisfies the “Level 1 FHQ” criteria.

The specified design envelope will be presented first in this chapter and then the controller structure will be introduced. Then the controller structure in the NASA study[14] will be explanined for the purpose of comparison with the H_∞ Loop Shaping controller. Finally, the mathematical method followed in optimization problem will be mentioned.

5.1 Flight Envelope and Open-Loop Plants

It is aimed to have Level 1 FHQ criteria along the flight envelope seen in the Figure 5.1 as a shaded area. The upper limit of the Mach number is determined as 0.6 since the aerodynamic data was defined up to this speed. There is a triangular upper left section which was not included into a square shaped envelope since AoA Limiter is active in this area. In order to keep the comparison with controller in NASA document, only flight points which has a value of AoA lower than 15 are evaluated. Last, upper altitude limit is determined as 20000 ft to shape the fligth envelope. The nominal design point is located in the middle of this flight envelope as 0.45 Mach and 10000 ft. The nominal and other design points can be seen in the Figure 6.1 as black dots and their data is presented in the Table 5.1.

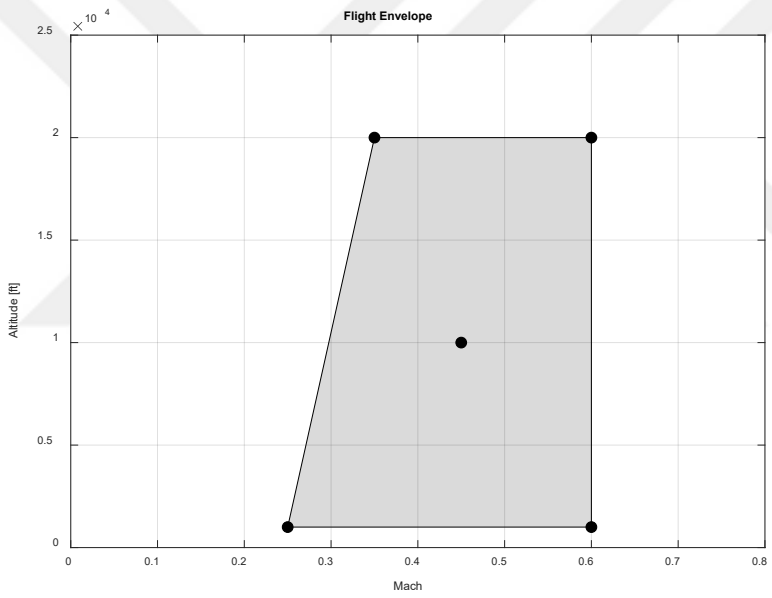

Figure 5.1 : Selected flight envelope and design points.

Table 5.1 : Design Points.

Design Point	Mach	Altitude [ft]	AOA [deg]
1	0.25	1000	12.1
2	0.6	1000	1.03
3	0.6	20000	3.84
4	0.35	20000	12.95
5	0.45	10000	4.93

The linear system in the design point 5 is given below with the state order of $x = [V_t \quad \alpha \quad q \quad \theta]$, the output order of $y = [V_t \quad \alpha \quad q \quad \theta \quad n_x \quad n_z \quad \gamma]$ and a single elevator input.

$$A = \begin{bmatrix} -0.0555 & -1.1052 & 1.0826 & -9.81 \\ -0.0010 & -3.5379 & 0.6922 & 0.0003 \\ 0 & 1.9673 & -0.73 & 0 \\ 0 & 0 & 1 & 0 \end{bmatrix}, \quad B = \begin{bmatrix} 0.1673 \\ -0.0078 \\ -0.1277 \\ 0 \end{bmatrix}$$

$$C = \begin{bmatrix} 1 & 0 & 0 & 0 \\ 0 & 57.2958 & 0 & 0 \\ 0 & 0 & 57.2958 & 0 \\ 0 & 0 & 0 & 57.2958 \\ -0.0057 & -0.1127 & 0.0406 & 0 \\ 0.0152 & 53.2936 & 4.6357 & 0 \\ 0 & -57.2958 & 0 & 57.2958 \end{bmatrix}, \quad D = \begin{bmatrix} 0 \\ 0 \\ 0 \\ 0 \\ 0 \\ 0 \\ 0 \end{bmatrix}$$

The short period model is considered during the design of H_∞ Loop Shaping controller design so the short period state-space representation of the aircraft at 10000 ft altitude and 0.45 Mach with state order of $x = [q \quad \alpha]$, output order of $y = [V_t \quad \alpha \quad q \quad \theta \quad n_x \quad n_z \quad \gamma]$ and a single elevator input is seen below.

$$A_{sp} = \begin{bmatrix} -0.73 & 1.9673 \\ 0.6922 & -3.5379 \end{bmatrix}, \quad B_{sp} = \begin{bmatrix} -0.1277 \\ -0.0078 \end{bmatrix}$$

$$C_{sp} = \begin{bmatrix} 0 & 0 \\ 0 & 57.2958 \\ 57.2958 & 0 \\ 0 & 0 \\ 0.0404 & -0.1127 \\ 4.6357 & 53.2936 \\ 0 & -57.2958 \end{bmatrix}, \quad D_{sp} = \begin{bmatrix} 0 \\ 0 \\ 0 \\ 0 \\ 0 \\ 0 \\ 0 \end{bmatrix}$$

The damping ratio and natural frequencies at the nominal design point for short period mode is given in the Table 5.2.

Table 5.2 : Short period properties.

Damping Ratio (ζ)	Natural Frequency (ω)
-1	-0.3083
1	-3.9595

The open loop bode response of the plants at the design points can be seen in the Figure 5.2 below.

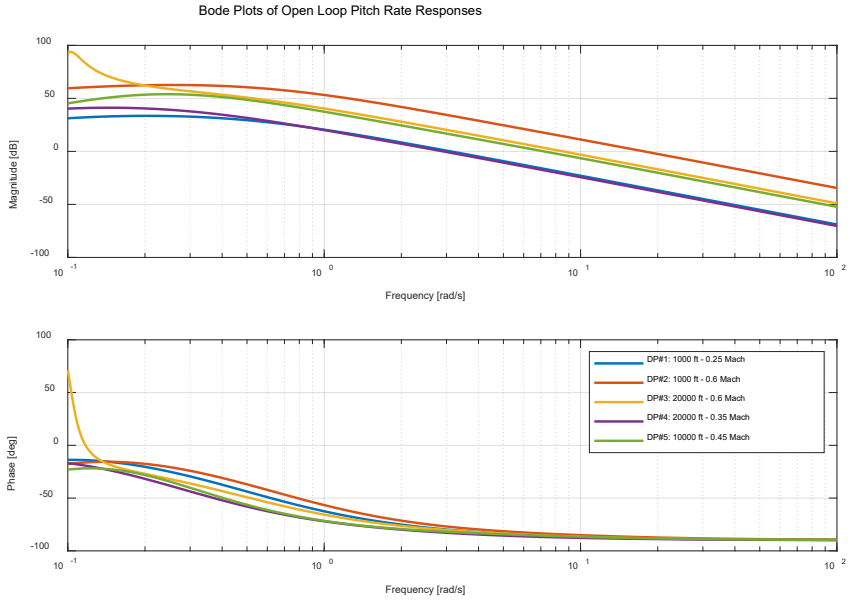

Figure 5.2 : Open loop bode plots of the pitch rate responses.

Also, pole-zero map of the open loop transfer functions from elevator command to pitch rate can be seen in the Figure 5.3.

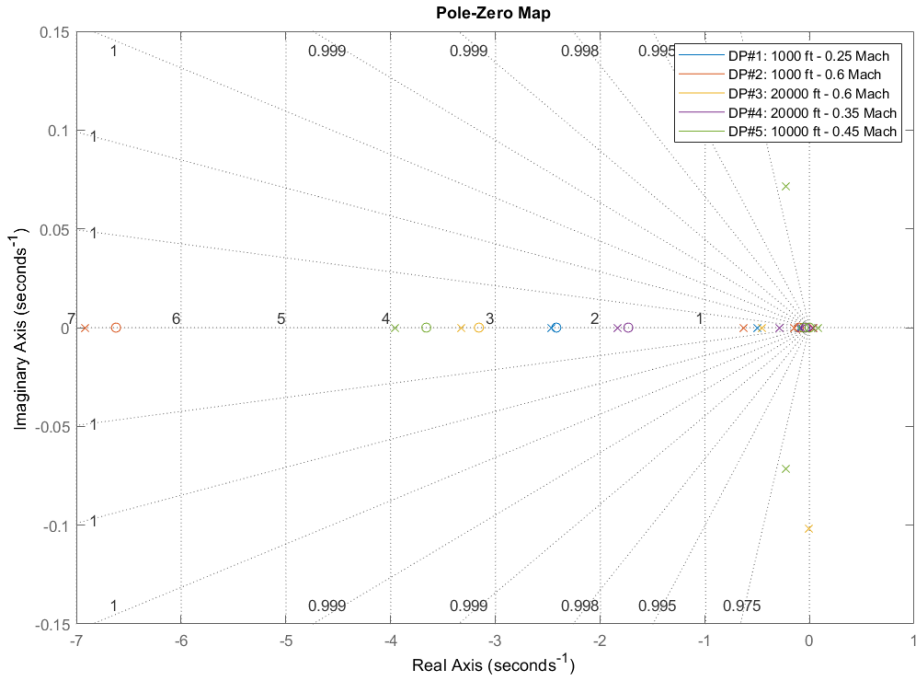

Figure 5.3 : Open loop poles and zeros of the pitch rate transfer functions.

5.2 System Architecture

The handling qualities chosen to evaluate the performance of the flight control law algorithm in Chapter 3 are mostly based on the response of the pitch rate. There are handling qualities such as dropback to examine the pitch attitude response which is the integrated value of the pitch rate actually. For these reasons, the controlled parameter for the control of the longitudinal axis was chosen as "pitch rate" and architecture proposed in the previous chapter for 2 degree-of-freedom H_∞ Loop Shaping Controller is applied with pitch rate parameter feedback. The system architecture for longitudinal axis of the aircraft can be seen in the Figure 5.4 below.

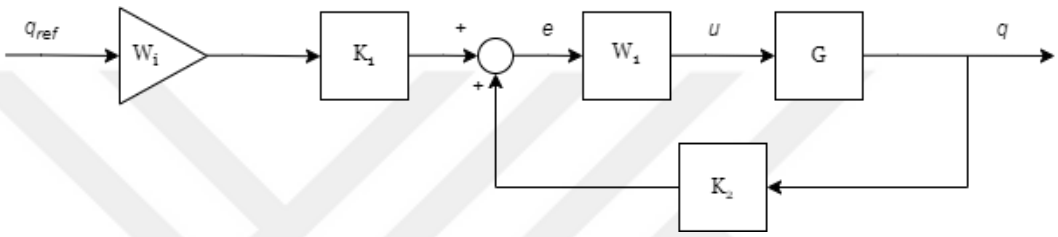

Figure 5.4 : System architecture.

The pre-compensator is in the form of PI controller as in equation 5.1. The parameters of this pre-compensator will be found with the optimization.

$$W_1 = k\left(1 + \frac{a}{s}\right) \tag{5.1}$$

The plant is symbolized as the block G in the Figure 5.4 which is the system composed of actuator, the short period longitudinal state-space model and the sensor as in equation 5.2.

$$G = sensor * G_{sp} * actuator \tag{5.2}$$

Then the controllers resulted from the model using short period approximated are introduced to the full state longitudinal system in order to represent the longitudinal dynamics better. This higher order system is used for the analyses of the system. The results of the nominal and uncertain systems along with the FHQ analyses will be conducted with the higher order system.

5.3 PID Controller

The technical report published by NASA[14] proposes a controller structure for the F-16 aircraft which is the studied aircraft in the scope of this thesis. This controller structure includes longitudinal, lateral and directional control structures and named as FLCS which employs classical control manners. The longitudinal flight control law of the FLCS involves AoA, pitch rate and normal acceleration feedbacks in order to stabilize and control the aircraft in longitudinal axis with a PI controller[14]. Furthermore, there are envelope protection logics such as AoA limiter and normal acceleration limiter.

The purpose of the longitudinal axis controller of the FLCS is to control the instable behaviour of the F-16 by limiting the demanded normal acceleration command to the permitted normal acceleration[15]. The pilot command passes through a command gradient which can be seen in the Figure 5.5 which converts pilot force input to a commanded "g" input as normal acceleration. Then the g command is limited due to the dynamic pressure scheduling as seen as in Figure 5.6. The maximum commanded normal acceleration is limited at 8 g while minimum bound of commanded normal acceleration is -4 g.

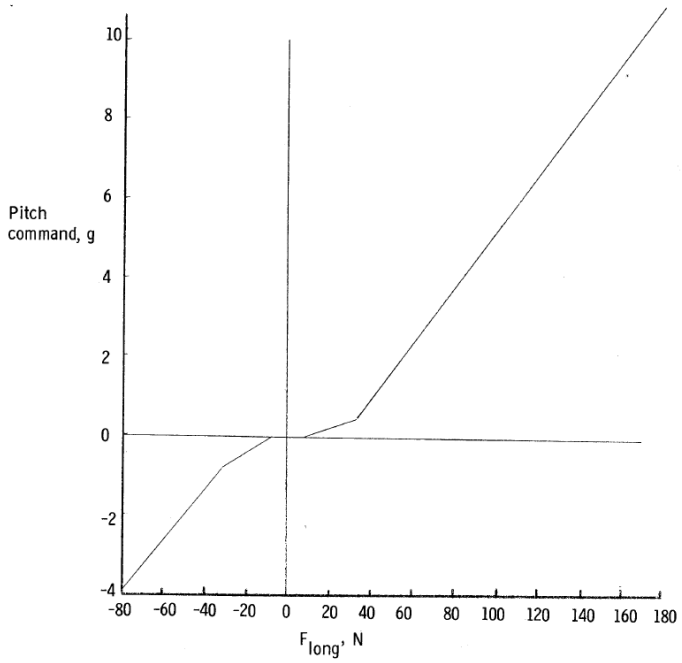

Figure 5.5 : Pitch command gradient of the longitudinal axis of FLCS. [14]

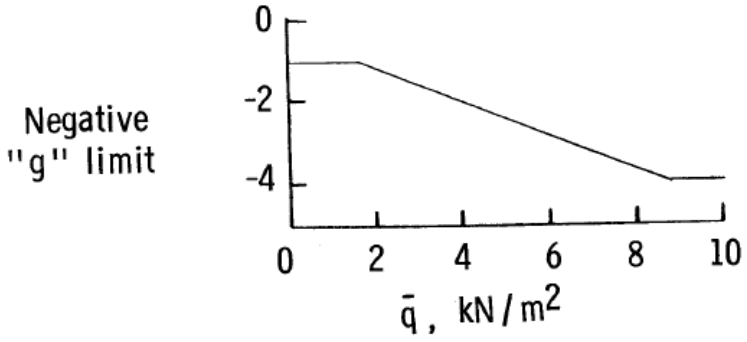

Figure 5.6 : Scheduled “g” limiting of FLCS. [14]

Then the “limited g command” passes through a pilot prefilter which is a low pass filter and after the AoA Limiter feedback and normal acceleration feedbacks are closed, the error passes throgh a PI controller. Finally, horizontal tail and differential deflection signals are obtained after the SAS feedback is closed in order to satisfy the stability.

The AoA Limiter system takes AoA and pitch rate signals as inputs and delivers two output signals one for feedback path and one for pilot command path. This AoA limiter system is activated once the AoA increases above 15° as two deadband blocks limits the signal below this AoA value.

The feedback path consists of two signals normal acceleration and pitch rate. The pitch rate signal passes through a high pass filter and then added to the normal acceleration feedback. Then the blended feedback signal is summed with one output of the AoA limiter logic then summed with pilot command path by passing through a lead-lag filter. The obtained error signal passes through a PI controller to minimize the normal acceleration error.

For the purpose of this thesis study, the longitudinal control structure of FLCS is used to compare the results of the H_∞ Loop Shaping controller. Thus, any envelope protection logics are discarded as the maximum AoA of the design points is lower than 15° which is the activation point of the AoA limiter. A feedback architecture in Figure 5.7 is used as a comparison system.

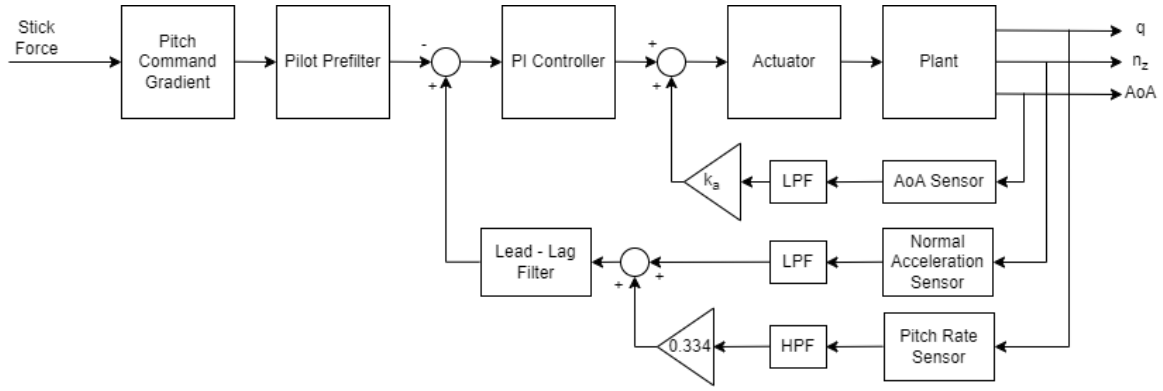

Figure 5.7 : Block diagram of the longitudinal axis FLCS.

5.4 Optimization Problem

In the scope of this thesis, it is aimed to design an H_∞ Loop Shaping controller which results in Level 1 FHQ in the desired flight envelope. The selected criteria in the Chapter 3 which are pitch attitude dropback and pitch attitude bandwidth are used as an evaluation criteria and CAP parameter is used as a guideline to shape the desired transfer function. This desired transfer function is a reference transfer function for 2 degree-of-freedom H_∞ Loop Shaping algorithm. The closed loop pitch rate time response will track this reference model to increase the performance properties defined according to the FHQ requirements mentioned above.

An ideal pitch rate transfer function should be defined in order to introduced as a reference model for controller algorithm. The transfer function to pitch rate from stick force or elevator deflection can be seen in the equation 5.3 [9].

$$\frac{q(s)}{\delta_e(s)\ or\ F_s(s)} = \frac{K_\theta s\left(s+\frac{1}{T_{\theta_1}}\right)\left(s+\frac{1}{T_{\theta_2}}\right)e^{-\tau_e s}}{\left[s^2+2\zeta_{ph}\omega_{ph}s\ +\omega_{ph}^2\right]\left[s^2\ +2\zeta_{sp}\omega_{sp}s\ +\omega_{sp}^2\right]} \tag{5.3}$$

However, since the controller is to be desiged on the short period approximated model, only short period terms of the equation above is in interest. The ideal pitch rate transfer function for short period model is seen in equation 5.4.

$$\frac{q(s)}{\delta_e(s)\ or\ F_s(s)} = \frac{K_\theta\left(s+\frac{1}{T_{\theta_2}}\right)e^{-\tau_e s}}{\left[s^2\ +2\zeta_{sp}\omega_{sp}s\ +\omega_{sp}^2\right]} \tag{5.4}$$

The characteristic equation parameters of the ideal pitch rate transfer function are optimized in order to satisfy the desired performance all over the specified flight

envelope. Thus ζ_{sp} and ω_{sp} are searched along with the pre-compansator gains of the H_∞ Loop Shaping controller a and k to meet the Level 1 FHQ. The CAP criteria is a good guideline to set the limits on natural frequency while short period damping ratio limits[8] can be used for the bounds of the damping ratio of the characteristic equation. Since the nominal plant is selected as the middle point in the flight envelope, the bounds for short period damping ratio and short period natural frequency are determined according to the values belongs to the flight point 10000 ft altitude and 0.45 Mach.

The defined limits of short period damping ratio with respect to the equivalent level responses can be seen in the Table 5.3 below.

Table 5.3: FHQ Level responses due to the short period damping ratio. [8]

Level	Category A and C Flight Phases		Category B Flight Phases	
	Minimum	Maximum	Minimum	Maximum
1	0.35	1.30	0.30	2.00
2	0.25	2.00	0.20	2.00
3	0.15	-	0.15	-

Since Level 1 response is desired, lower and upper limits of short period damping ratio are assumed as 0.30 and 2.00 respectively. Also the bounds for short period natural frequency can be found by calculating equation 3.3 for the flight point. It gives the n/α ratio of 54 for airspeed of 147 m/s and $1/T_{\theta_2}$ value of 3.66. Then the short period natural frequency range is determined for lower and upper bounds as 2 and 12 roughly as seen as red arrow in the Figure 5.8 as a red arrow.

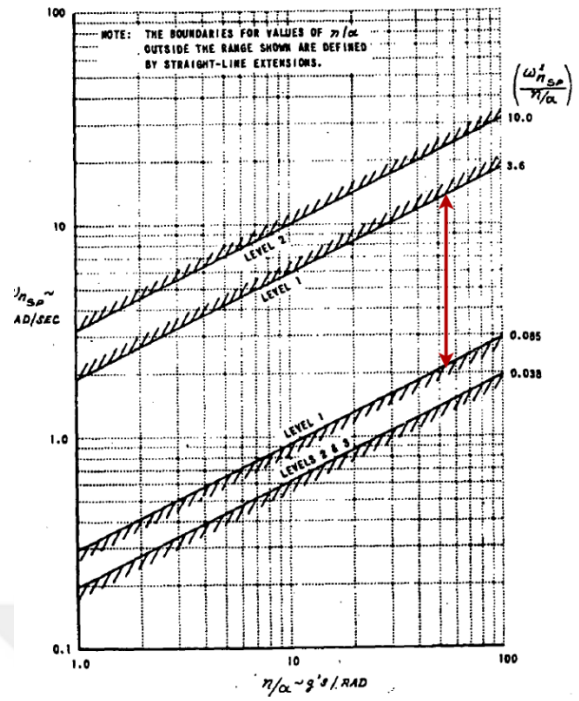

Figure 5.8 : Short period natural frequency range according to the CAP criteria.

After defining the upper and lower bounds for the short period natural frequency and damping ratio, the parameter bounds for the pre-compensator parameters k and a are determined as 0.5 and 10 for lower and upper bounds respectively. As a result, 4 parameters are defined as optimization variables x as in the equation 5.5.

$$x = [k\ a\ \zeta_{sp}\ \omega_{sp}] \tag{5.5}$$

The next step to set the optimization in order to have Level 1 FHQ for the specified flight envelope is to define a cost function to be minimized. For the purpose of having satisfactory time response and relatively similar FHQ for the specified design points, the pitch rate responses are needed to be as much as close to the ideal transfer function response. The grey shaded area in Figure 5.9 represents the difference between ideal pitch rate response and system response sybolically in time domain. This area is aimed to be minimised by minimizing root mean square error of the difference between ideal and system responses at each time interval.

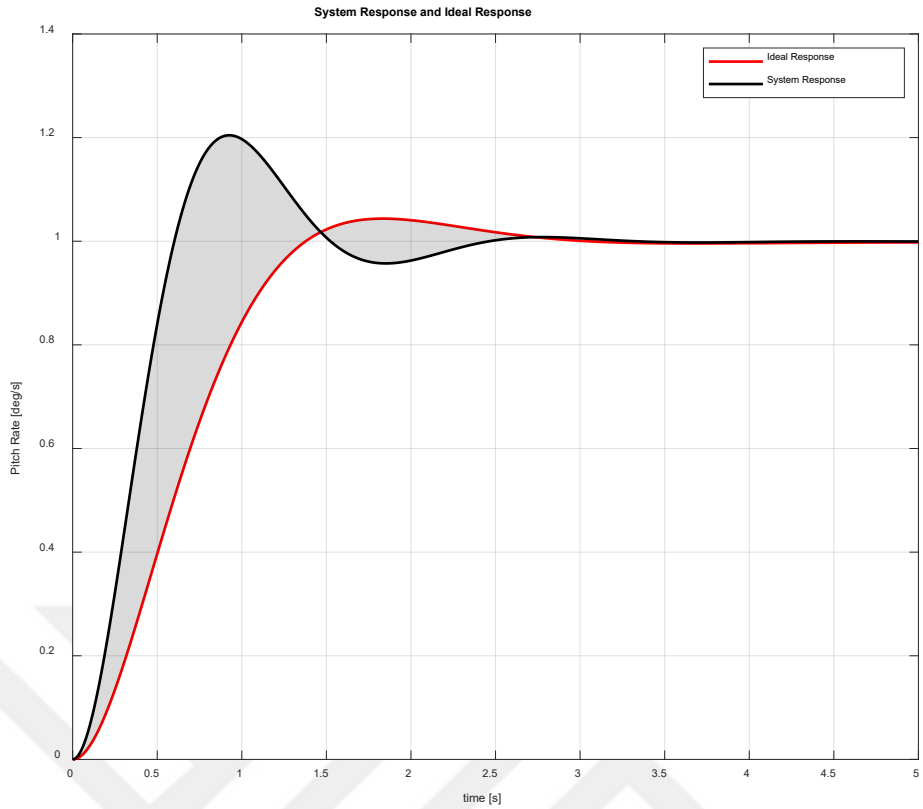

Figure 5.9 : Difference in system response and ideal response.

The optimization algorithm updates the variables in equation 5.5 at each iteration to find both a suitable ideal transfer function to be followed by each system in each design point and pre-compensator parameters that will shape the open-loop plant in order to satisfy the closed-loop goals determined by the ideal transfer function. Root-mean-square error which defined in equation 5.6[43] is used to measure the difference between the two responses.

$$RMSE = \left[\frac{1}{n}\sum_{t=0}^{n}[y_{sys}(t_i) - y_{id}(t_i)^2]\right]^{\frac{1}{2}} \tag{5.6}$$

At each time step, the difference of two responses is squared an then summed along the specified time interval. Then average of this value is taken by dividing the number of time samples. Finally square-root of value is taken in order to have identical units in measurement. The purpose is to have pitch rate responses along the flight envelope as close as ideal pitch rate response so the similarity cost is determined as average RMSE errors of all design points as in equation 5.7 below.

$$avg_{RMSE} = \left(\sum_{i=1}^{n} RMSE_i \right) / n \tag{5.7}$$

RMSE deals with the response over specified time interval however both pitch attitude bandwidth and dropback criteria deals with the transient response of the pitch rate characteristics too. In both FHQ criteria, effective time delay is a significant measurement which can affect the level responses in analyses. Thus, effective time delay cost is included in total cost in order to ensure the desired transient pitch rate response and turns optimization problem into a multiobjective optimization problem. A multiobjective optimization problem is a problem whose solution depends on more than one objective function[44]. Here, one objective of the optimization problem is to have a pitch rate response as much as similar to the ideal response in the given time interval. The other objective is to satisfy transient response requirements by analyzing effective time delay parameter mentioned in the Chapter 3. The purpose is to set an upper limit to the allowed effective time delay. So, it is aimed to minimize the maximum effective time delay within the set of design points. The maximum effective time delay for the Level 1 FHQ is 0.12 seconds as in Table 3.1 in Chapter 3. In order to get a good Level 1 FHQ, maximum allowed effective time delay is defined as 0.11 seconds. If any of 5 design points resulted a effective time delay value than 0.11 seconds, then the difference between the maximum effective time delay value and 0.11 seconds is taken as an effective time delay cost. If none of design points resulted in higher than 0.11 seconds as effective time delay, the effective time delay cost is taken as zero. The cost depending on time delay can be seen in the equation 5.8.

$$cost_{etd} = \begin{cases} 0 & if \ \max(etd) \leq 0.11 \\ |\max(etd) - 0.11| & if \ \max(etd) > 0.11 \end{cases} \tag{5.8}$$

Then, these two objectives are formed to obtain a single cost function which is the weighted sum of RMSE and time delay cost. A weighted sum can be expressed as in equation 5.9 below[44].

$$\bar{f}(x) = \sum_{i}^{N} \omega_i f_i(x) \tag{5.9}$$

Finally the cost function to be minimized in order to satisfy the Level 1 FHQ criteria all over the defined flight envelope by optimizing the pre-compensator and ideal transfer function parameters is given in equation 5.10.

$$cost = avg_{RMSE} + cost_{etd} \tag{5.10}$$

The minimization problem is solved by using MATLAB function “fmincon” which is used to solve nonlinear optimization with constrained variables[45]. The default algorithm of “interior-point” was preferred to solve this minimization problem.

6. RESULTS

Throughout this thesis study, it was purposed to design a longitudinal pitch rate controller that will results in Level 1 FHQ within the specified flight envelope. An optimization has been conducted to satisfy this purpose and detailed in the previous Chapter 6. In this chapter, the results of the optimization problem will be presented, time and frequency domain closed loop responses will be detailed. It will be explained that how the controller affected the open loop frequency response and how this difference is related to closed loop design purposes. FHQ analyses will be performed over the flight envelope to observe if the design purposes has been met. And finally, resultant closed loop system responses with the 2 degree-of-freedom H_∞ Loop Shaping controller will be compared with the responses of the system uses pre-existant controller in NASA study.

First of all, the optimization algorithm needed an initial point given below to iterate the solution up to the optimal point.

$$x_{init} = \left[k_{init} \;\; a_{init} \;\; \omega_{sp_{init}} \;\; \zeta_{sp_{init}}\right] = [\,1 \;\; 1 \;\; 3 \;\; 0{,}85\,]$$

Then, the optimization algorithm has converged to an optimal point with the solution of optimization variables seen below. As seen from the variations of the variables between the initial point and final optimal solution, both gain and integrator parameters are increased in order to keep all design points inside Level 1 FHQ value.

$$x_{opt} = \left[k_{opt} \;\; a_{opt} \;\; \omega_{sp_{opt}} \;\; \zeta_{sp_{opt}}\right] = [9{,}0539 \;\; 3{,}4877 \;\; 5{,}6295 \;\; 0{,}8893]$$

So, the optimal pre-compensator $W_{1_{opt}}$ can be seen in the equation 6.1.

$$W_{1_{opt}} = 9{,}0539\left(1 + \frac{3{,}4877}{s}\right) \tag{6.1}$$

Figure 6.1 shows how the ideal pitch rate time response changes from initial guess to the optimized ideal transfer function.

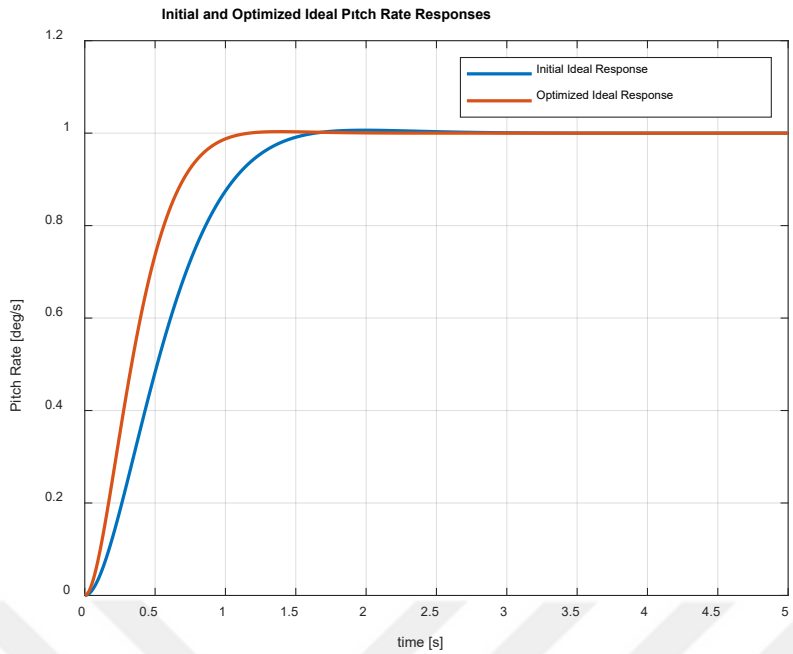

Figure 6.1 : Initial and optimized ideal transfer functions for pitch rate response.

From the Figure 6.1, it can be said that the ideal transfer function has changed to satisfy the FHQ requirements as the rise time gets faster with less overshoot.

The Figure 6.2 shows the closed loop system responses at the initial design variables and optimized design variables. The effect of change in both ideal transfer fuction and pre-compensator parameters can be observed between the two graphs.

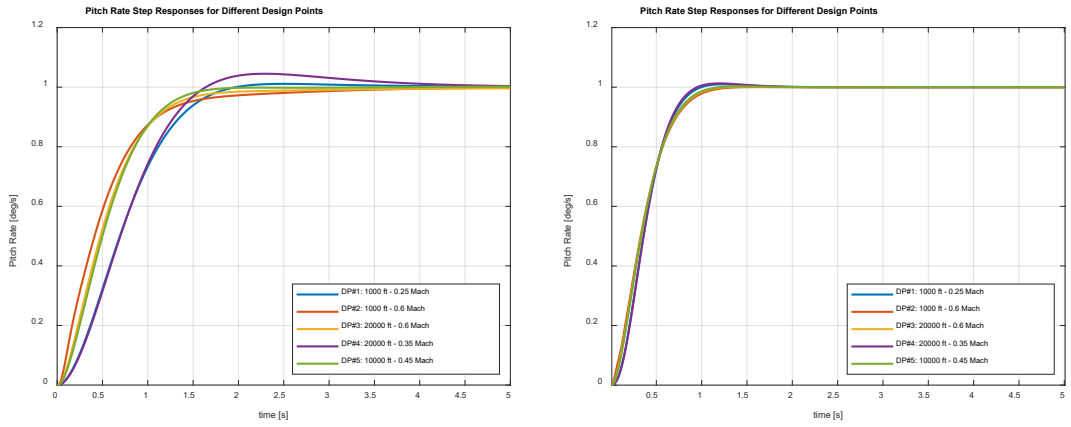

Figure 6.2 : Pitch rate responses of design points before[left] and after[right] optimization.

It can be seen that the pitch rate responses are groupped as the optimization converges to an optimal point that meets the design requirements defined. This means that the pitch rate response dependent Flying and Handling Quality criteria evaluations will be

similar in each design point within the flight envelope. Also, by examining further it is said to be all the nominal responses are following the time response of the ideal transfer function as in Figure 6.3 with a smaller scale in time.

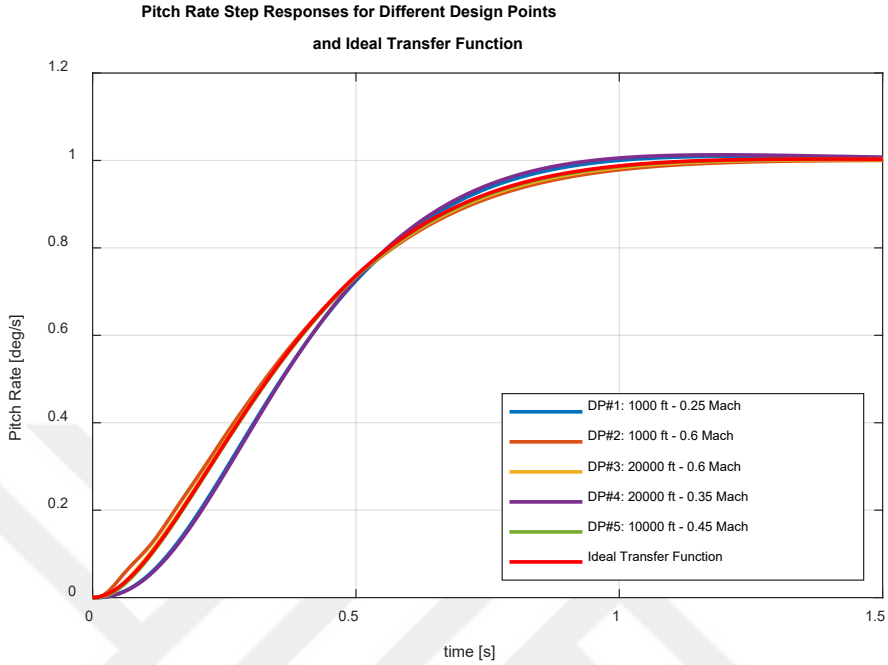

Figure 6.3 : Pitch rate responses of design points and ideal transfer function.

The resultant sigma value plot of the both plant and shaped plant are given in the Figure 6.4.The low frequency gain is boosted as the PI controller is applied as a pre-compensator. This boosted gain affects the disturbance rejection characteristics of the system. The Figure 6.5 gives more insight about how loop transfer function affects the sensitivity and complementary sensitivity functions. For nominal plant, boosted loop transfer function gain for low frequencies decreases the sensitivity function gain and ensures disturbance rejection. This effect can be seen in time domain analysis in the Figure 6.6. The system rejects the given $1deg/s$ disturbance under 1 second. Having a low frequency gain of 1 ensures accurate command tracking for the closed loop system. In Figure 6.5 the complementary sensitivity function has low frequency gain of 1. The tracking performance of the system at nominal design point(10000 ft – 0.45 Mach) can be seen in the Figure 6.7 which shows zero steady state error for unit pitch rate step input and exact matching to the ideal transfer function response.

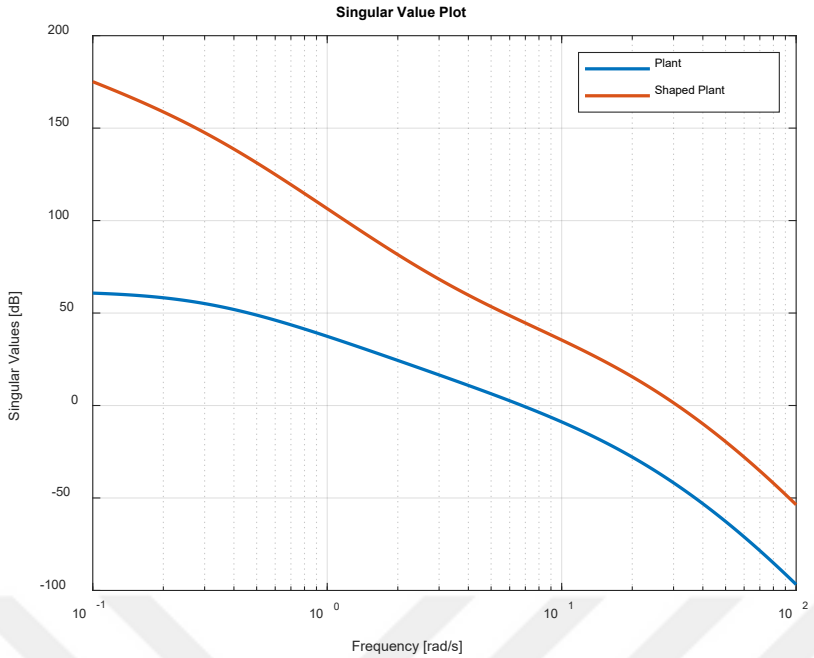

Figure 6.4 : Shaped plant singular values.

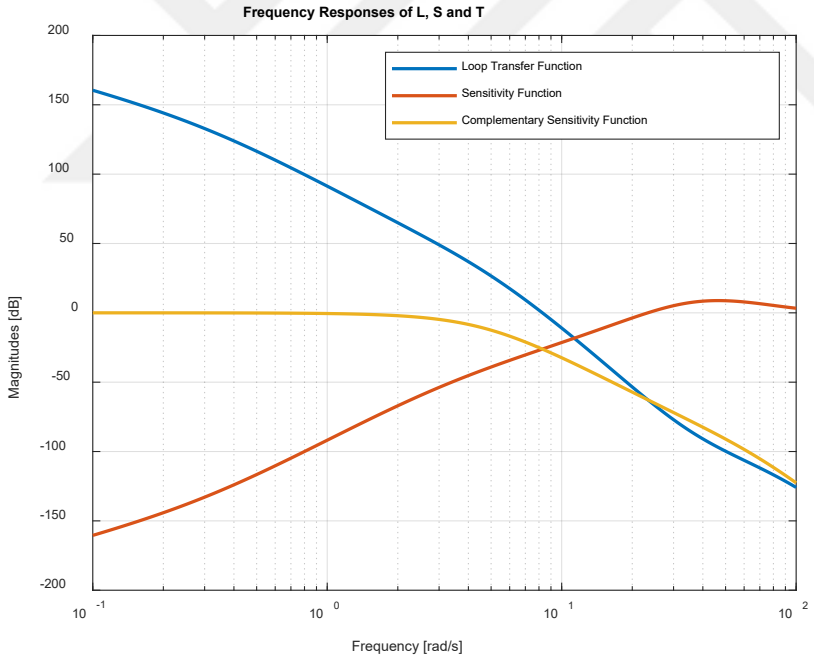

Figure 6.5 : Loop transfer, sensitivity and compementary sensitivity frequency responses.

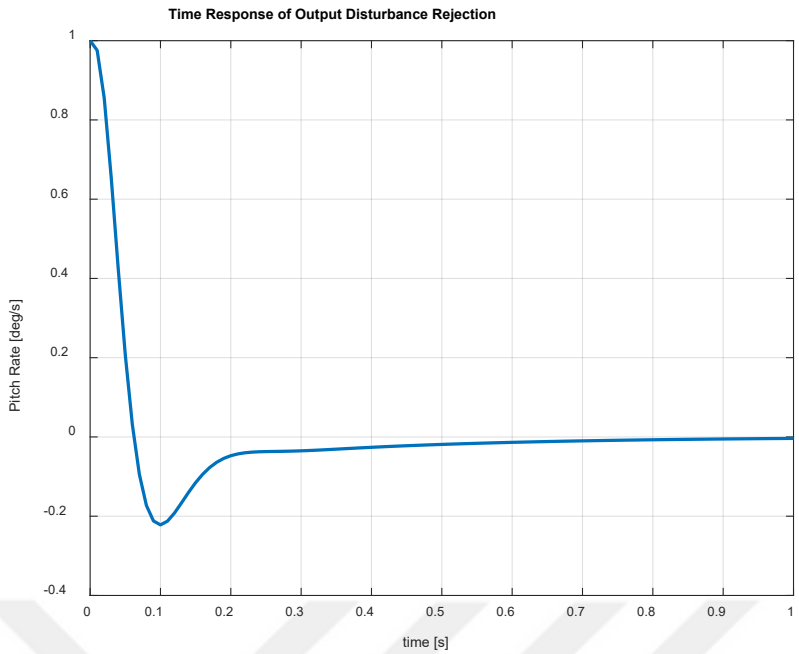

Figure 6.6 : Disturbance rejection in time domain.

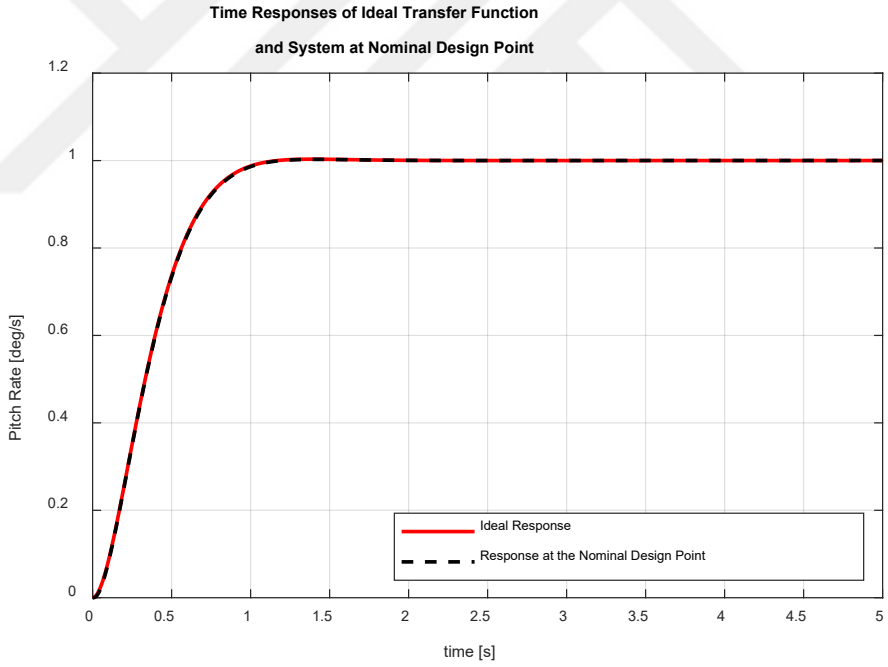

Figure 6.7 : The time responses of ideal transfer function and system at nominal design point.

The results of the design process is evaluated with the two FHQ requirement mentioned in the Chapter 3; pitch attitude bandwidth and pitch attitude dropback. The pitch attitude bandwidth criterion result for the nominal design point can be seen in the Figure 6.8 for the nominal design point. The design resulted in Level 1 bounds as expeced.

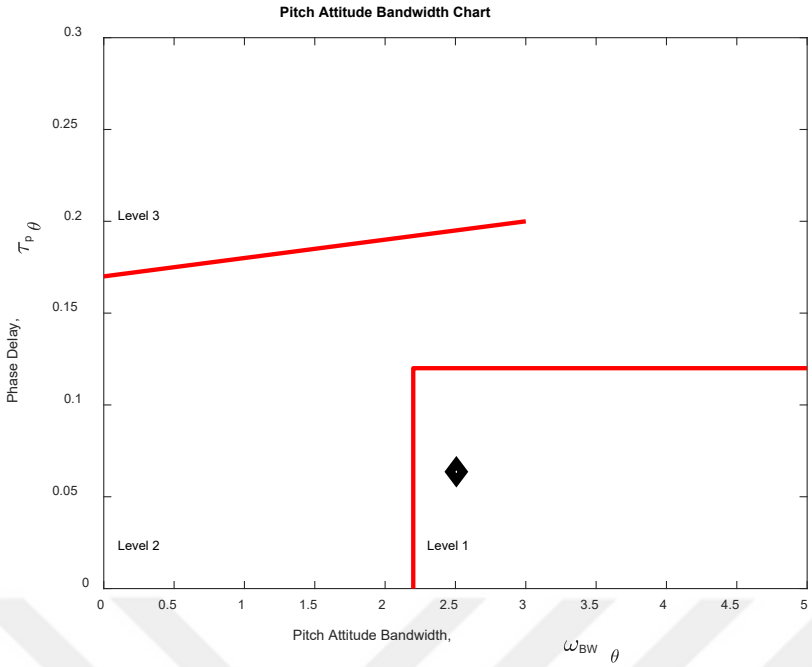

Figure 6.8 : Pitch attitude bandwidth FHQ result for nominal design point.

The pitch attitude dropback criterion result can be seen in the Figure 6.9 below. The design resulted in "satisfactory" characteristics which states there is neither dropback in pitch attitude response nor overshoot in pitch rate response.

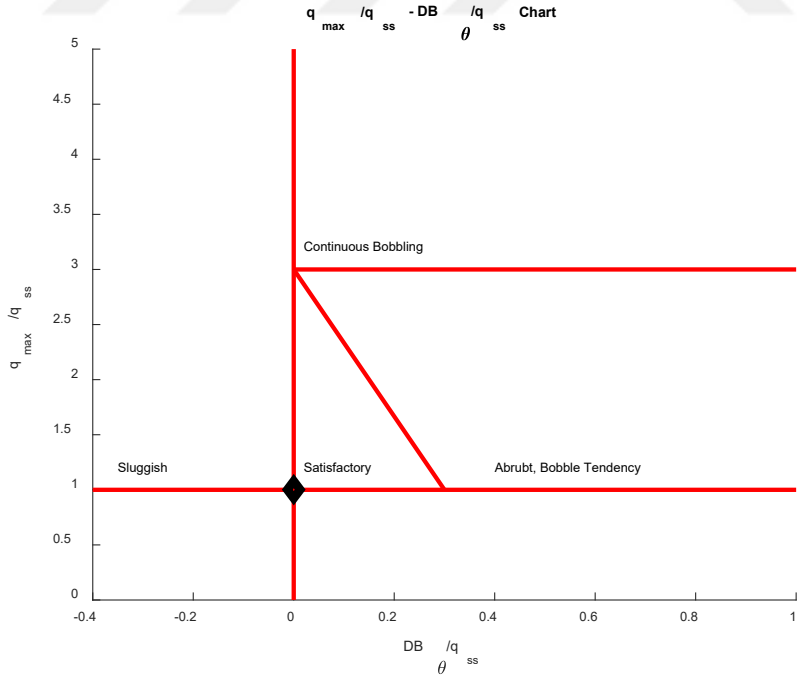

Figure 6.9 : Pitch attitude dropback FHQ result for nominal design point.

The Figure 6.10 shows the pitch attitude response due to the pulse input which released at 5 seconds. As it can be seen in figure, pitch attitude tracks its angle after the input was released.

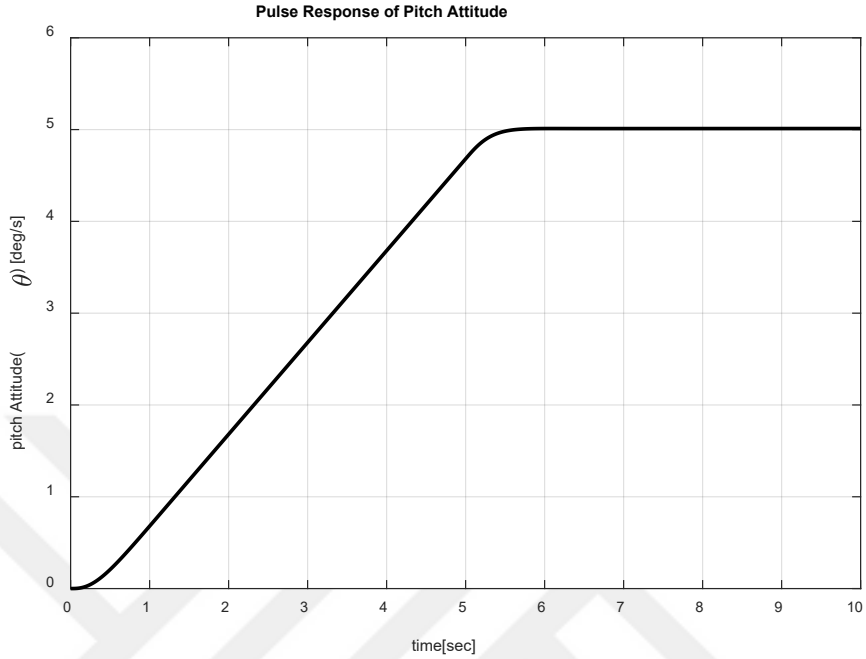

Figure 6.10 : Pitch attitude pulse input result for nominal design point.

The resultant gamma value for the design is $\gamma = 3.2$ and relatively, the maximum robust stability margin is resulted in $\epsilon_{max} = 0.3125$.

As it was stated earlier, the design purpose is to satisfy the FHQ criteria in Level 1 all over the specified flight envelope. So, the results given above which resulted Level 1 FHQ criteria chosen in Chapter 3 should apply the remainder of the flight envelope either. The Figure 6.11 shows that step responses of the controlled pitch rate response follows the ideal response used during the design phase of the nominal design point.

The pitch attitude bandwidth criteron results in Level 1 FHQ for all the considered design points along the flight envelope as seen in the Figure 6.12. Also, depending on the pitch rate responses in the Figure 6.11, dropback criteria results may be seen in the Figure 6.13. All 5 design points are within the satisfactory region which states both overshoot of the pitch rate and dropback of pitch attitude response over steady state pitch rate are desirable.

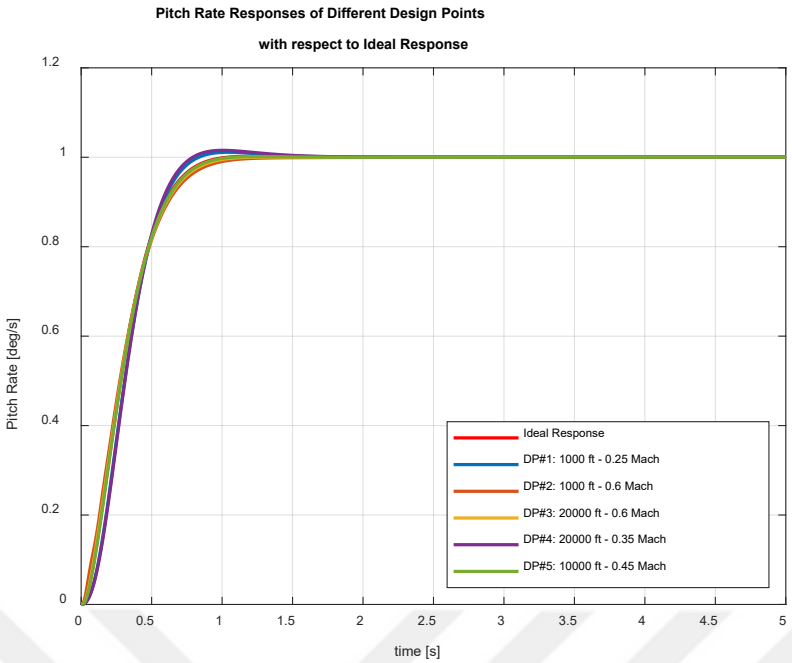

Figure 6.11 : Pitch rate responses along the flight envelope.

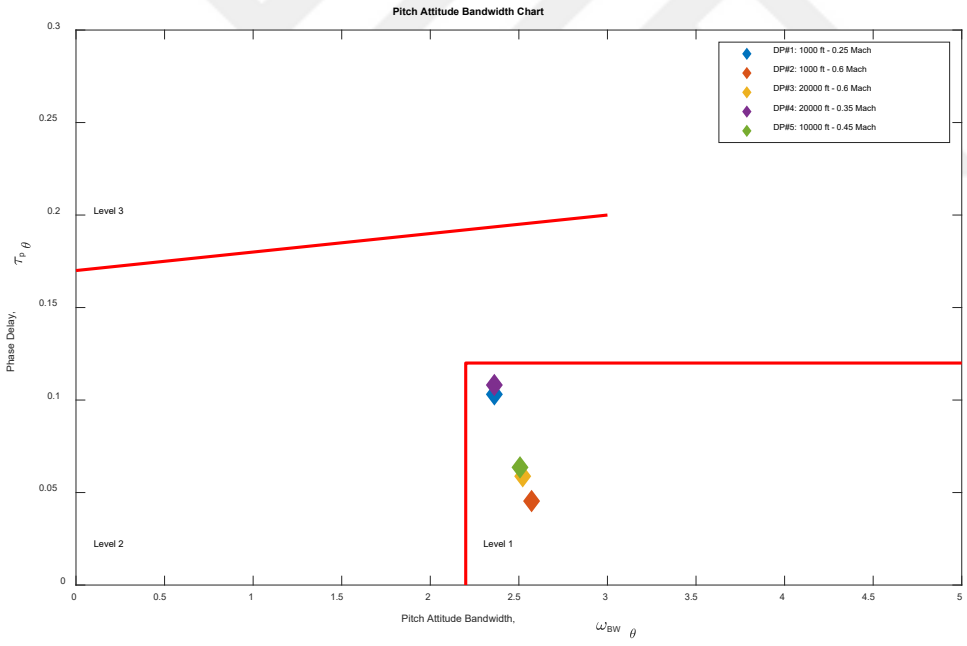

Figure 6.12 : Pitch attitude bandwidth FHQ result along the flight envelope.

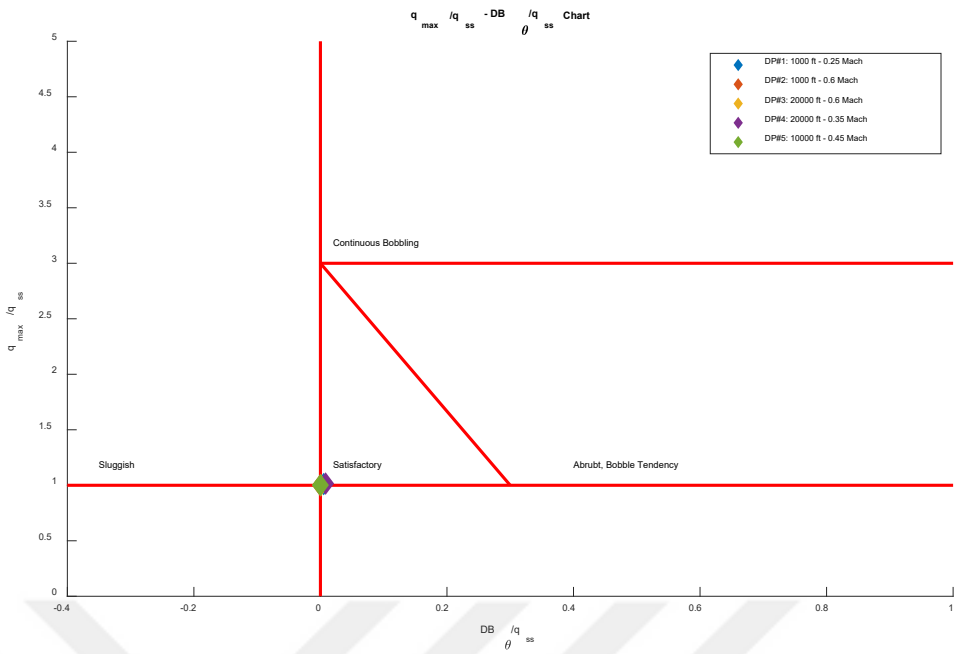

Figure 6.13 : Pitch attitude dropback FHQ result along flight envelope.

The Figure 6.14 shows how pitch attitude response changes after the stick was released. The results of all design points follows the pitch attitude at the time instance when the command was diminishes. Again, all pitch attitude results are following the result of the nominal design point which ensure zero dropback.

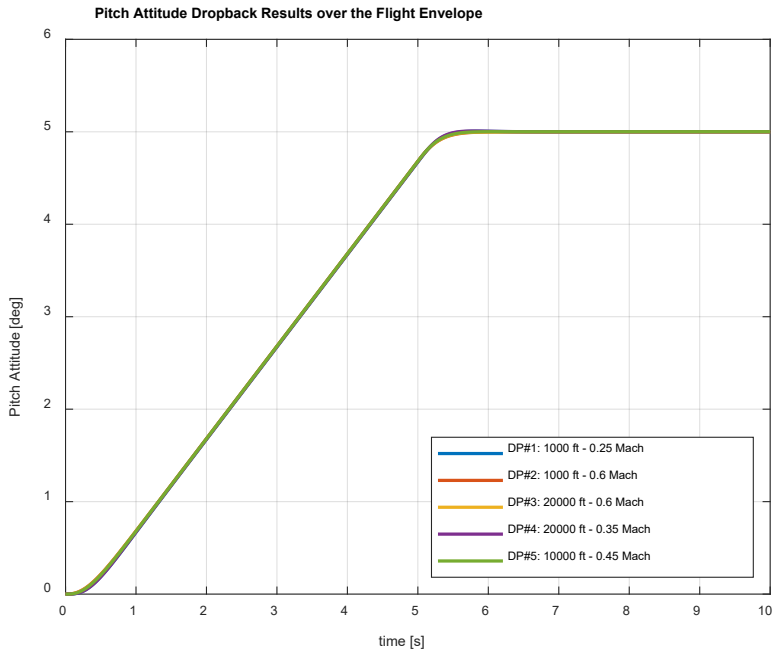

Figure 6.14 : Pitch attitude pulse input results along the flight envelope.

The Figure 6.15 shows the time delay results of each design point within the flight envelope. It can be seen that the all design points resulted in Level 1 FHQ as it was purposed and represented in the optimization cost.

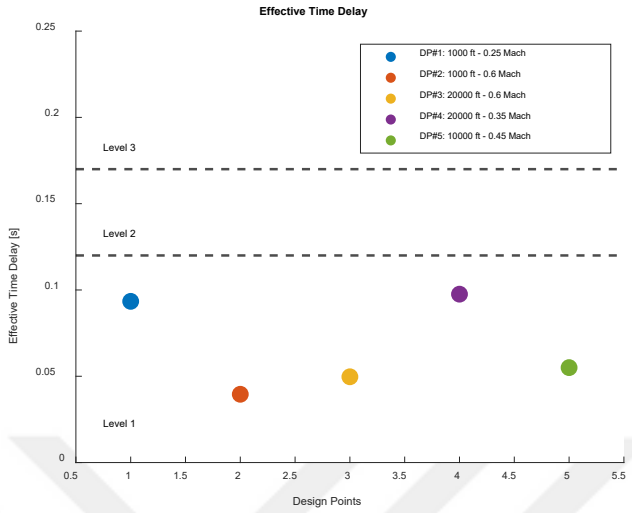

Figure 6.15 : Effective time delay results along the flight envelope.

Also, Figure 6.16 shows the pitch rate time responses of a step input given to different uncertain plants at different flight conditions. The uncertainty definition in Chapter 5 is used to represent the plant uncertainty.

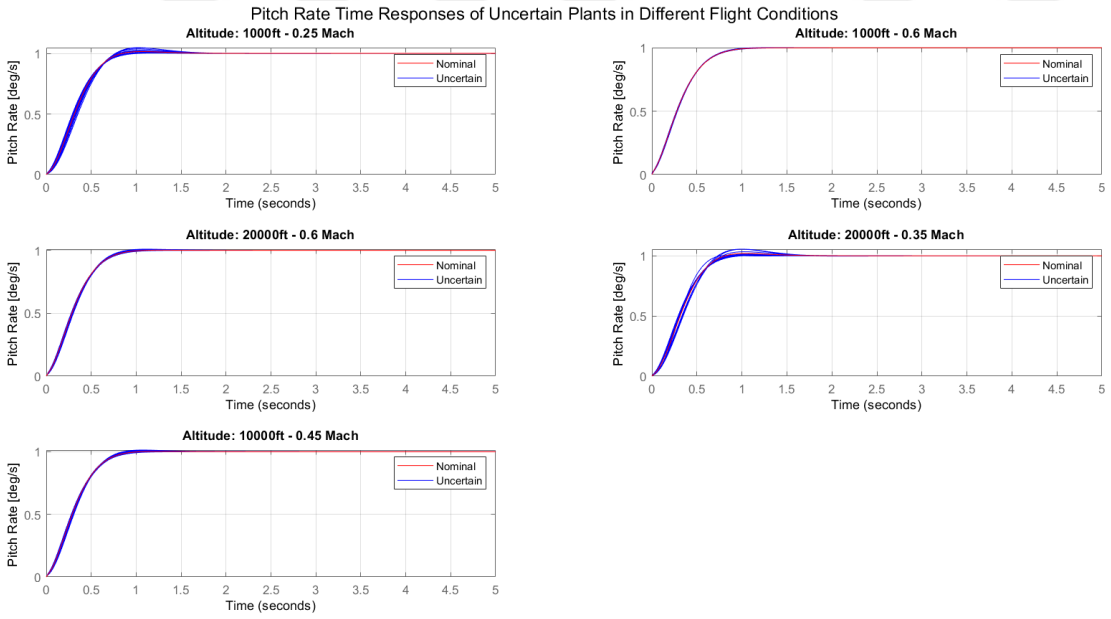

Figure 6.16 : Pitch rate time responses of uncertain plants.

It can be seen that the uncertain time responses follows the nominal plant response for all the flight conditions. The flight point of 1000 ft – 0.6 Mach has lower sensitivity for uncertainty while flight point 20000 ft – 0.35 Mach shows higher sensitivity. Thus, it is said to be the plant is more sensitive to the uncertainty as the dynamic pressure decreases and angle of attack increases relatively. The Figure 6.17 supports the results above as the pitch rate frequeny responses for uncertain plants have a distribution around the nominal plant. The results presented in Figure 6.16 and Figure 6.17 shows the performance robustness of the system that had been designed.

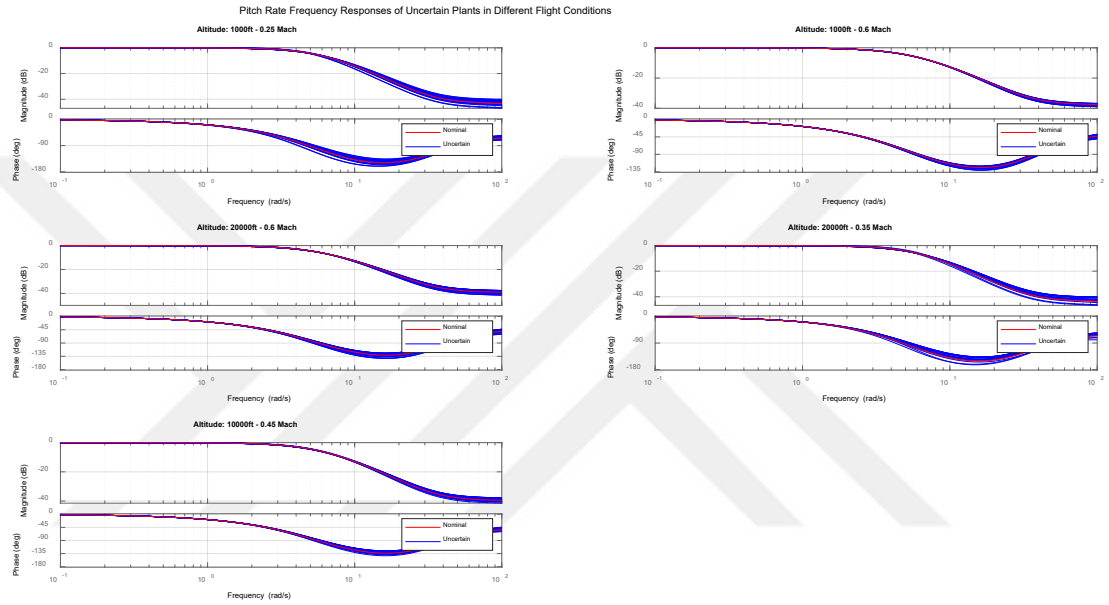

Figure 6.17: Pitch rate frequency responses of uncertain plants.

The stability robustness is another requirement that the system has to meet. For uncertain plants within the flight envelope, all closed loop responses need to remain outside of the nichols exclusion zone defined in Chapter 5. Figure 6.18 shows the nichols plot of the broken loop results from the input of the actuator over the selected design points with uncertain responses.

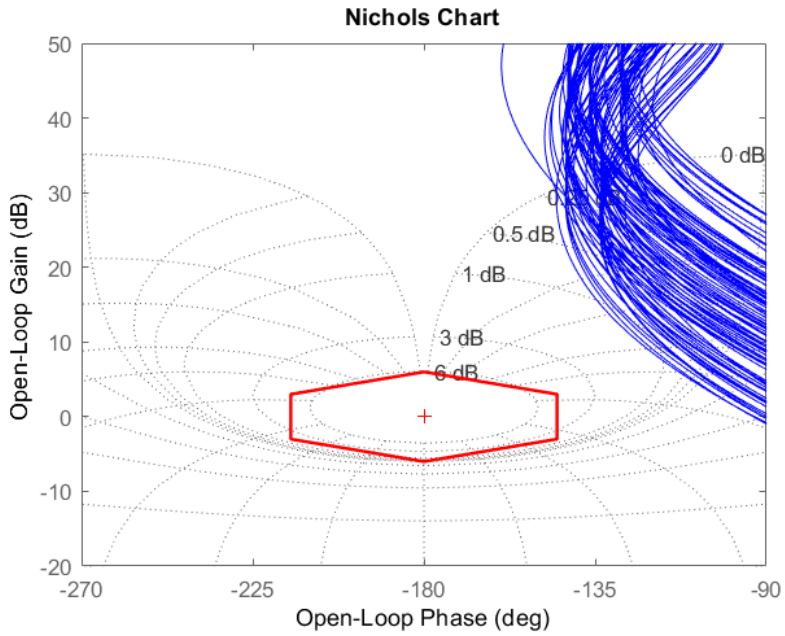

Figure 6.18 : Nichols plot of uncertain plants with respect to nichols exclusion zone.

It is said to be that the system is robustly stable over the flight envelope as the all uncertain responses remain outside of the nyquist exclusion zone. The closed loop system with 2 degree-of-freedom H_∞ Loop Shaping controller architecture is both satisfies performance criteria as all systems within the flight envelope resulted in Level 1 FHQ criteria that has been evaluated and stability criteria as all the uncertain plants within the designated flight envelope does not interferes nichols exclusion zone.

The results of 2 degree-of-freedom H_∞ Loop Shaping controller architecture are compared with the pre-existant PI controller of F-16 aircraft studied by NASA[14]. This comparison includes time response characteristics and FHQ evaluations of H_∞ controller and PI based NASA controller. The NASA controller emphasizes normal acceleration demand system and Figure 6.19 shows the normal acceleration responses after 1 g step input for design points discussed throughout this thesis. It can be seen that the aircraft follows the 1 g input for given points within the flight envelope. The Figure 6.20 shows the pitch rate time responses after 1 g step input. It can be seen that the pitch rate responses differs from each other with various flight conditions. The pitch rate responses need to be normalized in order to compare with the results of the H_∞ controller on the basis of tracking performance. The Figure 7.21 presents the pitch rate responses of both H_∞ controller and NASA PI controller with normalization side by side

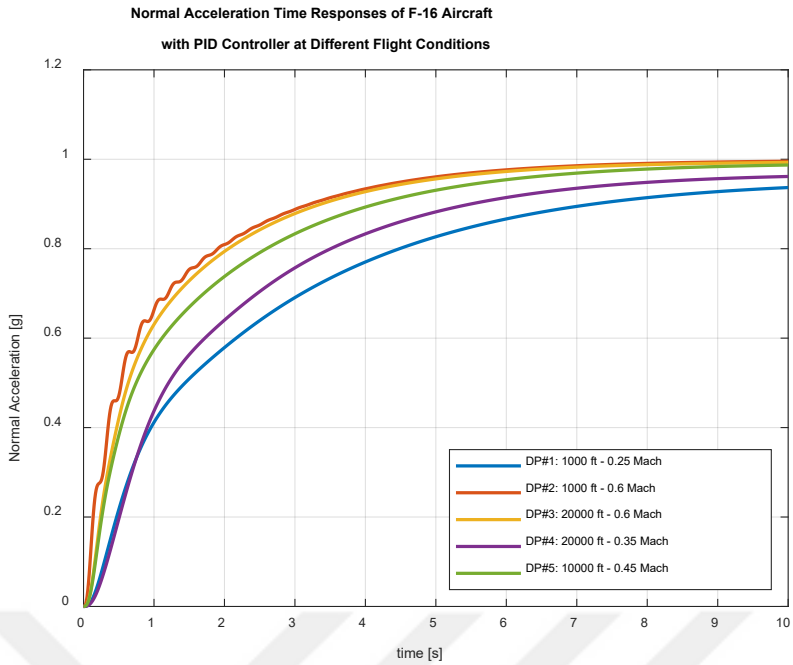

Figure 6.19 : Normal acceleration responses of NASA PI controller after step input.

As it can be easily seen from the figure, H_∞ controller has better rise time, settling time and overall response when compared to the NASA PI controller since the H_∞ controller employs pitch rate command system. This fact is expected since these two controller architecture has different demand systems. This difference creates a major difference in terms of FHQ criteria since the selected criteria are based on pitch rate and pitch attitude responses.

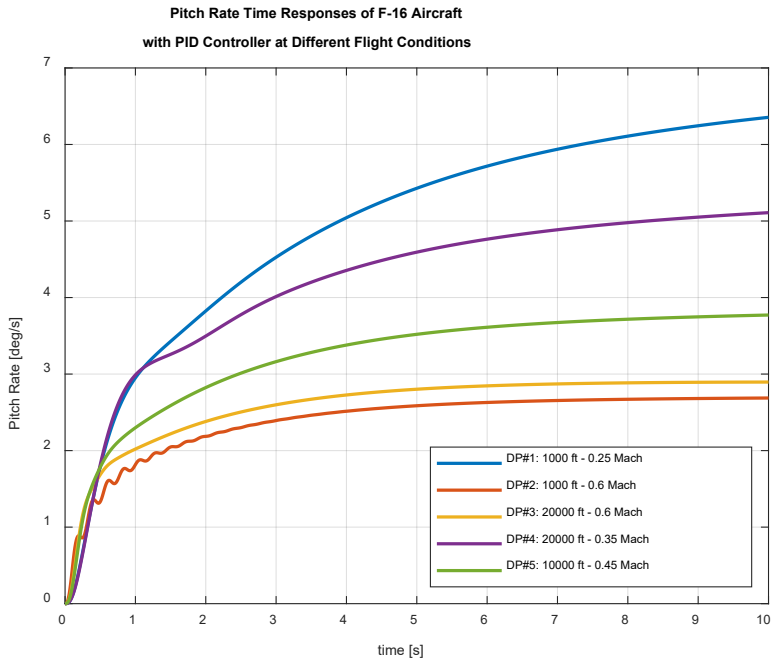

Figure 6.20 : Pitch rate responses of NASA PI controller after step input.

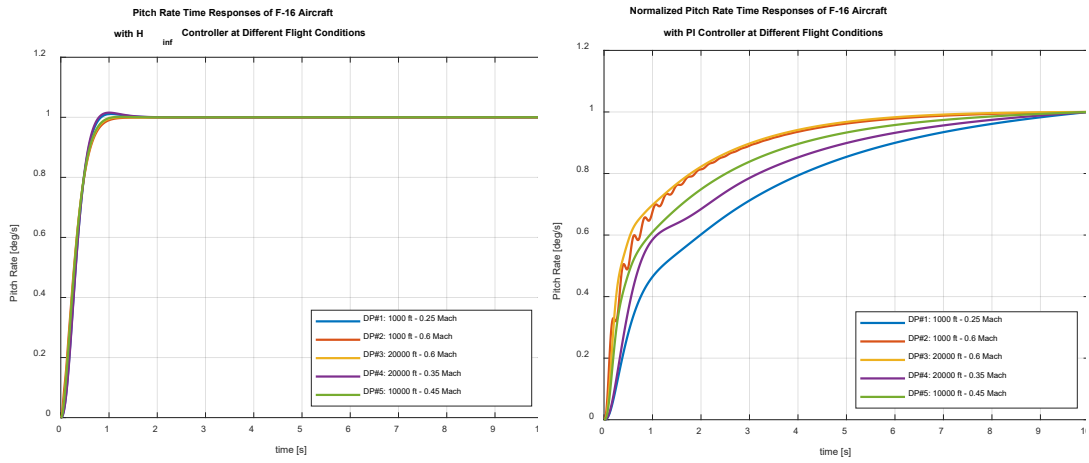

Figure 6.21 : Pitch rate time response comparison between $\boldsymbol{H}_\infty$ controller[left] and NASA PI controller[right].

First, pitch attitude bandwidth criterion results of both H_∞ controller and NASA PI controller is given in Figure 6.22 side by side. The H_∞ controller outperforms the NASA PI controller since all the FHQ evaluations of design points resulted in Level 1 while NASA PI controller has some Level 2 results especially for the points having high angle of attack.

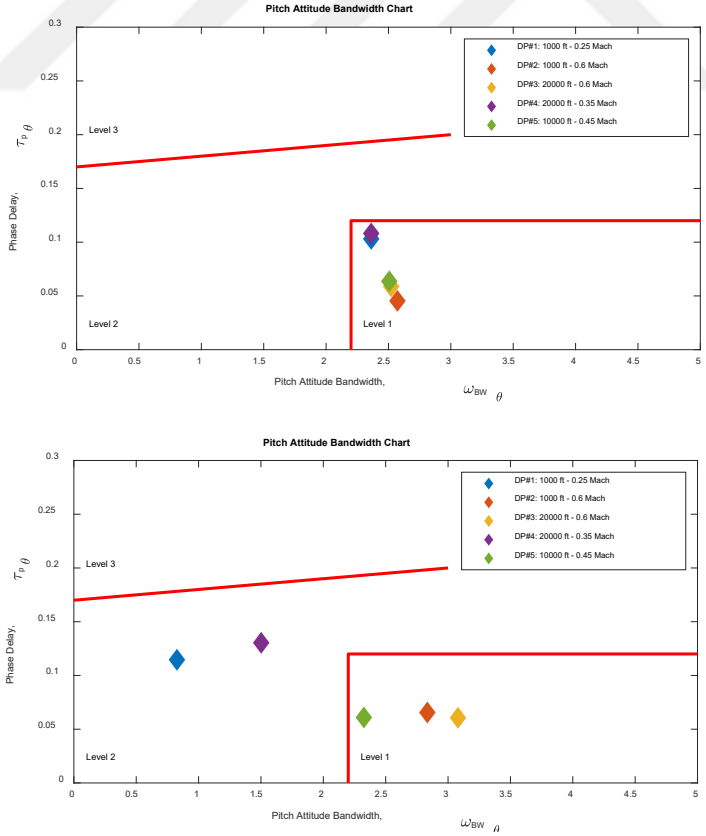

Figure 6.22 : Pitch attitude bandwidth criterion comparison between $\boldsymbol{H}_\infty$ controller[up] and NASA PI controller[down].

The Figure 6.23 shows the dropback criteria results of both H_∞ controller and NASA PI controller.

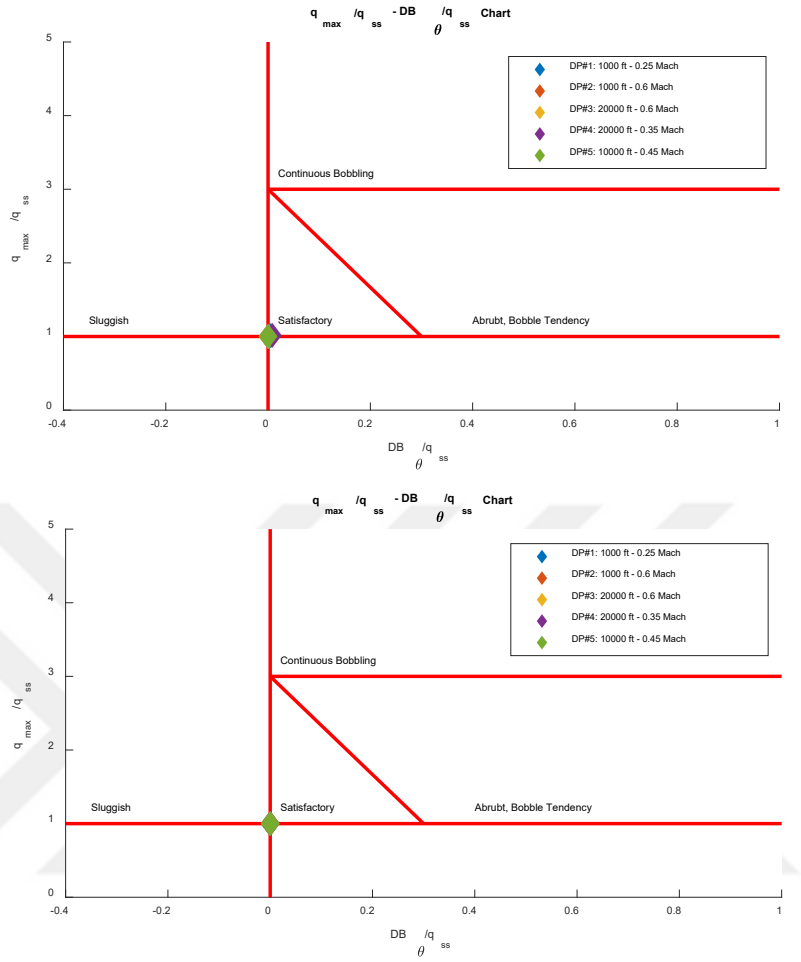

Figure 6.23 : Pitch attitude dropback criterion comparison between H_∞ controller[up] and NASA PI controller[down].

Both H_∞ controller and NASA PI controller satisfiy the pitch attitude dropback criterion as both pitch responses does not show large overshoot characteristics and pitch attitude shows any dropback when the command is released. On the basis of pitch attitude dropback criterion, the main difference steps forward on time delay responses shown in the Figure 6.24. Both H_∞ controller and NASA PI controller have Level 1 results for all the design points within the flight envelope however, the effective time delay result of 4th design point 20000 ft – 0.35 Mach for NASA PI controller is at the edge of the Level 2 FHQ boundary. It is clearly seen that H_∞ controller resulted in slightly less effective time delay.

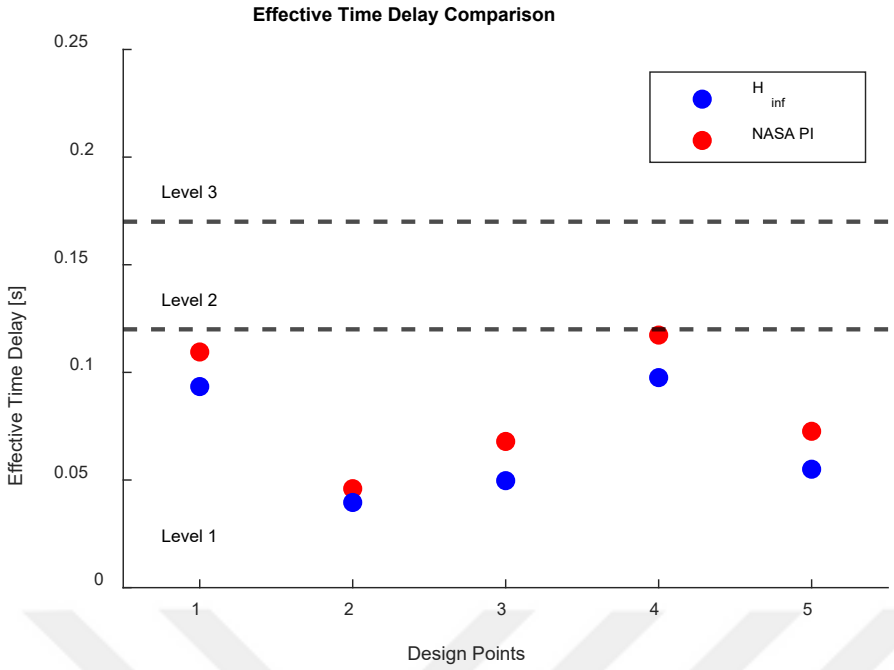

Figure 6.24 : Effective time delay criterion comparison between $\boldsymbol{H}_\infty$ controller and NASA PI controller.

To sum up all the results presented throughout this chapter, the parameters of 2 degrees-of-freedom H_∞ Loop Shaping controller are found by optimization are satisfactory for the design purpose which is to remain within the Level 1 FHQ for all the design points within the flight envelope. First, the ideal pitch rate transfer function is shaped with respect to optimization cost, then the controller design of a nominal design point has been done. Both the nominal design point and the design points along the flight envelope resulted in Level 1 FHQ. The performance robustness and stability robustness throughout the flight envelope demonstrated with the time and frequency domain responses. Finally, the results of the 2 degrees-of-freedom H_∞ Loop Shaping controller compared to the pre-existant NASA study which employs PI controller approach. The evaluated FHQ criteria shows the H_∞ controller outperforms NASA PI controller in both time and frequency domain.

7. CONCLUSION

In the scope of this thesis study, a robust control method of two degrees of freedom H_∞ Loop Shaping architecture has been applied to F-16 aircraft. It is purposed that for all the plants within the specified flight envelope, Level 1 FHQ evaluations resulted for a closed loop system. The specified flight envelope ranges from minimum altitude of 1000 ft to 20000 ft and minimum speed of 0.25 Mach to 0.60 Mach. This purpose has been achieved as all the plants resulted in Level 1 FHQ for both time and frequency domain. Also, whole systems within the flight envelope have robust stability and performance robustness. All uncertain responses follows the nominal responses corresponding to that flight condition as well as all uncertain responses stays outside of a nichols exclusion zone in frequency domain.

A comparison study has been completed in order to compare the results of the two degrees of freedom H_∞ Loop Shaping controller with the NASA PI controller in longitudinal axis. The two degrees of freedom H_∞ Loop Shaping controller outperforms the NASA PI controller as designated controller has better performance in both time and frequency domains.

A further work may be studied based on this thesis in the lateral directional axis of F-16 aircraft. The control method can be applied to MIMO system with similar manners. The ideal transfer function intervals can be found then the optimization problem can be defined in order to satisfy Level 1 lateral and directional FHQ evaluations within a specified flight envelope.

Furthermore, the optimization problem can be defined in other ways to find the optimal parameters that satisfies Level 1 FHQ evaluations. The problem defined in the scope of this thesis is a multiobjective optimization problem. Different approaches may be suitable such as multiobjective pareto solutions and particle swarm optimizations.

REFERENCES

[1] **Cassard, J.,** (2008). Dictionnaire d'historie de Bretagne, *Skol Vreizh,* France

[2] **Url-1** < https://www.leonardo-da-vinci.net/ornithopter/> date retrieved 07.01.2022

[3] **Atkinson, S., Dunne J.,** (2013). The Aircraft Book: The Definitive Visual History, *Dorling Lindersley,* London

[4] **Cayley, G.,** (1810), On Aerial Navigation, *Nicholson's Journal of Natural Philosophy,* February 1810

[5] **McRuer, D., Graham D.,** (2003). A Flight Control Century: Triumphs of the Systems Approach, *Journal of Guidance, Control and Dynamics*, Vol. 27, No. 2, pp. 161-173, 2003

[6] **Gates, S.B.,** (1924) "Notes on the Aerodynamics of Automatic Directional Control" Royal Aircraft Establishment (Britain), RAE Rept. BA 487, Feb. 19, 1924; and "Notes on the Aerodynamics of an Altitude Elevator Control", RAE Rept. BA 494, March 19, 1924

[7] **AGARD-CP-333** (1982). Criteria for Handling Qualities of Military Aircraft

[8] **MIL-F-8785C** (1980). Military Specification-Flying Qualities of Piloted Aircrafts.

[9] **MIL-STD-1797A** (2004). Flying Qualities of Piloted Aircraft .

[10] **Mitchell, David G., Hoh, Roger H., Aponso, Bimal L., Klyde, David H.** (1994). Proposed Incorporation of Mission-Oriented Flying Qualities into MIL-STD-1797A*,* CA.

[11] **Cooper, George E., Harper Jr. Robert P.** (1969). The Use of Pilot Rating in the Evaluation of Aircraft Handling Qualities*.,* NASA

[12] **Balas, G.G., and Hodgkinson.** (2009). Control Design Methods for Good Flying Qualities. *AIAA Atmospheric Flight Mechanics Conferance,* Chicago

[13] **Skogestad, S., Postlethwaite, I.** (2001). Multivariable Feedback Control, Analysis and Design. John Wiley&Sons

[14] **Nguyen, Luat T., Ogburn, Marilyn, E., Gilbert, William, P., Kibler, Kemper S., Brown, Philip W., Deal, Perry L.** (1979). Simulator Study of Stall/Post-Stall Characteristics of a Fighter Airplane with Relaxed Longitudinal Static Stability. Technical Paper 1538. National Aeronautics and Astronautics Administration, 1979.

[15] **Revealing the Dark Side of the F-16 FLCS,** Flight Model (FM) Developer's Notes Part 4

[16] **Gibson, J.** (1999). Development of a Design Methodology for Handling Qualities Excellence in Fly-by-Wire Aircraft *(Master's Thesis).*

[17] **Gautrey, J.** (1998). *Flying Qualities and Flight Control System Design for a Fly-by-Wire Transport Aircraft (Doctorate Thesis).*Cranfield University,Collage of Aeronautics, Cranfield.

[18] **Tichler, M., Lee, J., Colburne, J.,** (2001). Optimization and Comparison of Alternative Flight Control System Design Methods Using a Common Set of Handling-Qualities Criteria, *AIAA Guidance, Navigation and Control Conferance and Exhibit,* Montreal, Canada

[19] **Berger, T., Tichler, M., Hagerott, S., Gangsaas, D., Saeed, N.,** (2012). Longitudinal Control Law Design and Handling Qualities Optimization for a Business Jet Flight Control System, *AIAA Atmospheric Flight Mechanics Conference,* Mineapolis, MN

[20] **Berger, T., Tichler, M., Hagerott, S., Gangsaas, D., Saeed, N.,** (2013). Lateral/Directional Control Law Design and Handling Qualities Optimization for a Business Jet Flight Control System, *AIAA Guidance, Navigation and Control,* Boston, MA

[21] **Glover, K., Doyle, J.,** (1988). State-space formulae for all stabilizing controllers that satisfy an H_∞-norm bound and relations to risk sensitivity, *Systems & Control Letters*

[22] **Glover, K., Mcfarlane, D.C.,** (1989). Robust Stabilization of Normalized Coprime Factor Plant Descriptions with H_∞-Bounded Uncertainty, *IEEE Transactions on Automatic Control,* Vol. 34, No. 8, August 1989.

[23] **Glover, K., Sefton, J., Mcfarlane, D.C.,** (1990). A Tutorial on Loop Shaping Using H-Infinity Robust Stabilization, *IFAC 11th Trennial World Congress,* Tallinn, Estonia, USSR. 1990

[24] **Limebeer D.J.N., Kasenally E.M., Perkins J.D.** (1993). On the Design of Robust Two Degree of Freedom Controllers, Pergamon Press Ltd.

[25] **Hyde R.A.** (1991). H_∞ Aerospace Control Design-A VSTOL Flight Application. Berlin, Springer-Verlag

[26] **Application of Multivariable Control Theory to Aircraft Control Laws** (1996). Flight Dynamics Directorate Wright Laboratory

[27] **Magni, J.F., Bennani, S., Terlouw, J.,** (1997). Robust Flight Control: A Design Challenge. Springer-Verlag

[28] **Bates D.G., Kureemun R, Postletwaite I.** (2001). Quantifying the Robustness of Flight Control Systems Using Nichols Exclusion Regions and the Structured Singular Value, *Proceedings of the Instutituon of Mechanical Engineers, Part I: Journal of Systems and Control Engineering 2001 21 (pp.625-638)* SAGE.

[29] **Forssell, L., Nilsson U.,** (2005). ADMIRE The Aero-Data Model In a Research Environment Version 4.0, Model Description, FOI-Swedish Defence Research Agency Systems Technology.

[30] **Zhou K., Doyle J.C.** (1999). *Essentials of Robust Control.* Prentice Hall

[31] **Sidi M.,** (2001). *Design of Robust Control Systems, From Classical to Modern Practical Approaches,* Malabar FL, Krieger Publishing Company

[32] **Skogestad S., Postlethwaite I.** (2001). *Multivariable Feedback Control, Analysis and Design.* John Wiley&Sons

[33] **Stevens, B. L., Lewis, F. L., & Johnson, E. N.** (2016). *Aircraft Control and Simulation* . Wiley & Sons, Inc.

[34] **U.S. Standard Armosphere** (1976). National Aeronautics and Astronautics Administration, Washington DC., 1976.

[35] **Chapra Steven C., Canale Raymond P.** (2015). *Numerical Methods for Engineers, Seventh Edition.* McGraw Hill Education.

[36] **Stengel Robert F.,** (2004). *Flight Dynamics.* Princeton University Press

[37] **Nelson Robert C.,** (1998). *Flight Stability and Automatic Control.* WCB/McGraw-Hill

[38] **Roskam H.,** (2001). *Airplane Flight Dynamics and Automatic Flight Controls.* Design, Analysis and Research Corporation(DARcorporation)

[39] **Freudenberg J.S., Hollot C.V., Looze D.P.** (2003). *A First Graduete Course in Feedback Control*.

[40] **McFarlane D.C., Glover K.** (1990). *Lecture Notes in Control and Information Sciences, Robust Controller Design Using Normalized Coprime Factor Plant Descriptions.* Berlin, Springer-Verlag

[41] **Chen W.** (2005). *The Electrical Engineering Handbook,* London UK, Elsevier Academic Press

[42] **Ackermann J.** (2002). *Robust Control: The Parameter Space Approach, 2nd Edition.* London, Springer-Verlag

[43] **Terrell G.R.** (1999). *Mathematical Statistics: A Unified Introduction*, New York USA, Springer-Verlag

[44] **Martins J., Ning A.** (2020). *Engineering Design Optimization,* Cambridge, Cambridge University Press

[45] **Optimization Toolbox User's Guide** (2021), *Mathworks Inc.*

CURRICULUM VITAE

Name Surname **:** Zafer KAÇAN

EDUCATION **:**

- **B.Sc.** **:** 2017 , Istanbul Technical University, Aeronautical and Astronautical Engineering, Aeronautical Engineering

PROFESSIONAL EXPERIENCE:

- 2017-to present: Turkish Aerospace

OTHER PUBLICATIONS, PRESENTATIONS AND PATENTS:

- Cakin, U., **Kaçan, Z.**, Aydoğan, Z.A., & Kuvvetli, I. (2020). Initial Sizing of Hybrid Electric VTOL Aircraft for Intercity Urban Air Mobility, *AIAA Aviation 2020 Forum*